

**Static and Dynamic Theoretical Studies on Vibronic
Model Based Potential Energy Surface(s): Locating
Transition Structures and Fundamental Investigations in
Time-resolved Spectroscopy**

by

Prateek Goel

A thesis
presented to the University of Waterloo
in fulfillment of the
thesis requirement for the degree of
Doctor of Philosophy
in
Chemistry

Waterloo, Ontario, Canada, 2017

© Prateek Goel 2017

Examining Committee Membership

The following served on the Examining Committee for this thesis. The decision of the Examining Committee is by majority vote.

External Examiner: Artur Izmaylov
Associate Professor, Dept. of Chemistry, University of Toronto Scarborough

Supervisor(s): Marcel Nooijen
Professor, Dept. of Chemistry, University of Waterloo

Internal Member: Pierre-Nicholas Roy
Professor, Dept. of Chemistry, University of Waterloo

Internal-External Member: Wing-Ki Liu
Adjunct Faculty, Dept. of Physics, University of Waterloo

Other Member(s): Scott Hopkins
Associate Professor, Dept. of Chemistry, University of Waterloo
German Sciaini
Associate Professor, Dept. of Chemistry, University of Waterloo

Author's Declaration

This thesis consists of material all of which I authored or co-authored: see Statement of Contributions included in the thesis. This is a true copy of the thesis, including any required final revisions, as accepted by my examiners.

I understand that my thesis may be made electronically available to the public.

Statement of Contributions

Chapter 4 of this thesis is written by author's supervisor: Prof. Marcel Nooijen. In addition, Figures 5.5 - 5.7 and Figures 5.10 - 5.12 are made by author's collaborator: Amanda Kwan.

Rest of the material presented in this thesis is author's contribution.

Abstract

Construction and exploration of Potential Energy Surfaces (PES) is central to the study of many interesting chemical phenomena, such as computing the rate of a chemical reaction or elucidating structure of a complex molecule. Locating a transition state structure on a PES is an important problem as it provides a qualitative as well as quantitative understanding of reaction rates and mechanisms. A powerful example of this is the celebrated Transition State Theory (TST). Finding a transition state structure is a nontrivial and challenging task for reasons such as the lack of a good starting geometry or the PES having complicated topological features. The problem of characterizing critical points on a PES can be classified as "static" approaches to understand chemical structure and reactivity. When the interest lies in understanding dynamical processes, one needs to solve the time-dependent Schrödinger equation (TDSE). Although solving TDSE contains more "Physics", however, it also becomes harder to interpret the complex information it carries and to provide simple answers.

In this work, an attempt has been made on both static and dynamic fronts to address problems of fundamental importance, while proposing new and unconventional solutions to these problems. In first part of the thesis, a strategy to locate transition states using the vibronic model based PES has been proposed, implemented, and tested on a primary test set of unimolecular reactions. The approximate representation of the ground state PES using vibronic model serves as a powerful tool for transition state search by providing cheap means to compute the gradient and hessian on the PES, which are essential (or desirable, in particular the hessian) quantities for geometry optimization techniques. On the dynamic front, in second part of the thesis a new scheme for time-dependent photoelectron spectroscopy has been proposed, denoted as pump-repump-cw-photoelectron spectroscopy (PRP-CW-PES), which provides vibronically resolved fingerprints for a series of time-delay between pump-and repump pulses. In principle, the proposed scheme can be used to distinguish between closely related molecular structures, and can also serve as a new tool to study wave packet interferometry (WPI). The basic theory of the proposed scheme is outlined with application to simple model systems. Attention of the experimental community is called for realization of the experiment in the laboratory.

Acknowledgements

A PhD by its very nature is a long journey full of ups and downs (at least for most people), the successful completion of which depends heavily on a direct or indirect support of a number of people. I would like to thank and acknowledge efforts of some such people in this small note.

I would first like to thank my supervisor Prof Marcel Nooijen for devoting large amount of time and energy towards my PhD and being patient with my average level of intelligence and slow pace of progress. Since he has an open-door-walk-in policy for all students, he was always available for discussions and answered my questions patiently, including personal matters at times. He also allowed and encouraged me to attend a variety of conferences and participate in short term research visits, which helped me gain a broader perspective on scientific research, as well as allowed to meet new people and discuss new ideas. His extremely thorough approach to doing research, combined with utmost honesty and ethics, has laid a strong foundation for my journey in academia, or otherwise.

I am highly indebted to the very talented and extremely hardworking collaborator of mine, Amanda Kwan, who is a second year undergraduate student, for helping me with analyzing large amounts of data in a short span of time. You have a bright future, and I wish you the best.

I am thankful to Prof German Sciaini, who happens to be one of my committee members, for providing positive support, along with the great tasting coffee! In addition, the discussions on time-resolved spectroscopy with him and his group members were insightful. Prof LeRoy and Prof McCourt in the theoretical chemistry group have continued to be a source of inspiration. Prof Michael Palmer, much like during the course of my Masters, has been a great support and I enjoyed the discussions with him on Science and life.

I would also like to thank Dr. Jake Fisher, with whom I did most of my TA duties, for his positive outlook and good advice on life. Many colleagues in the Chemistry department especially Olivier (Gauthier Group), Eric (Palmer Group), KK (Murphy Group), and Chuda (Taylor Group) were very supportive and helpful, and with them there are many good memories to cherish and remember as part of my PhD journey.

Towards the end, I cannot afford to not mention some old friends, who continue to stand by me and tolerate my shenanigans, while making life a bit more meaningful and a lot more fun - Nilesh Mishra, Kailash Kasala, Ketan Sharma, Shantanu Kumar, Amit Vikram, Ankur Jalan, and Anjana Babu thank you for everything. Finally, thanks Mom and Dad for teaching me the core values of honesty, karma and compassion at an early age, along with standing up for what is right. I have tried to keep up with these values, to the best of my capabilities, albeit not without some room for being vulnerable and making mistakes, which is invariably part of being human. Perhaps there are some people who are above making mistakes, but sadly I am not amongst one of them.

Dedication

This thesis is dedicated to Prof **Pinaki Gupta-Bhaya (aka PGB)**, (now retired) Professor at IIT Kanpur, India, who will always hold a special place in my life.

Table of Contents

Examining Committee Membership	ii
Author's Declaration	iii
Statement of Contributions	iv
Abstract	v
Acknowledgements	vi
Dedication	vii
List of Tables	xi
List of Figures	xiii
List of Abbreviations	xv
Introduction	1
PART-A	7
1 Theoretical Background	8
1.1 Geometry Optimization	9
1.1.1 A Newton-Raphson Primer	10
1.1.2 Interpolation Methods	14
1.2 Approximate representation of BO PES	15
1.3 Geometry Optimization on Approximate BO PES	17
2 Construction of Vibronic Model to represent Adiabatic Ground State Potential Energy Surface	19
2.1 Introduction	19
2.2 Illustration of the proposed scheme using a 1D model system	21

2.3	Formulation of Gradient and Hessian for Vibronic Model	26
2.3.1	Computation of analytical gradient	26
2.3.2	Computation of analytical hessian	28
2.3.3	Numerical Gradient and Numerical Hessian	29
2.4	Determination of Vibronic Model Parameters	30
2.4.1	Determination of constant term E_{ab}	32
2.4.2	Determination of linear coupling terms \mathbf{g}_{ab}	32
2.4.3	Determination of quadratic coupling terms \mathbb{H}_{ab}	33
2.4.4	Self-consistent solution for all parameters	33
2.5	Choice of Coordinates	33
2.6	Results & Discussions	39
2.6.1	Scans of Potential Energy Surface	39
2.6.2	A note on quantum chemical calculations	41
2.6.3	Reaction Test Set	41
2.6.4	Results for HF/3-21G: A detailed discussions of three reactions	47
2.6.5	Results for B3LYP/cc-pVTZ	48
2.6.6	Conclusions	49
3	Alternative Vibronic Model Construction for Transition State Search: VMTS-c	64
3.0.1	Recipe for construction of new vibronic model	65
3.0.2	Illustrative and Representative Example	66
3.0.3	Conclusions	67
4	Transition State Optimization on Vibronic Model: VMTS-o	71
4.1	Characterization of Transition States	71
4.2	Potential Advantages of Vibronic Model Transition State Optimization (VMTS-o)	72
4.3	Limitation of Vibronic Model Transition State Optimization (VMTS-o)	73
4.4	Basic algorithmic steps employed in VMTS-o	75
4.5	Main VMTS-o Algorithm	78
5	Vibronic Model Transition State Search: Results	80
5.1	Introduction	80
5.2	Potpourri of VMTS Schemes	81
5.2.1	Note on the starting guess geometry	83
5.2.2	Note on the analogous schemes in Gaussian09	83
5.2.3	Reaction Data Set: Unimolecular reactions	84
5.3	Results and Discussions	92
5.3.1	Results for VMTS <i>small</i> scheme	92

5.3.2	Results for VMTS <i>large</i> schemes	94
5.4	Conclusions and Perspective on VMTS Future Work	97
5.4.1	VMTS: A positive outlook and the road ahead	97
5.4.2	VMTS: A critical outlook	98
PART-B		110
6	A proposed new scheme for vibronically resolved time-dependent photoelectron spectroscopy: pump-repump-continuous wave-photoelectron spectroscopy (prp-cw-pes)	111
6.1	Introduction	111
6.2	Schematics of the pump-repump-cw-photoelectron scheme	114
6.2.1	General discussions of the proposed scheme	114
6.2.2	Various realizations of prp-cw-pes	120
6.3	Application of prp-cw-pes to a 2x2 vibronic model	124
6.4	Concluding Remarks	136
References		142

List of Tables

2.1	Different forms of window function and their derivatives	30
2.2	Unimolecular Reactions	46
2.3	Comparison of Energies for Reaction-9: H-shift [HF/3-21G]	50
2.4	Comparison of Gradients for Reaction-9: H-shift [HF/3-21G]	51
2.5	Comparison of Energies for Reaction-1: Ring Opening [HF/3-21G]	52
2.6	Comparison of Gradients for Reaction-1: Ring Opening [HF/3-21G]	53
2.7	Comparison of Energies for Reaction-3: Claisen Rearrangement [HF/3-21G]	54
2.8	Comparison of Gradients for Reaction-3: Claisen Rearrangement [HF/3-21G]	55
2.9	Comparison of Energies for Reaction-9: H-shift [B3LYP/cc-pVTZ]	56
2.10	Comparison of Gradients for Reaction-9: H-shift [B3LYP/cc-pVTZ]	57
2.11	Comparison of Energies for Reaction-1: Ring Opening [B3LYP/cc-pVTZ]	58
2.12	Comparison of Gradients for Reaction-1: Ring Opening [B3LYP/cc-pVTZ]	59
2.13	Comparison of Energies for Reaction-3: Claisen Rearrangement [B3LYP/cc-pVTZ]	60
2.14	Comparison of Gradients for Reaction-3: Claisen Rearrangement [B3LYP/cc-pVTZ]	61
2.15	Comparison of V_{ab} and Window function for Reaction 9	62
2.16	Comparison of V_{ab} and Window function for Reaction 10	63
3.1	Data for Reaction-8 during TS search using original definition of the vibronic model	66
3.2	Data for Reaction-8 for new definition of the model at geometries during TS search using original definition of the vibronic model	67
3.3	Energy and Gradient Norm Comparison for Reaction 8 at first guess geometry ($\frac{Q_A+Q_B}{2}$) using the original definition of the vibronic model	68
3.4	Energy and Gradient Norm Comparison for Reaction 8 at first guess geometry ($\frac{Q_A+Q_B}{2}$) using the modified definition of the vibronic model	69
3.5	Energy and Gradient Norm Comparison for Reaction 8 at an intermediate geometry using the modified definition of the vibronic model, where original model can not be constructed	70
5.1	A summary of schemes used for TS search using Vibronic Models (VMTS)	82
5.2	A statistical summary of VMTS small (HF/3-21G) results	94

5.3	A statistical summary of VMTS large (HF/6-31G*) results	96
5.4	A statistical summary of VMTS large (B3LYP/cc-pVTZ) results	97
5.5	Number of cycles it takes to reach 1 negative eigenvalue regime starting from $\frac{Q_A+Q_B}{2}$ guess for VMTS small scheme	100
5.6	Energy and gradient as a function of VMTS cycles for Reactions 3, 17 and 16 respectively	106
6.1	Parameters for the 2D vibronic model Hamiltonian. All quantities in electron Volts.	126
6.2	Change in populations as a function of pump-repump time-delay for select vibronic levels in excited states depending on the vibronic overlap with the ground state. All time-delays are in <i>fs</i>	135

List of Figures

1.1	Diabatic States of the EVB model and the off-diagonal coupling term	17
1.2	Adiabatic ground state obtained as a linear combination of the diabatic states in Figure 1.1	17
2.1	The red solid curve line is the known adiabatic ground state potential, which will be modeled using vibronic model scheme discussed in this chapter	22
2.2	Vibronic model constructed with only the constant term in the off-diagonal, unable to capture the ground state PES correctly	23
2.3	Vibronic model with a full quadratic off-diagonal term, but no window included. TS region is captured correctly, but not the minima regions.	24
2.4	Vibronic model with a quadratic off-diagonal term times a Gaussian window function. Vibronic model energies follow true adiabatic energies closely.	25
5.1	Algorithm employed in VMTS small scheme using full ab initio hessian at each cycle	85
5.2	Algorithm employed in VMTS 2A scheme using ab initio hessian at a lower level of theory	86
5.3	Algorithm employed in VMTS 2B scheme using mixed hessian update strategy	87
5.4	Reaction Test Set for VMTS: 36 Unimolecular Reactions	91
5.5	VMTS small scheme with starting geometry QST2(1) vs. Gaussian’s QST2	101
5.6	VMTS small scheme: comparison of starting guess geometries	102
5.7	VMTS small scheme: comparison of max distance parameter used in VMTS-o	103
5.8	VMTS small scheme: intermediate geometries during TS search for Reaction 3	104
5.9	VMTS small scheme: intermediate geometries during TS search for Reaction 17	105
5.10	VMTS large scheme 2A comparison with Gaussian’s QST3 for HF/6-31G*	107
5.11	VMTS large scheme 2B comparison with Gaussian’s QST3 for HF/6-31G*	108
5.12	VMTS large scheme 2B comparison with Gaussian’s QST3 for B3LYP/cc-pVTZ	109
6.1	A diagrammatic representation of pump and repump pulse sequence with a time delay of $\tau = t_2 - t_1$	119

6.2	Snapshots of prp-cw-pes for a 1D model system at different values of pump-repump time-delays.	122
6.3	Rapid oscillations of populations in vibronic levels of excited state on a short time-scale.	123
6.4	Snapshots of prp-cw-pes for the 2D vibronic model at select values of pump-repump time-delays.	128
6.5	Populations in vibronic levels of excited states for the 2D vibronic model at select values of pump-repump time-delays. Eigenvalues characterize the vibronic levels.	129
6.6	Select fingerprints of vibronic excited states for the 2D vibronic model displaying the <i>primary</i> character of excited electronic state of its origin	130
6.7	1d cut of PES along the normal mode v_t for excited states S_1 and S_2 corresponding to the parameters shown in Table 6.1	131
6.8	Results of fitting for the snapshot corresponding to time-delay 10.0 fs for the 2D vibronic model with varying number of fingerprints. Convergence is reached at 35 fingerprints.	137
6.9	RMSE values associated with the fitting of snapshots with varying number of fingerprints for select time-delays. The pattern is similar for all time-delays and convergence is reached after 35 fingerprints.	138
6.10	Snapshots of prp-cw-pes for the 2D vibronic model at select values of pump-repump time-delays for the case when the state S_1 is bright.	139
6.11	Population dynamics associated with vibronic levels in excited state at select values of time-delays. Some eigenstates display large changes while others only have small effect of time-delay on the net population.	140

List of Abbreviations

AIMD	Ab initio Molecular Dynamics
CMD	Centroid Molecular Dynamics
CTP	Cubic Transit Path
DFT	Density Functional Theory
DG-EVB	Distributed Gaussian - Empirical Valence Bond
EVB	Empirical Valence Bond
HF	Hartree-Fock
IRC	Intrinsic Reaction Coordinate
MCMM	Multiconfiguration Molecular Mechanics
MCTDH	Multi-configuration Time Dependent Hartree
MEP	Minimum Energy Path
PES	Potential Energy Surface
PRP-CW-PES	Pump-repump-cw-photoelectron spectroscopy
QMDFE	Quantum-mechanically derived Force Fields
QTP	Quadratic Transit Path
RPH	Reaction Path Hamiltonian
RPMD	Ring Polymer Molecular Dynamics
SC-IVR	Semiclassical Initial Value Representation
TRPES	Time-resolved Photoelectron Spectroscopy
TS	Transition State
VCI	Vibrational Configuration Interaction
VMTS	Vibronic Model Transition State
VMTS-c	Vibronic Model Transition State - construction
VMTS-o	Vibronic Model Transition State - optimization
WPI	Wave packet Interferometry

Introduction

A long standing goal of Chemistry has been the understanding of reaction mechanisms, i.e. obtaining answers to questions such as how a reaction proceeds from reactants to products, what are the steps and intermediates involved in the process, which are the preferred pathways, what are the energy bottlenecks which can lead to prediction of reaction rates and others. At a microscopic molecular level, most reactants have to cross an energetic "barrier" in order to convert into products. These barriers are characterized by a type of intermediate structure, referred to as a transition state or transition structure (TS) ¹ on the molecular Potential Energy Surface (PES). [1, 2] These transition states are important as they play a crucial role in determination of energy barriers which help in proposing a mechanism or verifying an experimentally proposed reaction mechanism, and predicting the thermal rates (albeit approximately, but qualitatively correct), using the much celebrated Transition State Theory (TST). [3] TST has become a cornerstone in theoretical chemical reaction dynamics and is used widely as a practical tool to model the kinetics of complex chemical reactions, for example in combustion chemistry. [4] In the context of proposing mechanism and pathways, knowing TS energy helps to propose a pathway, when there are more than one possible TS for a particular reaction channel, by selecting the preferred route to be the one with lower(est) energy barrier. Much of these predictions often work reasonably well as a guiding tool in understanding the complicated chemical reaction networks and provide chemists a toolbox to make sense of complex underlying processes.

The importance of transition states in Chemistry is thus well established and the success of TST is a testament to this fact. The challenging task itself is to locate and characterize these structures. Experimentally, this is a difficult goal to achieve as TS can only be observed in an indirect manner during the course of a reaction. There have been continued efforts towards spectroscopic characterization of transition states, [5] but this is not yet a routine and robust procedure. In addition, such experiments can also be costly affairs, making it out of reach of most researchers. This is where theory comes into picture and it plays a vital role indeed in this quest. A large amount of effort has been dedicated towards developing methods to locate transition states in the past (for a recent survey, see [6]). While significant progress has been made on this front in the

¹Although there are differences in the terminology for these two words associating somewhat different meaning, in this thesis these two are used interchangeably, most of the times "transition state".

past couple of decades, combined with exponential growth in computational power and resources², there is not one method that can be called the panacea of transition state search problem. *A major focus of the work carried out in this thesis is the development of a new method for locating transition states.* In addition to the TS geometry, the *minima* structures corresponding to reactant and product geometries also need to be located and characterized. This is a relatively simpler task, both experimentally and theoretically. The minima and TS structure together are referred to as *critical points* on the PES, and are often the starting points and building blocks of many computational studies. At times, there are also other important geometries of interests, such as a *conical intersection* (CI), but these are far and few in between so long as one restricts oneself to studying processes on the *ground state* PES (corresponding to the lowest eigenstate of electronic Schrödinger equation).

While a successful theory like TST needs information only about critical points, one needs to have a global representation of a PES in order to perform a detailed and more accurate dynamical studies. The goals of such elaborate studies are often to compute branching ratios for different products and reaction rates using accurate rate theories (which go beyond TST approximation) such as RPMD. [7] Constructing a PES is a field in itself, an important branch of theoretical chemistry, and a variety of strategies have been developed in the past. A conceptually simple yet an appealing method to build an approximate reactive PES was developed by Miller and coworkers, famously known as Reaction Path Hamiltonian (RPH). [8] After locating the TS, one constructs a minimum energy path (MEP) such as an IRC. MEP is a one dimensional coordinate parameterized by the its arclength. For the remaining degrees of freedom, harmonic valleys perpendicular to the MEP are created. This defines a global PES in terms of all $(3N - 6)$ internal coordinates. Another conceptually straightforward, but technically difficult way to construct a PES is to obtain a global fit of the energy surface at multiple ab initio energies. [9] However, such an effort quickly becomes unfeasible because of the exponential increase in the number of ab initio energies that will be needed for a global fit. Moreover, even if one can obtain the ab initio energies for a large number of geometries, obtaining a fit using a flexible and accurate expansion in analytical basis function is not an easy task. As a result of the impracticality of brute-force fitting approach, one turns towards using "direct dynamics" type of approaches to study reaction dynamics, in which no apriori knowledge of PES is needed. [10] The potential energy is calculated on-the-fly at each time step using electronic structure theory - often using an inexpensive method such as the Density Functional Theory (DFT). Direct dynamics approaches also suffer from computational expense, both with an increase in system size and with an increasing level of accuracy in the electronic structure method. It should be noted that while the fitting approach is more commonly used for accurate spectroscopic studies ("wavenumber accuracy") in conjunc-

²A personal laptop these days can easily have 16GB of random-access memory and 1TB of hard disk space with powerful multi-core processors, sufficient to run small-scale simulations at home!

tion with accurate quantum nuclear dynamical methods such as VCI or MCTDH, the direct dynamics approach is often used to study kinetics or photochemical processes in combination with approximate quantum dynamics methods such as surface hopping, Ab initio molecular dynamics (AIMD), path integral based approaches such as RPMD and CMD, and semi-classical methods such as SC-IVR.

The Empirical Valence Bond (EVB) [11] approach presents a good alternative for constructing a (ground state) PES, which is based on a matrix representation of local potential energy surfaces. The diagonal elements of this coordinate dependent matrix represent the potential for different reactants and products valleys, while the off-diagonal elements represent the coupling elements between them. The lowest eigenvalue of this coordinate dependent matrix gives the approximate ground state PES. The off-diagonal element is chosen such that the correct barrier height (and possibly also curvature) at the transition state geometry is reproduced. There are a variety of EVB methods depending on how the diagonal and off-diagonal elements are modeled. Some of these methods will be briefly mentioned in the next chapter. What is important to note here that many applications of the EVB based methods focus on extended systems or complex biological systems, where the diagonal elements are modeled based on molecular mechanics force fields, which can be thought of as "basis functions" for representing chemical reactions. Such force fields are based on a particular "bonding pattern" (in the spirit of VB theory) and are known to be able to capture most features of the PES around a minimum region and are suitable to describe conformational degrees of freedom. In this thesis, we have also employed the "EVB based" approach to construct an approximate PES, but our formulation tends to be closer to some alternative definitions of EVB models, which do not make use of force field potentials. Our goals are limited to gas phase organic reactions of small (to medium) sized molecules and for the reactant and product local PES description, we employ the standard harmonic approximation.

In fact, we prefer to see our EVB based PES in a somewhat different light, different from most other practitioners. We prefer to use the term *vibronic model* instead of EVB because of the close similarity of our model to the commonly used *vibronic model Hamiltonian* for the description of excited states. [12] Known by the name of its pioneers, Köppel-Domcke-Cederbaum (KDC), vibronic model Hamiltonians have been extensively used to study excited state dynamics, in particular short-time dynamics such as the simulation of absorption spectra or photoelectron spectra, often in conjunction with accurate quantum dynamics algorithms such as MCTDH. [13] The mathematical structure of our vibronic model, in order to describe the ground state PES, is analogous to the (quadratic) KDC Hamiltonian. The determination of parameters that go in the model is entirely different for the two cases. The KDC Hamiltonian has *true* coupling between real excited state surfaces, which is determined using a suitable diabaticization scheme. In our description the upper surface has no particular meaning associated with it. The off-diagonal cou-

pling elements in our model are determined such that the ab initio energy, gradient and hessian at the transition state geometry are reproduced exactly. It should also be noted that the KDC vibronic model is also part of this thesis, in the context of simulation of time-resolved spectra, though only rudimentary model systems have been studied for this purpose.

One major motivation for building EVB type PES is to apply them in the study of reaction dynamics, in particular to calculate rate constants. Their cheap construction and limited (but often satisfactory) accuracy makes them an ideal candidate to study dynamical processes and calculate rate constants, where order-of-magnitude accuracy is often sufficient. A prime example of such application is the extensive work done by Truhlar et al, [14] and also the work of Schlegel et al. [15] We would like to note that our journey towards constructing a ground state PES based on a vibronic model started because of an interest in calculating reaction rates for unimolecular reactions. The attraction of a vibronic model in this context is that it can provide a convenient model to construct complicated potential energy surfaces. As an additional benefit, the definition of reactant and product becomes lucid in terms of projection operators on electronic Hilbert space, bypassing the need of a (vague) definition of dividing surface in phase space. The calculation of rates for unimolecular reactions is a challenging problem because of the bound nature of PES. If one considers an isolated gas-phase system, quantum mechanically the thermal wave packets oscillate (or bifurcate) forever, and it is unclear how one can extract a meaningful rate constant from such a formulation. The practical strategies include introducing the "bath" degrees of freedom (and a system-bath coupling), or a complex absorbing potential (CAP) explicitly in the Hamiltonian, which forces the wave packet recurrence to vanish and a long time limit of the thermal correlation function provides information on the rate. Our goal was to extract the rate solely based on system information, much in the spirit of equilibrium statistical mechanics where the thermal properties can be calculated once one has the knowledge of all eigenstates of the system. In the end, this endeavor proved too hard for us and the focus of the thesis shifted to the problem of modeling sections of PES using a vibronic model, and in particular a transition state search algorithm based on a vibronic model representation of the PES. It is important to note that the problem of calculating reaction rates is not a part of the thesis and the majority of the thesis revolves around the problem of locating transition states.

The thesis is organized as follows. In Chapter-2, the construction of vibronic model in order to represent the ground state potential energy surface (GS-PES) is discussed at length including the technical details. The methodology is then applied to a set of unimolecular reactions and the results have been compared to the true ab initio data along some specific reaction paths, such as the IRC. Such a comparison provides a measure of the quality and validity of the vibronic model. It should be noted that both the minima and transition state region are captured correctly by design, employing an iterative procedure to determine the parameters of the model. In Chapter-

3, some modifications in the vibronic model construction strategy are discussed such that it can best suit the needs of transition state search. It is important to emphasize that unlike the previous chapter, where both minima and TS region are captured correctly, here only the (guess) TS region is modeled accurately. This is certainly not a desirable feature but the reasons for such a limitation will be discussed in the chapter.

In Chapter-4, optimization algorithms to locate transition state on a vibronic model are discussed. One constructs the vibronic model using ab initio data at a guess geometry for the TS to model the off-diagonal element. The transition state on this model, or the closest approximation to it is found and checked whether it is a true transition state. If it is not a true transition state, a new model is built at this geometry and the process is repeated. We call this strategy as VMTS (Vibronic Model Transition State), while the two components of VMTS - construction of vibronic model, and locating a transition state on a given model are denoted as VMTS-c and VMTS-o respectively. The VMTS scheme, along with its variants, is discussed in detail in Chapter-5. Two sets of ab initio data are employed for this study - one at a lower level of theory with a smaller basis set (HF/3-21G) while other at a higher level of theory with a larger basis set (B3LYP/cc-pVTZ). The variations in VMTS scheme occur mainly because of how the hessian is updated at each VMTS cycle. In addition, effects of changing the initial guess structure have also been studied. The VMTS scheme is applied to a set of unimolecular reactions and the results have been compared to the popular TS search methods in Gaussian09, namely QST2 and QST3.

In Chapter-6, the discussion shifts towards a different direction where a new scheme of time-dependent photoelectron spectroscopy is discussed. There is no direct connection between this chapter and other chapters as such, though these two parts of thesis can be considered as two sides of a coin - static and dynamic studies on a PES - which can often complement each other quite well. A summary of the work presented in this chapter is as follows:

We propose a new scheme for time-resolved photoelectron spectroscopy denoted as pump-repump-continuous wave-photoelectron spectroscopy (prp-cw-pes). The scheme is comprised of two femtosecond laser (pump) pulses under cw illumination (probe). By changing the time-delay between pump and repump laser one can manipulate the populations of vibronic levels in electronic excited states. The cw laser acts on for a long time and establishes resonance between excited states and the continuum photo-ionized states. Sharp spectra can be obtained from the resonance condition $\hbar\omega_{cw} = E_{kin}^{(\vec{k})} + (E_{v^+}^{ion} - E_v^{exc})$. The intensities in the spectra are sensitive to the time-delay between the pump-repump pulses, but only depend on the populations of excited states, not the phase relations (coherences). As a result, each time-delayed snapshot spectrum is a weighted sum of so-called fingerprints, where a fingerprint is the vibrationally resolved photoelectron spectrum for a single vibronic excited state. The latter information can potentially be simulated reliably using vibronic models and wave packet propagation methods. In the easiest application of the

experiment, different time-delays produce different spectra, for a single molecular system. This wealth of experimental data can be fitted to an, ideally small, set of theoretical fingerprints by adjusting the populations as fitting parameters. This technique might be able to distinguish between closely related molecular species. Adopting a different viewpoint, the proposed scheme can also be employed to monitor the time-dependent dynamics by changing the phase relationship between the pump and repump laser that can be viewed as a "control mechanism" employed in wave packet interferometry. Simplifications arise as the change in the spectra are due to the changing populations, not because of the coherences. The ideas behind the scheme are outlined and illustrated theoretically using simple model systems.

PART-A: Transition State Search using Vibronic Model

Chapter 1

Theoretical Background

A chemical reaction within the realm of the *Born-Oppenheimer Approximation* (BOA) is thought of as structural changes occurring due to changing positions of nuclei on a multidimensional Potential Energy Surface (PES). From a classical point of view, the reaction proceeds along a minimum energy path (MEP) connecting the reactant and product, both of which correspond to a minimum on the PES. The highest energy point on such a path is referred to as transition state (TS). Since a TS is a maximum of energy along the reaction coordinate (MEP, in general) and minimum along all the other directions, it is a *saddle point* of the first order on the PES, which is also a *stationary point*¹ just like the minima. Locating and characterizing such stationary points on a PES then becomes a building block of chemistry and is also of fundamental interest to chemists, as it provides a means to understand complex reaction mechanisms or calculate reaction rates in terms of simple, intuitive concepts. As noted in Introduction, the much celebrated Transition State Theory (TST) relies on such information. Let us note that a PES is a multidimensional hypersurface, where the electronic energy of a molecule is a continuous (not necessarily differentiable) function of nuclear coordinates of its N nuclei, where N is the number of atoms in the molecule. While the most useful points on PES are often minima and TS structures, there are other points such as a Valley Ridge Inflection (VRI) or a Conical Intersection (CI) which must be located to describe more complicated reactions / phenomena when the simple picture does not provide a satisfactory or correct explanation of events. Below, the focus will be on minima and TS, in particular the latter, in addition to finding an approximate *analytic* representation of a PES.

Stationary points on PES can be characterized according to the eigenvalues of the Force Constant Matrix (FCM), also referred to as Hessian (a matrix of second derivatives of energy with respect to nuclear coordinates). The FCM in Cartesian coordinates will have six (five for linear

¹A stationary point is a geometry where the gradient (first derivative) of electronic energy as a function of nuclear coordinates is zero.

molecules) zero eigenvalues, corresponding to the overall translation and overall rotation of the molecule. When the remaining $3N - 6$ eigenvalues are all positive, it is representative of a minimum geometry, while if there is exactly one negative eigenvalue, the structure corresponds to a TS. Once a TS has been located, a reaction path can be found by tracing the intrinsic reaction coordinate (IRC) from reactant to product. The IRC corresponds to a steepest descent path when mass-weighted Cartesian coordinates are used.

The concepts and methods discussed in this chapter should be helpful in order to navigate the rest of thesis, while also putting things into perspective and providing a larger picture. Many of the ideas, although not discussed with too many details, are important in many areas of theoretical chemistry and an interested reader can refer to the respective references for further reading. There are three sections in this chapter, which are a logical breakdown of the narrative in the thesis (Part-A, in particular):

- Geometry Optimization Techniques
- Construction of approximate PES based on EVB approach
- Characterizing stationary points on the above EVB based PES

1.1 Geometry Optimization

The techniques and methods to locate the stationary points on a PES, such as minima and TS as introduced above, are collectively known as *Geometry Optimization*. One usually has to start with geometry optimization to locate minima, and TS if desired, in order to study thermodynamic, kinetic or spectroscopic properties of a system. Since Geometry Optimization is essentially a minimization problem (somewhat tricky to define for transition states though), there are several methods which can be employed for this purpose as mathematical optimization is an evolved field in itself. [16] The most common methods are based on the evaluation of energy derivatives of first and second order, i.e. gradient and hessian, though hessian based methods generally tend to be much faster. [16] The bottleneck of hessian based methods is often the evaluation of hessian itself, which tend to be computationally expensive for *ab initio* electronic structure methods. Later in this section, approximate schemes of hessian updates will be briefly touched upon.

Before some of the popular methods for TS optimization are discussed, it is important to emphasize that there are optimization methods which *guarantee* to keep lowering a function value until it finds a minimum (such as steepest descent), even though the process can be excruciatingly slow, it will converge in the end. In contrast, no such general method exist which can guarantee to locate saddle points, such as a transition state. A myriad of strategies have been proposed to locate transition state structures, a large subset of which can be classified into two categories: a)

interpolation methods, based on the interpolation of geometries between reactant and product, and b) *local methods*, which utilize only the local information at a given point. Since it is beyond the scope of this thesis to have a comprehensive discussion of all the methods, a specific choice has been made which aligns with the goals of this thesis.

1.1.1 A Newton-Raphson Primer

Newton-Raphson (NR) is one of the most popular methods for locating transition states, which is a hessian based approach. [16] It is based on a Local Quadratic Approximation (LQA) of the PES, meaning that the true energy of the PES at the current geometry \mathbf{q}_0 is expressed as a second order Taylor expansion around this point:

$$V(\mathbf{q}) = E(\mathbf{q}_0) + \mathbf{g}^T \cdot (\mathbf{q} - \mathbf{q}_0) + \frac{1}{2}(\mathbf{q} - \mathbf{q}_0)^T \cdot \mathbb{H} \cdot (\mathbf{q} - \mathbf{q}_0) \quad (1.1)$$

Where \mathbf{g} is the gradient vector, and \mathbb{H} is the hessian matrix, evaluated at geometry \mathbf{q}_0 . The validity of the approximation in a region around \mathbf{q}_0 is decided by a *trust radius*, which can be either a constant, or can change dynamically during the optimization process. A related and more general concept of *trust region* is used widely in mathematical optimization, where it is used to represent part of the region where the objective function is approximated using a model function (such as a quadratic function in this case). The concept of *trust region* will be encountered again in the context of vibronic model and will be used frequently throughout the thesis.

If one wants to find a minimum on the quadratic potential introduced above, one has to set the gradient of this function to zero, which gives the following step:

$$\Delta \mathbf{q} = \mathbf{q} - \mathbf{q}_0 = -\mathbb{H}^{-1} \mathbf{g} \quad (1.2)$$

If the real energy function is truly quadratic, one will find the minimum in just one step! One could be sitting on the moon, but a *Newton-Raphson step* (more commonly used as *Newton step*) will land them on the minimum in one step. That is the beauty and simplicity of a quadratic potential. Unfortunately, the true PES can have a rather complicated topology, therefore one uses the NR method in an iterative fashion to descend towards a minimum. A huge advantage of the NR method is that near a stationary point, it converges in a quadratic fashion. [16] Therefore, once the algorithm has reached a local region, the convergence is achieved very quickly.

It is often advantageous to work in the hessian eigenvector basis, since the hessian becomes diagonal; the Newton step can then be rewritten as:

$$\begin{aligned} \Delta \mathbf{q} &= \sum_i \Delta q_i \\ \Delta q_i &= -\frac{f_i}{\epsilon_i} \end{aligned} \quad (1.3)$$

Where f_i is the projection of the gradient along the hessian eigenvector with eigenvalue ϵ_i .

It is known that close to a TS geometry, one of the hessian eigenvalues is negative, by definition, therefore the Newton step in this direction is along the gradient component, which can be seen from the above equation. This implies that there will be an increase in energy along this direction. For all the other directions, the step is taken in the opposite direction of the gradient direction, thus decreasing the energy. This is a favorable situation for transition state search. However, if all the eigenvalues of the initial hessian are positive, the Newton step along the TS eigenvector will point in the wrong direction. This emphasizes a very important point: all Newton type schemes depend on a direction along which the energy should be maximized, and this direction is typically provided by one of the eigenvectors of the hessian. The eigenvector associated with the lowest eigenvalue of the hessian will not necessarily point towards the TS direction, in particular at geometries which are a bit far away from the true TS. In such a scenario, the Newton method may fail to locate a transition state.

In addition to the above, the Newton method can also encounter other problems. Four main problems will be listed and discussed below:

- A Newton step can become unbound if one or more eigenvalues of the hessian are close to zero (i.e. the hessian is close to being singular). In such a case, the step size will be huge and will likely take the geometry to a region, which is far away from the *trust region*.
- As discussed above, the initial hessian may lack the desired structure by not having exactly one negative eigenvalue, while the corresponding eigenvector points along the reaction coordinate.
- Hessian methods for quantum chemistry methods can be very expensive, such that in practice it becomes prohibitive to perform a large number of hessian calculation during the optimization process.
- A good starting geometry is an important requirement for Newton methods.

Below, these problems will be briefly discussed along with possible solutions to resolve some of the issues.

Step-Size Control

Since the quadratic approximation to the potential energy surface is only reasonable for a small region (inside the *trust radius*), the length of the Newton step should be such that it does not exceed the *trust radius*. This is dependent on the magnitude of the eigenvalues of the hessian matrix. In addition to the length of the Newton step, the direction of the step should also be in the correct direction, as discussed earlier. A common solution to both these problems is to add a suitable shift parameter to the hessian matrix. The step is parameterized by subtracting a constant

λ from the eigenvalue of hessian (denominator in Equation 1.3) as follows (note that $\lambda = 0$ will correspond to pure Newton step):

$$\Delta q_i = -\frac{f_i}{\epsilon_i - \lambda} \quad (1.4)$$

Since the energy should increase along the reaction coordinate, $\lambda_{TS} > \epsilon_{TS}$, while for all the other modes $\lambda < \epsilon_{i \neq TS}$. By choosing a reasonably large λ_{TS} and negative λ values, one can make the step size arbitrarily small. Such methods, which modify the nature of the hessian matrix by adding a shift parameter, are commonly referred to as *Augmented Hessian* methods. [17–20] This will be seen again in Chapter 4 in the context of transition state search using vibronic models.

There are many schemes for the determination of λ parameters, but it is beyond the scope of this thesis to discuss them. One of the better known method in this context is the Partitioned Rational Function Optimization (PRFO). An interested reader should refer to [21–25] for further details. It should be noted in passing that the Augmented Hessian techniques increase the radius of convergence to some extent compared to the standard Newton method, and a transition state can be located even if the initial hessian does not have the desired structure, on one condition that the lowest eigenvector is in the *correct* uphill direction.

Hessian Update

During geometry optimization, several different molecular configurations are explored for which the hessian can be very different. The hessian is not constant for a molecule (it would be if PES was truly quadratic). This means that for Newton methods, a new hessian must be calculated at every step. Since hessian evaluations can be computationally expensive, one must seek to update the hessian in some approximate way. Methods which use such approximate hessian are referred to as *Quasi-Newton* methods. The basic premise of the hessian updating schemes is that the hessian at a new configuration can be updated from the hessian at the old configuration by making use of the Newton step $\Delta \mathbf{q}$ and the difference in the gradient between the current and last step, $\Delta \mathbf{g}$. A simple update scheme is the Murtagh-Sargent update [26]:

$$\Delta \mathbb{H}^{MS} = \frac{(\Delta \mathbf{g} - \mathbb{H}^{old} \Delta \mathbf{q})(\Delta \mathbf{g} - \mathbb{H}^{old} \Delta \mathbf{q})^T}{(\Delta \mathbf{g} - \mathbb{H}^{old} \Delta \mathbf{q})^T \Delta \mathbf{q}} \quad (1.5)$$

The above hessian update can run into numerical issues if $|\Delta \mathbf{g} - \mathbb{H}^{old} \Delta \mathbf{q}|$ is very small. The Broyden-Fletcher-Goldfarb-Shanno (BFGS) hessian update [27–30] overcomes this issue, in addition it ensures that the hessian is positive definite, which makes it a suitable choice for minima optimization.

$$\Delta \mathbb{H}^{BFGS} = \frac{\Delta \mathbf{g} \Delta \mathbf{g}^T}{\Delta \mathbf{g}^T \Delta \mathbf{q}} - \frac{\mathbb{H}^{old} \Delta \mathbf{q} \Delta \mathbf{q}^T \mathbb{H}^{old}}{\Delta \mathbf{q}^T \mathbb{H}^{old} \Delta \mathbf{q}} \quad (1.6)$$

Since for transition state optimization, the hessian must have one negative eigenvalue, therefore a hessian update scheme should force the hessian to be positive definite. Therefore, the BFGS update is not a good choice here. The Powell-symmetric-Broyden (PSB) update [31] does not force the hessian to be positive definite, it is written as:

$$\Delta\mathbb{H}^{PSB} = \frac{(\Delta\mathbf{g} - \mathbb{H}^{old}\Delta\mathbf{q})\Delta\mathbf{q}^T + \Delta\mathbf{q}(\Delta\mathbf{g} - \mathbb{H}^{old}\Delta\mathbf{q})^T}{\Delta\mathbf{q}^T\Delta\mathbf{q}} - \frac{(\Delta\mathbf{q}^T(\Delta\mathbf{g} - \mathbb{H}^{old}\Delta\mathbf{q}))\Delta\mathbf{q}\Delta\mathbf{q}^T}{(\Delta\mathbf{q}^T\Delta\mathbf{q})^2} \quad (1.7)$$

The Bofill update [32] is a combination of MS and PSB update, and has been found to perform better in the context of locating transition states:

$$\Delta\mathbb{H}^{Bofill} = \phi\Delta\mathbb{H}^{MS} + (1 - \phi)\Delta\mathbb{H}^{PSB} \quad (1.8)$$

Where

$$\phi = \frac{((\Delta\mathbf{g} - \mathbb{H}^{old}\Delta\mathbf{q})^T\Delta\mathbf{q})^2}{|\Delta\mathbf{g} - \mathbb{H}^{old}\Delta\mathbf{q}|^T\Delta\mathbf{q}|^2|\Delta\mathbf{q}|^2} \quad (1.9)$$

Extrapolations using GDIIS

In Geometry optimization by using Direct Inversion of Iterative Subspace (GDIIS), the idea is to construct a new geometry as a linear combination of previous geometries such that the size of the Newton step can be minimized. [33–35]

$$\mathbf{q} = \sum_i c_i \mathbf{q}_i \quad \mathbf{g} = \sum_i c_i \mathbf{g}(\mathbf{q}_i) \quad \sum_i c_i = 1 \quad (1.10)$$

The quantity $|\mathbf{q}^{new} - \mathbf{q}|^2$ needs to be minimized with respect to c_i , where $\mathbf{q}^{new} = \mathbf{q} - \mathbb{H}^{-1}\mathbf{g}$.

The GDIIS is an iterative procedure and is similar in spirit to methods such as Lanczos algorithm. [36] It is possible that the GDIIS for transition state optimization might converge to the nearest saddle point instead of the actual transition state. It is advised that one compares the predicted geometry with the corresponding Newton step geometry. If the dot product of two geometries (angle between them) is large, it is considered safer to take the Newton step. GDIIS converges faster at times towards the end of a minimization, during the final few cycles it tends to become faster than Quasi-Newton methods, therefore a combination of Quasi-Newton and GDIIS might prove to be more effective.

In summary, the main concern of Newton methods is the requirement that one should have a good starting guess geometry. In addition, the convergence radius can be small at times, such that the lowest eigenvector of the hessian only provides proper uphill search direction when one is very close to the TS geometry. Last but not the least, if the hessian has many small eigenvalues, the applicability of the Newton method seems dubious.

1.1.2 Interpolation Methods

Interpolation methods which locate transition states require the knowledge of reactant and product beforehand. The basic assumption made is that there is a transition state between these two end-points. The underlying idea behind interpolation methods is based on the idea that a *reaction path* exists between the two minima, and the transition state can be found as the highest energy point on this path. The methods differ in how the path is constructed, or equivalently, how the interpolation between end-points is performed. Since these methods primarily focus on obtaining a minimum energy path, often they do not locate the actual TS, but end up at a nearby geometry. Starting from this geometry as a guess, the local methods, such as those discussed in previous section, can then be employed to refine the result and converge to the true TS geometry. A myriad of interpolation methods have been developed in the past and it is beyond the scope of this thesis to discuss all of them. Below, a few of these methods will be briefly touched upon. In addition, few important characteristic points of interpolation methods will be mentioned.

A popular interpolation method to locate transition states is known as the Linear Synchronous Transit (LST) and its quadratic variant, the Quadratic Synchronous Transit (QST). [37] In LST, the geometry corresponding to highest energy is located along a line connecting the minima geometries. In QST, the reaction path is approximated by a parabola rather than a straight line. The LST maximum geometry is relaxed by minimizing the energy in the perpendicular direction to the LST path. A maximum of energy is then searched along the QST path. LST alone often does not lead to a good guess of the TS. The synchronous transit-guided quasi-Newton (STQN), [38] which is a variant of QST, uses a circular arc in place of a parabola for the interpolation. The tangent to the circle is then used to guide the search towards the transition state region. Once inside the TS region, the algorithm switches to a Newton-Raphson search. This is essentially the scheme used in Gaussian’s popular QST2 (or QST3) method to locate transition states.

Another class of methods used widely is based on the chain-of-states idea, [39] where one initially calculates the energy at a series of equidistant points along a suitably chosen reaction coordinate (usually a quadratic path). The highest energy point on this path is relaxed along a direction which is defined by the component of gradient orthogonal to the line between two neighboring points. This step is repeatedly performed until the gradient become tangential to the path. The current highest energy point can not be relaxed any further, and becomes the (guess to) transition state geometry. There are many variants of the chain method, such as the Conjugate Peak Refinement (CPR) method, [40] or the Self-penalty Walk (SPW) method. [41] A very closely related method to SPW is the Nudge Elastic Band (NEB) method, [42] which is considered to be the most effective among the current interpolation methods and is widely used in condensed matter physics.

Certain characteristic features of the interpolation methods are discussed below:

- It is possible that no TS exists between the reactant and product directly. In such a situation, the algorithm in question may end up at an intermediate geometry, which may be far removed from a stationary point.
- An interpolation can find a TS, but it may not be the one desired. One should perform an IRC calculation to check whether the obtained TS indeed connects the desired reactant and product.
- User intervention might be necessary to guide the TS search if more than one TS exist between the two minima considered.

1.2 Approximate representation of BO PES

An *exact* representation of a multidimensional PES is possible only for small molecules. A point-by-point calculation on a multidimensional grid and additionally obtaining a fitted analytic functional form is way too cumbersome. Although significant progress has been made towards fitting strategy and automating the task of PES construction, it remains a specialized and highly technical task limited to small molecules. [43] There are a number of approximate strategies to build a PES, many of which seek an accurate representation only in a limited region. The harmonic approximation comes to the mind first, which only needs the knowledge of energy, gradient and hessian at a single geometry, usually a minimum. The harmonic approximation can provide a good qualitative, sometimes even semi-quantitative accuracy for certain thermodynamic and spectroscopic properties. Additional anharmonic corrections can make up for most of the error, and are also used to describe the correct asymptotic behavior (bond breaking) which the harmonic approximation lacks completely. An alternative strategy, conceptually appealing and computationally much cheaper, is the use force-field type of potentials, which is often employed for larger systems. [1]

The issue with force-field type potential is that they are not able to describe a reactive PES, since they are based on a particular "bonding pattern". These bonds can break as one moves towards the asymptotic dissociative region, but they will not turn into a new structure describing a different bonding pattern, or even into a new conformer, which is what chemical reactions are all about. A celebrated method to resolve this problem and construct a reactive PES efficiently is the Empirical Valence Bond (EVB) idea developed by Warshel. [44] In the EVB description, the reactant and product PES are described using force-field, according to their own bonding patterns. They are the "diabatic states", smooth potentials preserving the electronic character on the PES. The adiabatic reactive PES is described as a linear combination of the reactant and

product diabatic states. The energy matrix is built similar to the VB theory, except now the coupling term is also determined empirically to get the correct barrier height (or more generally also the curvature). A cartoon representing the EVB idea is depicted in Figure 1.1 and Figure 1.2. In Figure 1.1, the two diabatic states represent the minima PES (harmonic in this case), coupled by a term that is maximum at the crossing point, and drops off to zero near the minima wells. The resulting adiabatic ground state PES, shown in Figure 1.2 represents a reactive PES. The mixing of diabatic states is the maximum around the TS region.

There have been many attempts in the literature towards building a full dimensional ground state PES based on the EVB idea. One of the early approaches was that of Chang and Miller, [45] who used harmonic approximation for the minima potential and an exponential off-diagonal term (a generalized Gaussian function) as a function of nuclear coordinates. The parameters for off-diagonal elements were determined such that the transition state geometry, the model should reproduce correct barrier height as well as the correct curvature associated with the TS hessian. It was assumed that the relevant transition state has been located using ab initio electronic structure methods, and this data was used for parameterization. Their description becomes problematic as the coupling term does not necessarily drops off as smoothly as shown in Figure 1.1, but rather increases rapidly in some directions, causing troubles to define a correct PES. Truhlar and co-workers' MCMC [14] (now MCSI) utilized more ab initio data than just of minima and TS, and used Shepard interpolation between these additional data points to generate the off-diagonal coupling term. Naturally, their approach tends to be more accurate but at the cost of losing simplicity. The DG-EVB method of Sonneberg and Schlegel [15, 46] modeled the coupling term using a distributed Gaussian basis, and also proposed to use more reference data points than just minima and TS in order to get an accurate PES. More recently, Hartke and Grimme [47] proposed similar idea, the strength of which is more accurate minima potential, described by newly developed quantum-mechanically derived force field (QMDF). [48] Their method, termed as QMDF-EVB could be a promising method to obtain approximate reactive PES.

In Chapter-2, we propose a similar idea to build the ground state PES, which is quite close to Sonneberg and Schlegel's DG-EVB scheme, with some subtle differences, especially in terms of our choice of coordinates. All the relevant technical details will be provided in Chapter-2. One important thing to point out in this context is the use of term *vibronic model* by us, instead of EVB, as our minima potentials are quantum-mechanical harmonic approximation and are not based on empirical force fields. Our matrix based representation of the diabatic states and the coupling terms looks more in unison with the *vibronic model Hamiltonian* by Kopple-Domcke-Cederbaum, [12] which is used to study excited state dynamics. The upper surfaces in the latter are real excited state surfaces with physical meaning, while for us, it is merely an artifact of the modeling process.

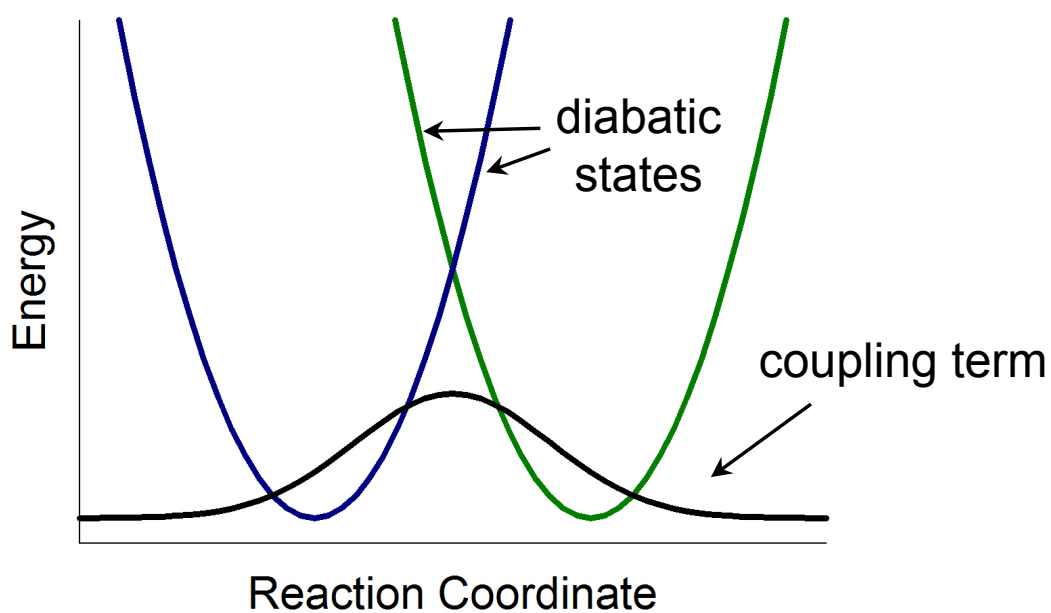


Figure 1.1: Diabatic States of the EVB model and the off-diagonal coupling term

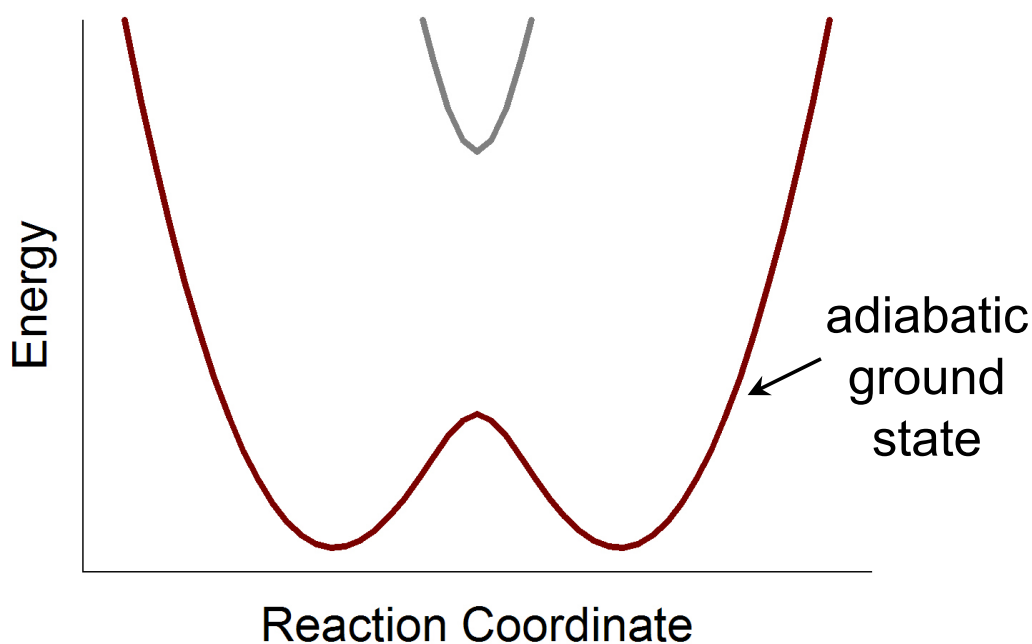


Figure 1.2: Adiabatic ground state obtained as a linear combination of the diabatic states in Figure 1.1

1.3 Geometry Optimization on Approximate BO PES

We will turn back our attention towards geometry optimization now, in particular towards locating transition states. In order to employ the strategies for searching transition states, one does not need to know a full PES beforehand. The gradient and hessian calculations are performed *on-*

the-fly. However, calculating the hessian ab initio at several points during the search process can be computationally very demanding. The most effective algorithms are based on information of hessian - such as the previously discussed Newton-Raphson method, which is one of the reasons that finding transition states is a tricky affair. EVB based PES provides a lucrative alternative to the conventional search algorithms based on ab initio PES, since the hessian computation becomes extremely cheap on such a surface.

The early ideas along these lines, i.e. to use an EVB based PES to locate a TS, was proposed by Jensen et al. [49] Their idea was to locate the minimum on the seam of intersection of two diabatic surfaces, which can be considered as an approximation to true TS, or could be used as a starting guess geometry for the transition state in the conventional search algorithms. Later, they proposed to use Truhlar's MCMM PES to perform geometry optimization in order to locate minima and TS. [50] Although Jensen's idea was somewhat unique, it was not implemented into a black-box tool. Sierka and Sauer [51] came up with a detailed algorithm for using the EVB based PES to locate transition states and implemented it into a black-box program by making interfaces between many sub-programs.

Our proposed VMTS approach, described in Chapter-4 and Chapter-5, happens to be in the same spirit of Sierka and Sauer, though the technical details will vary significantly. In terms of applications also, their focus was on simple proton transfer reactions in extended systems, while we are in this work mostly concerned with possibly complicated organic reactions involving small molecules in gas phase.

Chapter 2

Construction of Vibronic Model to represent Adiabatic Ground State Potential Energy Surface

2.1 Introduction

The methodology of constructing a reactive PES is based on a matrix representation of the local PES around the critical points. The diagonal elements $V_{aa}(\mathbf{q})$ of this coordinate dependent Hamiltonian \mathbf{V} are the quadratic potential corresponding to a particular minimum well, which can be represented as:

$$V_A(\mathbf{q}) = E_A + \mathbf{g}_A^T \cdot (\mathbf{q} - \mathbf{q}_A) + \frac{1}{2}(\mathbf{q} - \mathbf{q}_A)^T \cdot \mathbb{H}_A \cdot (\mathbf{q} - \mathbf{q}_A) \quad (2.1)$$

Where \mathbf{q}_A is the optimized geometry of the stationary point, E_A is the electronic energy, g_A and \mathbb{H}_A are the gradient and hessian respectively at the corresponding geometry. Given a suitable choice of off-diagonal elements, the ground state PES is obtained as the lowest eigenvalue $\lambda_0(\mathbf{q})$ of the model Hamiltonian. For a reactive system with n minima wells, the vibronic model Hamiltonian is represented as:

$$\mathbb{V}(\mathbf{q}) = \begin{pmatrix} V_{11} & V_{12} & \cdots & V_{1n} \\ V_{21} & V_{22} & \cdots & V_{2n} \\ \vdots & \vdots & \ddots & \vdots \\ V_{n1} & V_{n2} & \cdots & V_{nn} \end{pmatrix} \quad (2.2)$$

Diagonalizing this coordinate dependent matrix will yield n surfaces, each corresponding to a particular set of eigenvalues. While the lowest surface represents the ground state PES, the rest of the upper surfaces do not have any particular physical meaning associated with them. They are

simply an artifact of the modeling process. This is in sharp contrast to a *true* vibronic coupling Hamiltonian, such as for a set of excited states, where each diagonal element represents a true (diabatic) electronic surface and the off diagonal terms reflect the strength of the interstate coupling between diabatic surfaces. Diagonalizing such a true vibronic coupling Hamiltonian will give the corresponding adiabatic surfaces for the excited states. The scheme discussed in this chapter, and employed elsewhere in this thesis, assumes that there are no other electronic states in the close proximity of the ground state, unless stated otherwise.

The choice of off-diagonal elements for the vibronic model Hamiltonian is less obvious. One can start with listing certain desirable features for this function:

- It should go to zero or near-zero as it approaches the minima regions.
- The approach towards minima should be slow and continuous.
- The choice should be such that at the transition state geometry, diagonalizing the model Hamiltonian yields correct barrier height, zero gradient, and correct curvature (hessian) of the corresponding transition state.
- A scan of the PES in the reactive regime, such as along an intrinsic reaction coordinate, should follow ab initio data as closely as possible, and ideally away from it as well.

In order to accomplish these goals, we propose the form of off-diagonal element as a quadratic polynomial (similar to the diagonal elements) times a Gaussian function, both centered at the transition state geometry. It can be represented as:

$$V_{ab}(\mathbf{q}) = \{E_{ab} + \mathbf{g}_{ab}^T \cdot (\mathbf{q} - \mathbf{q}_{TS}) + \frac{1}{2}(\mathbf{q} - \mathbf{q}_{TS})^T \cdot \mathbb{H}_{ab} \cdot (\mathbf{q} - \mathbf{q}_{TS})\} \cdot e^{(-\frac{1}{2}(\mathbf{q} - \mathbf{q}_{TS})^T \cdot \mathbb{A} \cdot (\mathbf{q} - \mathbf{q}_{TS}))} \quad (2.3)$$

The parameters E_{ab} , \mathbf{g}_{ab} , and \mathbb{H}_{ab} are chosen such that diagonalization of the model Hamiltonian reproduces correct barrier height, zero gradient and correct hessian at the transition state geometry, respectively. One can systematically obtain these parameters, in a step by step manner. Below, a simple example will be presented to illustrate the process and importance of each term.

The Gaussian function, referred to as the window function hereafter, becomes important in order to satisfy the first two conditions, in particular because the quadratic term alone increases rapidly quite often and does not vanish near the minima geometries. Examples of such behaviour will be discussed in the results section. The width parameter of the Gaussian window is chosen such that it drops off to near-zero for the closer minima, naturally vanishing on the other side as well. The quadratic form of the argument of the exponential is flexible and other choices can also be exercised to best suit the needs of specific problem. In this work, the matrix \mathbb{A} is always taken to be $\alpha \mathbb{I}$, and one has a single parameter of choice.

2.2 Illustration of the proposed scheme using a 1D model system

In this section, the proposed scheme will be illustrated with the help of a simple one-dimensional model system, without going into technical details. A one-dimensional reactive PES is created using two Morse potentials, which define the reactant and product regions of nuclear configurational space. The red curve in Figure 2.1 represents the true adiabatic PES, which will be modeled using the proposed scheme. The energies and second derivatives are known at the critical points numerically. The diagonal elements of the vibronic model are defined as quadratic potentials, such that the local regions around minima are captured accurately. For the off diagonal element, a constant term alone is chosen at first such that it reproduces the ab initio barrier height correctly. The PES generated from this model along with the true curve are shown in Figure 2.2. It can be seen that the vibronic model PES deviates significantly from the true curve. The primary reason for this deviation is the incorrect curvature at the TS geometry. In the next step, this is fixed by adding a quadratic term to the off-diagonal element in the model, such that in addition to reproducing the correct barrier height, it also reproduces the correct curvature around the TS geometry. The result from this updated model is shown in Figure 2.3. The improvement from the first model (with a constant off-diagonal term only) is substantial, in particular around the TS region. However, the minima region still deviate from the true curve, because the off-diagonal element does not vanish as one approaches the minima geometries. A solution for this problem is to introduce a Gaussian window function as discussed in the previous section, which will force the off-diagonal term to vanish near minima geometries. The results after including the window function are shown in Figure 2.4, which is a qualitatively correct description of the true PES, capturing the regions around critical points accurately.

The take away from this simple example is two-fold: i) a simple constant term on the off-diagonal is not sufficient to accurately model the true PES, and ii) a window function is important in order to preserve the character of the minima regions. This observation is applicable for real systems as well, as will be seen later while discussing the results for polyatomic molecules. In the preceding discussion, the details of parameter determination are not discussed, which is the focus of next couple of sections. The formalism presented below, including the computation of gradient and hessian, is applicable to a general n -state system, even though much of the focus in this thesis will be on 2×2 vibronic models, corresponding to Unimolecular reactions.

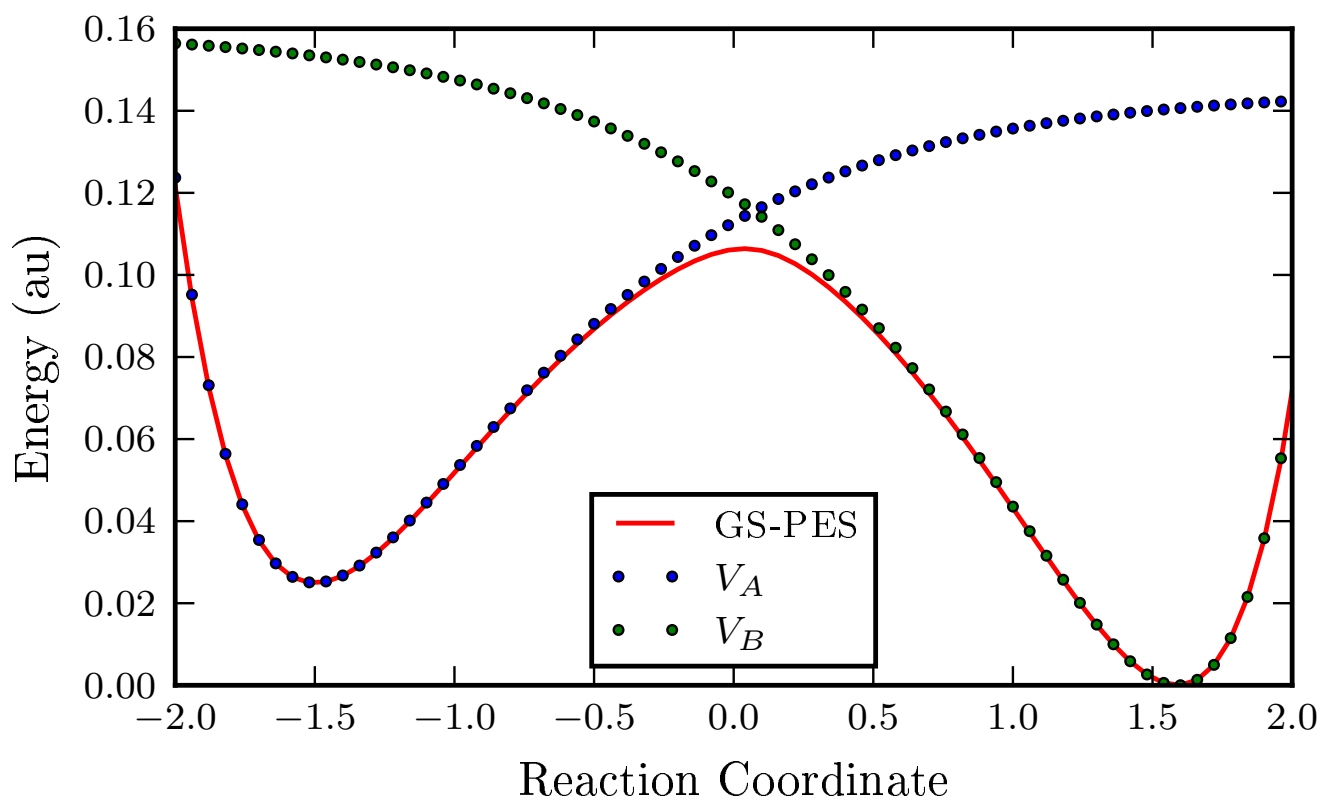


Figure 2.1: The red solid curve line is the known adiabatic ground state potential, which will be modeled using vibronic model scheme discussed in this chapter

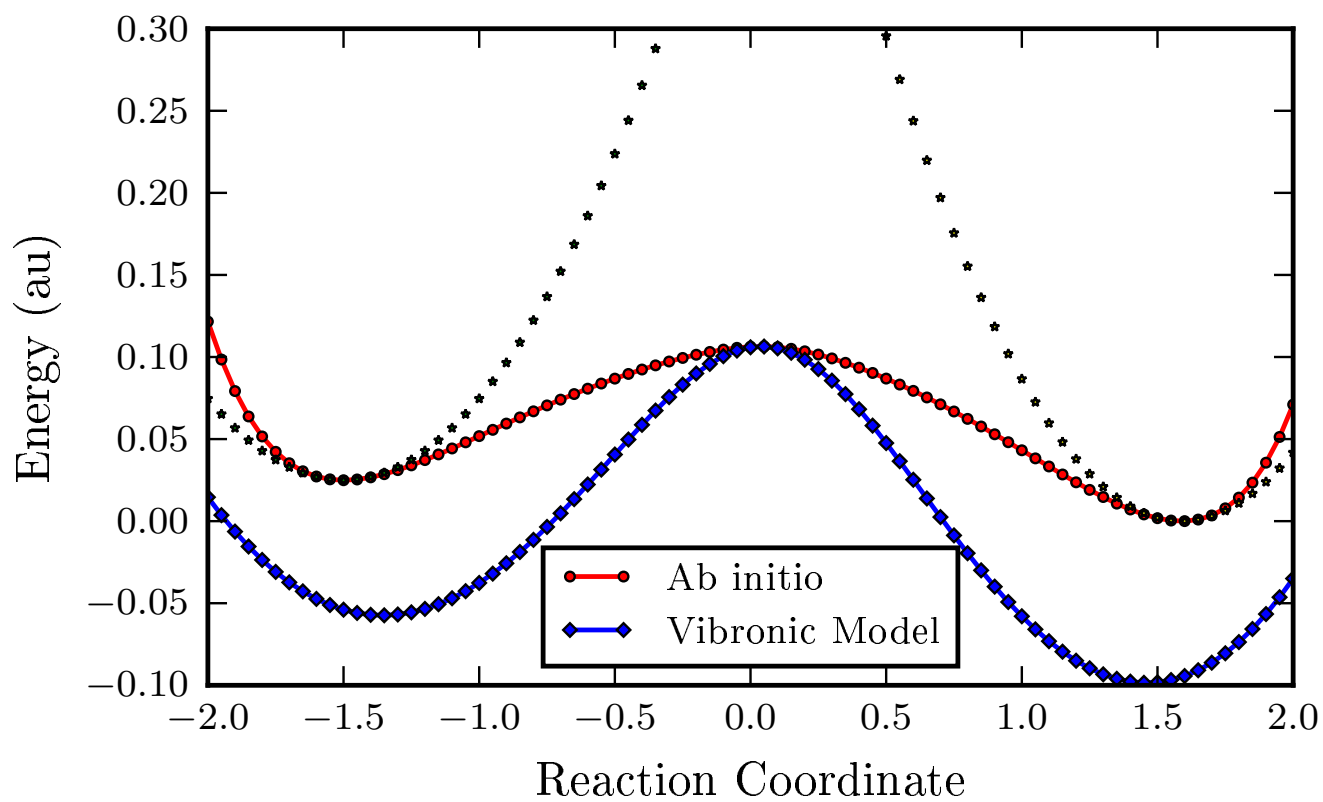


Figure 2.2: Vibronic model constructed with only the constant term in the off-diagonal, unable to capture the ground state PES correctly

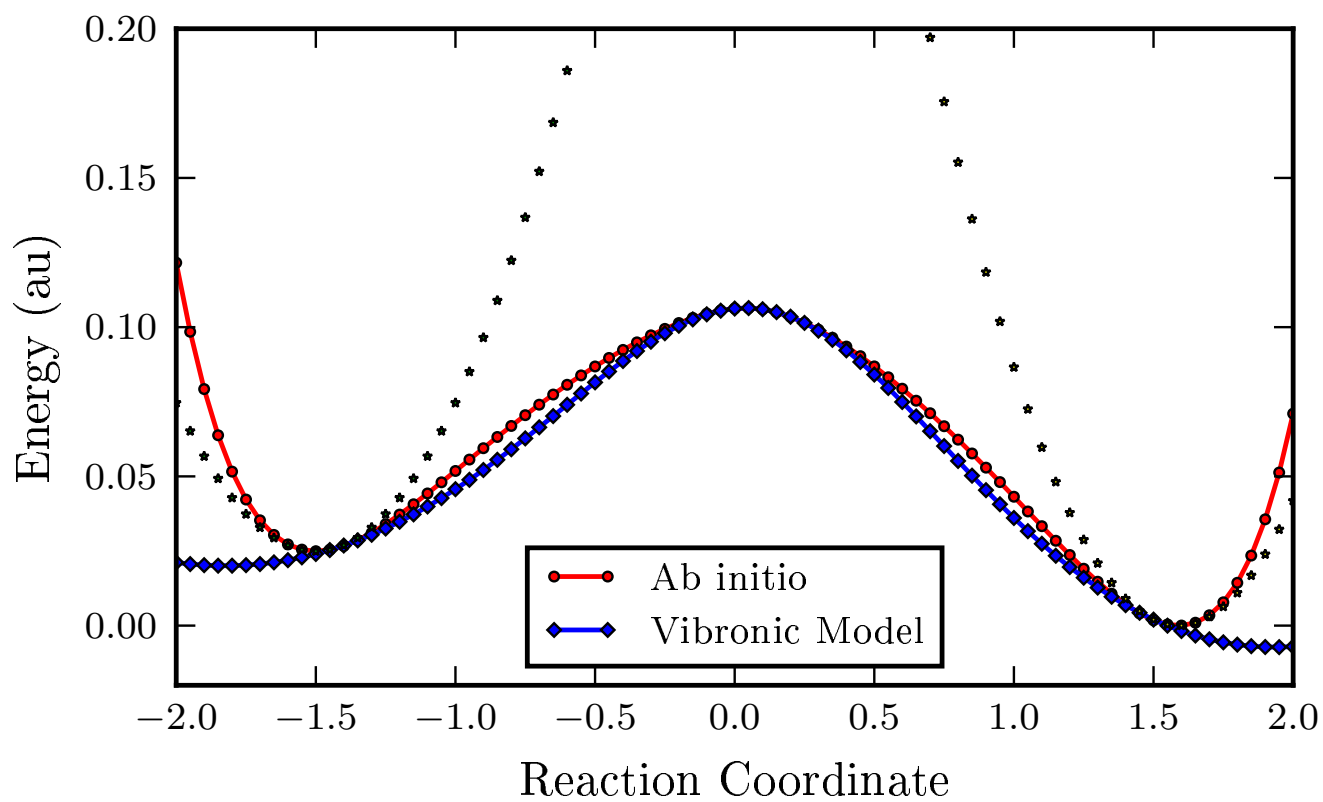


Figure 2.3: Vibronic model with a full quadratic off-diagonal term, but no window included. TS region is captured correctly, but not the minima regions.

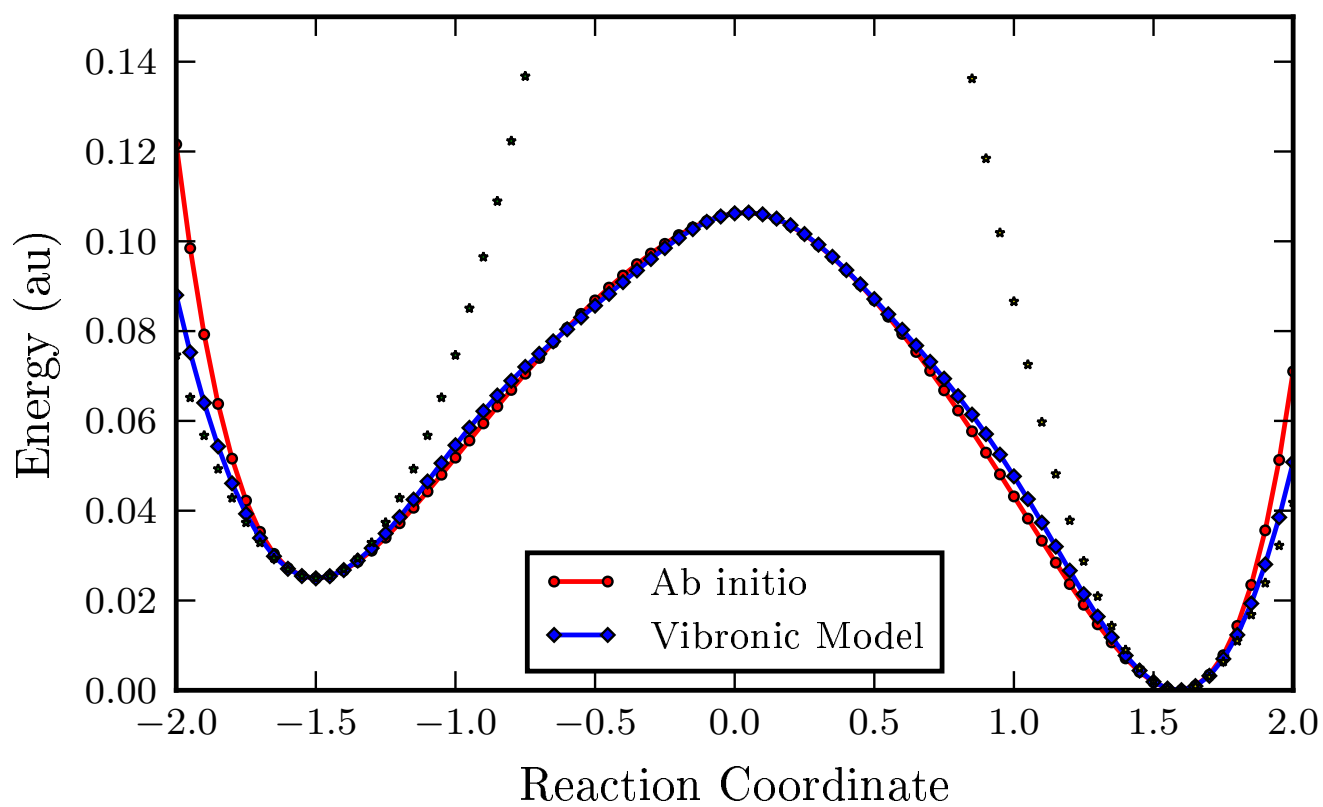


Figure 2.4: Vibronic model with a quadratic off-diagonal term times a Gaussian window function. Vibronic model energies follow true adiabatic energies closely.

2.3 Formulation of Gradient and Hessian for Vibronic Model

Until now, it has been mentioned how the ground state PES can be obtained approximately as the lowest eigenvalues of the coordinate dependent vibronic model Hamiltonian. In addition to the total energy, it is also important to be able to evaluate the gradient and hessian, for the model to be employed for geometry optimization techniques. Gradient and hessian are also required if one wants to carry out some approximate dynamical simulations on the PES, or trace out a reaction path, such as the Intrinsic Reaction Coordinate (IRC). Below, two complimentary approaches - analytical and numerical - for evaluating the energy derivatives are presented.

2.3.1 Computation of analytical gradient

The derivative of energy eigenvalue on the vibronic model with respect to nuclear coordinates can be evaluated using the Hellman-Feynman theorem:

$$\begin{aligned}
 \frac{\partial E}{\partial \mathbf{q}} &= \frac{\partial}{\partial \mathbf{q}} \langle \Psi | \hat{V} | \Psi \rangle \\
 &= \left\langle \frac{\partial \Psi}{\partial \mathbf{q}} \middle| \hat{V} \middle| \Psi \right\rangle + \left\langle \Psi \middle| \hat{V} \middle| \frac{\partial \Psi}{\partial \mathbf{q}} \right\rangle + \left\langle \Psi \middle| \frac{\partial \hat{V}}{\partial \mathbf{q}} \middle| \Psi \right\rangle \\
 &= E \underbrace{\left(\frac{\partial}{\partial \mathbf{q}} \langle \Psi | \Psi \rangle \right)}_{=0} + \left\langle \Psi \middle| \frac{\partial \hat{V}}{\partial \mathbf{q}} \middle| \Psi \right\rangle = \left\langle \Psi \middle| \frac{\partial \hat{V}}{\partial \mathbf{q}} \middle| \Psi \right\rangle
 \end{aligned} \tag{2.4}$$

where $|\Psi\rangle$ is the (coordinate dependent) eigenvector corresponding to the lowest eigenvalue of $\mathbb{V}(\mathbf{q})$ and $\frac{\partial \hat{V}}{\partial \mathbf{q}}$ is the matrix of gradients of individual diabatic potential elements, which can be written as:

$$\frac{\partial \mathbb{V}}{\partial \mathbf{q}} = \begin{pmatrix} \frac{\partial V_{11}}{\partial \mathbf{q}} & \frac{\partial V_{12}}{\partial \mathbf{q}} & \cdots & \frac{\partial V_{1n_{el}}}{\partial \mathbf{q}} \\ \frac{\partial V_{21}}{\partial \mathbf{q}} & \frac{\partial V_{22}}{\partial \mathbf{q}} & \cdots & \frac{\partial V_{2n_{el}}}{\partial \mathbf{q}} \\ \vdots & \vdots & \ddots & \vdots \\ \frac{\partial V_{n_{el}1}}{\partial \mathbf{q}} & \frac{\partial V_{n_{el}2}}{\partial \mathbf{q}} & \cdots & \frac{\partial V_{n_{el}n_{el}}}{\partial \mathbf{q}} \end{pmatrix} \tag{2.5}$$

Where the individual derivatives take the form (using definition of V_A from Equation 2.1):

$$\frac{\partial V_A}{\partial \mathbf{q}} = \mathbf{g}_A + \mathbb{H}_A \cdot (\mathbf{q} - \mathbf{q}_A) \tag{2.6}$$

Therefore, in the matrix-vector formulation the gradient can be expressed as:

$$\frac{\partial E}{\partial \mathbf{q}} = \begin{pmatrix} c_1 c_2 \cdots c_{n_{el}} \end{pmatrix} \cdot \begin{pmatrix} \frac{\partial V_{11}}{\partial \mathbf{q}} & \frac{\partial V_{12}}{\partial \mathbf{q}} & \cdots & \frac{\partial V_{1n_{el}}}{\partial \mathbf{q}} \\ \frac{\partial V_{21}}{\partial \mathbf{q}} & \frac{\partial V_{22}}{\partial \mathbf{q}} & \cdots & \frac{\partial V_{2n_{el}}}{\partial \mathbf{q}} \\ \vdots & \vdots & \ddots & \vdots \\ \frac{\partial V_{n_{el}1}}{\partial \mathbf{q}} & \frac{\partial V_{n_{el}2}}{\partial \mathbf{q}} & \cdots & \frac{\partial V_{n_{el}n_{el}}}{\partial \mathbf{q}} \end{pmatrix} \cdot \begin{pmatrix} c_1 \\ c_2 \\ \vdots \\ c_{n_{el}} \end{pmatrix} \tag{2.7}$$

It can be expressed in a more compact form as follows:

$$\frac{\partial E}{\partial \mathbf{q}} = \sum_a c_a^2 \left(\frac{\partial V_{aa}}{\partial \mathbf{q}} \right) + 2 \sum_{\substack{a,b \\ a>b}} c_a c_b \left(\frac{\partial V_{ab}}{\partial \mathbf{q}} \right) \quad (2.8)$$

where $a, b = 1, 2, \dots, n_{el}$ (number of minima).

Including the window for off-diagonal elements

The structure of the gradient essentially remains the same as before, the only thing that changes are the derivatives of the off-diagonal diabatic potential matrix as these objects are now associated with a window function now. The off-diagonal quadratic potential with window function can be expressed as:

$$V_{ab}^{window} = V_{ab} \cdot W \quad (2.9)$$

Where W is the Gaussian window function, represented as:

$$\begin{aligned} W &= \exp(\tilde{w}(q)) \quad \text{where,} \\ \tilde{w}(q) &= -\frac{1}{2}(\mathbf{q} - \mathbf{q}_{TS})^T \cdot \mathbb{A} \cdot (\mathbf{q} - \mathbf{q}_{TS}) \end{aligned} \quad (2.10)$$

Where \mathbb{A} is the *width matrix* of the multidimensional Gaussian function. The width matrix is diagonal since an isotropic Gaussian (with zero co-variances) will always be employed in this work. The width matrix then takes a simple form characterized by a single parameter α :

$$\mathbb{A} = \begin{pmatrix} \alpha & 0 & \dots & 0 \\ 0 & \alpha & \dots & 0 \\ \vdots & \vdots & \ddots & \vdots \\ 0 & 0 & \dots & \alpha \end{pmatrix} \quad (2.11)$$

The derivative of the window function with respect to nuclear coordinates can be expressed as:

$$\frac{\partial W}{\partial \mathbf{q}} = -W (\mathbb{A} \cdot (\mathbf{q} - \mathbf{q}_{TS})) \quad (2.12)$$

Therefore, the derivative of V_{ab}^{window} can be written as:

$$\begin{aligned} \frac{\partial V_{ab}^{window}}{\partial \mathbf{q}} &= \frac{\partial}{\partial \mathbf{q}} (V_{ab} \cdot W(\alpha)) \\ &= \frac{\partial V_{ab}}{\partial \mathbf{q}} \cdot W + \frac{\partial W}{\partial \mathbf{q}} \cdot V_{ab} \\ &= \frac{\partial V_{ab}}{\partial \mathbf{q}} \cdot W - W (\mathbb{A} \cdot (\mathbf{q} - \mathbf{q}_{TS})) \cdot V_{ab} \\ &= \left\{ \frac{\partial V_{ab}}{\partial \mathbf{q}} - (\mathbb{A} \cdot (\mathbf{q} - \mathbf{q}_{TS})) \cdot V_{ab} \right\} \cdot W \end{aligned} \quad (2.13)$$

Where $\frac{\partial V_{ab}}{\partial \mathbf{q}}$ is the regular gradient given by Equation 2.6. Substituting this expression in Equation 2.8, one can evaluate the gradient for vibronic model at any given geometry. If the form of the window function is changed, the only quantity that will need to be changed is $\frac{\partial W}{\partial \mathbf{q}}$ and rest of the formulation can be used as it is.

2.3.2 Computation of analytical hessian

The hessian can also be calculated based on the extension of the gradient formula as follows:

$$\begin{aligned} \frac{\partial^2 E}{\partial q_i \partial q_j} &= \frac{\partial^2 \langle \Psi | \hat{V} | \Psi \rangle}{\partial q_i \partial q_j} = \frac{\partial}{\partial q_i} \left\langle \Psi \left| \frac{\partial \hat{V}}{\partial q_j} \right| \Psi \right\rangle \\ &= \left\langle \frac{\partial \Psi}{\partial q_i} \left| \frac{\partial \hat{V}}{\partial q_j} \right| \Psi \right\rangle + \left\langle \Psi \left| \frac{\partial \hat{V}}{\partial q_j} \right| \frac{\partial \Psi}{\partial q_i} \right\rangle + \left\langle \Psi \left| \frac{\partial^2 \hat{V}}{\partial q_i \partial q_j} \right| \Psi \right\rangle \end{aligned} \quad (2.14)$$

The following quantities are needed to evaluate these terms:

$\frac{\partial \hat{V}}{\partial \mathbf{q}}$: Gradient matrix; already evaluated for the gradient calculation

$\frac{\partial \Psi}{\partial \mathbf{q}}$: Wavefunction response; perturbation theory will be used to evaluate this term

$\frac{\partial^2 \hat{V}}{\partial q_i \partial q_j}$: Hessian matrix; similar to gradient matrix, now using second derivatives of diabatic elements

Evaluation of wavefunction response

The wavefunction response can be evaluated as follows. One starts with the zeroth order eigenvalue equation for the current vibronic model guess:

$$\mathbb{V} \left| \Psi_l^{(0)} \right\rangle = E_l^{(0)} \left| \Psi_l^{(0)} \right\rangle \quad (2.15)$$

where l can take values $1, 2, \dots, n_{el}$. For the above equation, the derivative with respect to \mathbf{q} can be written as :

$$\frac{\partial \hat{V}}{\partial \mathbf{q}} \left| \Psi_l^{(0)} \right\rangle + \hat{V} \left| \frac{\partial \Psi_l^{(0)}}{\partial \mathbf{q}} \right\rangle = E_l^{(0)} \left| \frac{\partial \Psi_l^{(0)}}{\partial \mathbf{q}} \right\rangle + \left| \Psi_l^{(0)} \right\rangle \frac{\partial E_l^{(0)}}{\partial \mathbf{q}} \quad (2.16)$$

Such that

$$(E_l^{(0)} - \hat{V}) \left| \frac{\partial \Psi_l^{(0)}}{\partial \mathbf{q}} \right\rangle = \left(\frac{\partial \hat{V}}{\partial \mathbf{q}} - \frac{\partial E_l^{(0)}}{\partial \mathbf{q}} \right) \left| \Psi_l^{(0)} \right\rangle \quad (2.17)$$

One can transform this equation to eigenvector basis by inserting partition of unity as $\sum_n \left| \Psi_n^{(0)} \right\rangle \left\langle \Psi_n^{(0)} \right| = 1$, such that the wavefunction can be evaluated as:

$$\frac{\partial \Psi}{\partial \mathbf{q}} = \left| \Psi_l^{(1)} \right\rangle = \sum_{\substack{n \\ n \neq l}} c_{ln}^{(1)} \left| \Psi_n^{(0)} \right\rangle \quad (2.18)$$

where

$$c_{ln}^{(1)} = \frac{V_{nl}}{E_l^{(0)} - E_n^{(0)}} \quad (2.19)$$

and

$$V_{nl} = \left\langle \Psi_n^{(0)} \left| \frac{\partial \hat{V}}{\partial \mathbf{q}} - \frac{\partial E_l^{(0)}}{\partial \mathbf{q}} \right| \Psi_l^{(0)} \right\rangle \quad (2.20)$$

At the end, one can transform back to original basis. Note that the wavefunction response is formulated in terms of all the zeroth order quantities - eigenvalues and eigenvectors of the zeroth order Hamiltonian. These formulas are general and one can loop over l to calculate these quantities for both lower and upper surface(s) for any number of minima.

Finally, the hessian matrix can be expressed as:

$$\frac{\partial^2 \hat{V}}{\partial q_i \partial q_j} = \begin{pmatrix} \mathbb{H}_{11} & \mathbb{H}_{12} & \dots & \mathbb{H}_{1n_{nel}} \\ \mathbb{H}_{21} & \mathbb{H}_{22} & \dots & \mathbb{H}_{2n_{nel}} \\ \vdots & \vdots & \ddots & \vdots \\ \mathbb{H}_{n_{nel}1} & \mathbb{H}_{n_{nel}2} & \dots & \mathbb{H}_{n_{nel}n_{nel}} \end{pmatrix} \quad (2.21)$$

The diagonal elements are simply the hessian matrix of the minima objects as appearing in Equation 2.1. Just like for the case of gradient, second derivatives for off-diagonal elements need to be evaluated in the presence of the window function.

$$\frac{\partial^2 V_{ab}^{window}}{\partial q_i \partial q_j} = \left\{ \frac{\partial^2 V_{ab}}{\partial q_i \partial q_j} + \frac{\partial V_{ab}}{\partial q_i} \cdot \frac{\partial \tilde{w}}{\partial q_j} + \frac{\partial \tilde{w}}{\partial q_i} \cdot \frac{\partial V_{ab}}{\partial q_j} + \left\{ \frac{\partial^2 \tilde{w}}{\partial q_i \partial q_j} + \frac{\partial \tilde{w}}{\partial q_i} \frac{\partial \tilde{w}}{\partial q_j} \right\} \cdot V_{ab} \right\} \cdot W \quad (2.22)$$

The only new term appearing in the above equation is $\frac{\partial^2 \tilde{w}}{\partial q_i \partial q_j}$ which is simply the width parameter for an isotropic Gaussian window function. Rest of the quantities have been computed already. Substituting all relevant quantities in Equation 2.22 will provide the analytical hessian at a given geometry.

In the above discussion on evaluation of the gradient and hessian of the vibronic model, only a quadratic form of window is considered. In the forthcoming chapter on the usage of vibronic model for transition state search, a window function with a quartic exponent will rather be employed. Below, a small table is presented depicting the functional form of both the window functions, and the their first and second derivatives.

2.3.3 Numerical Gradient and Numerical Hessian

In addition to analytical evaluation of gradient and hessian, these quantities can also be computed numerically, with only the knowledge of energies (lowest surface eigenvalues). This approach primarily serves as a diagnostic tool to test that the analytical analog of these quantities

Window (\tilde{w})	Functional Form	First Derivative	Second Derivative $i = j$	$i \neq j$
Quadratic	$\exp(-\frac{1}{2}\alpha(\mathbf{q} - \mathbf{q}_{ts} ^2))$	$-\alpha(\mathbf{q} - \mathbf{q}_{ts})$	$-\alpha$	0
Quartic	$\exp(-\frac{1}{2}\delta(\mathbf{q} - \mathbf{q}_{ts} ^4))$	$-4\delta[\mathbf{q} - \mathbf{q}_{ts} ^2](\mathbf{q} - \mathbf{q}_{ts})$	$-4\delta[\sum_k (q_k - q_{k0})^2 + 2(q_i - q_{i0})^2]$	$-8\delta(q_i - q_{i0}) \times (q_j - q_{j0})$

Table 2.1: Different forms of window function and their derivatives

discussed above are correct, and a discrepancy between the two is either due to an error in implementation or due to a difference in meaning associated with these gradient and hessian. Such subtleties can occur when considering overall rotational motions of the molecule. The formulas for numerical gradient and hessian based on finite difference approximation (centered) are presented below:

$$\frac{\partial E}{\partial q_i} = \frac{E(q_i + \epsilon) - E(q_i - \epsilon)}{2\epsilon} \quad (2.23)$$

$$\frac{\partial^2 E}{\partial q_i \partial q_j} = \begin{cases} \frac{E(q_i + \epsilon) - 2E_0 + E(q_i - \epsilon)}{2\epsilon^2}, & \text{if } i = j \\ \frac{E(q_i + \epsilon, q_j + \epsilon) - E(q_i + \epsilon, q_j - \epsilon) - E(q_i - \epsilon, q_j + \epsilon) + E(q_i - \epsilon, q_j - \epsilon)}{\epsilon^2}, & \text{otherwise} \end{cases} \quad (2.24)$$

The numerical stability has been tested extensively for the above formulas using many examples, with respect to the choice of ϵ . A numerical value of 10^{-4} was chosen in the final implementation. In conclusion, computation of the gradient and hessian has been developed for a general n -state vibronic model in this section. From a practical implementation point of view, most of these formulas are embarrassingly parallel, and this can be utilized to speed up computations for larger systems. In addition, if one switches to a different coordinate system, gradient and hessian equations must also be transformed carefully in accord. Whenever there is a change of definition in the model, such as due to a change in the definition of the window function, it is advisable to ensure that the numerical and analytical results for gradient and hessian match at a random geometry, before employing the code for further applications.

2.4 Determination of Vibronic Model Parameters

Obtaining the off-diagonal optimal parameters that enter the vibronic model such that the model reproduces ab initio data at critical points is a rather straightforward task, in particular for the two minima problem, i.e., an elementary Unimolecular reaction. An important component of this process is knowledge of gradient and hessian computation on the vibronic model, which has been developed in the previous section. For the two minima problem, all the three terms, namely the

constant, linear, and quadratic terms can be obtained *analytically*, using the gradient and hessian definitions described in the previous section. Solving the equations to determine vibronic model parameters for the two minima case is tantamount to solving a linear equation as the number of unknown (ab initio data) equals the number of variables (vibronic model parameters).

An assumption has been made about the diagonal terms of the vibronic model that they are simply the local quadratic potential around the minima region, and are not affected by the virtue of the window function. This is only true if the window function is extremely small (near zero) close to the minima geometries. An extremely tight window might result in artificial features on the PES, therefore it is preferred that there is some flexibility in choosing the width parameter associated with the window function. This can result in the minima regions not being accurately represented, as the off-diagonal elements ($V_{ab} \cdot W$) might have significant non-zero value at the minima geometries. In such cases, the parameters for diagonal elements will also need to be optimized using the same procedures as for the off-diagonal element. As a result, the determination of model parameters becomes a series of solving a system of linear equations since only one set of parameters is optimized at a time. An attempt to find a *self-consistent solution* is always made such that both diagonal and off-diagonal parameters are converged to the unique solution. The width parameter is kept small due to the fact that a large window can cause problems to achieve self-consistency. At the end, the vibronic model should be able to reproduce the ab initio energies, gradient and hessian at all the three critical points, which is when it will be considered that a solution to the determination of model parameters has been found. This is a minimum requirement that must be met before proceeding further. In addition, as a diagnostic test for the technical accuracy of the model, the analytical gradient and hessian are compared to their numerical counterparts at a random geometry (not the critical points), which must be equal to each other. Once these conditions are met, the construction of vibronic model will be deemed complete.

The general idea for determination of vibronic model parameters is that given a starting guess for the parameters, one solves a linear equation like $A \cdot \Delta = R$, where A is the coefficient matrix, Δ the change in parameter, and R the residual vector. Since for a 2×2 vibronic model, there is a one to one mapping between the ab initio data and vibronic model parameters, and the equations are solved for each mode (or pair of modes) decoupled from the rest, it essentially becomes equivalent to solving a scalar equation for each parameter individually. It is important to note that since the form of gradient and hessian is known (previous section), the solution is *analytic* in nature, i.e., it does not depend on the initial guess and it does not require an *iterative solution*. It also must be added that one big equation can be solved together for all parameters, as is employed in the DG-EVB method, though it can quickly become large for bigger molecules as the total number of parameters grows as $1 + n_{mode} + \{n_{mode}(n_{mode} + 1)/2\}$ with respect to number of normal modes of the system n_{mode} (already taking the symmetry of hessian into account).

Finally, this procedure of solving linear equation for parameter determination can be extended to multiple minima cases, including under-determined cases where one set of ab initio data maps to more than one set of vibronic model parameters. However, the details of such generalization will not be presented here. Below, the equations for determination of model parameters are presented.

2.4.1 Determination of constant term E_{ab}

For a 2×2 system, the constant coupling term can be determined analytically as follows:

$$E_{ab} = \sqrt{E_{TS}^2 - E_{TS}(V_A + V_B) + V_A V_B} \quad (2.25)$$

Where V_A and V_B are values of the diagonal diabatic elements at Q_{TS} . However, in general, it can also be obtained numerically by an iterative Newton-Raphson procedure. The residual vector R is defined as the difference between true ab initio E_{TS} and the lower eigenvalue of the vibronic model at a given iteration as follows:

$$R = E_{TS} - E_0^{current} \quad (2.26)$$

The A matrix is simply the derivative $2c_a c_b$, where c_a and c_b are the components of eigenvector corresponding to the lowest eigenvalue. Therefore, Δ can be computed as

$$\Delta = \frac{E_{TS} - E_0^{current}}{2c_a c_b} \quad (2.27)$$

The new E_{ab} can be calculated as $E_{ab}^{old} + \Delta$. The cycle is repeated until Delta goes to zero.

2.4.2 Determination of linear coupling terms g_{ab}

The determination of linear coupling terms can be formulated based on the gradient Equation 2.8. At $q = Q_{TS}$, the gradient is explicitly expressed as:

$$\frac{\partial E}{\partial q_i} = \sum_a c_a^2 \left(\frac{\partial V_{aa}}{\partial q_i} \right) + 2c_a c_b \cdot g_{ab}^i \quad (2.28)$$

This equation can be simply solved for g_{ab}^i . In terms of $A \cdot \Delta = R$ formulation,

$$\begin{aligned} A &= 2c_a c_b \\ R &= \frac{\partial E}{\partial q_i} - \sum_a c_a^2 \left(\frac{\partial V_{aa}}{\partial q_i} \right) \\ \Delta &= \frac{R}{A} = \frac{\frac{\partial E}{\partial q_i} - \sum_a c_a^2 \left(\frac{\partial V_{aa}}{\partial q_i} \right)}{2c_a c_b} \end{aligned} \quad (2.29)$$

2.4.3 Determination of quadratic coupling terms \mathbb{H}_{ab}

The determination of quadratic coupling parameters is based on the same procedure as the linear coupling terms. Using Equation 2.14 in conjunction, one can arrive at an analytic expression as follows:

$$\mathbb{H}_{ab}^{ij} = \mathbb{K}_{TS}^{ij} - \left\langle \frac{\partial \Psi}{\partial q_i} \left| \frac{\partial \hat{V}}{\partial q_j} \right| \Psi \right\rangle - \left\langle \Psi \left| \frac{\partial \hat{V}}{\partial q_j} \right| \frac{\partial \Psi}{\partial q_i} \right\rangle - \sum_a c_a^2 \mathbb{H}_{aa}^{ij} - \frac{\partial^2 W}{\partial q_i \partial q_j} \cdot V_{ab} \quad (2.30)$$

Where \mathbb{K}_{TS}^{ij} is the ij^{th} element of the ab initio hessian at the TS geometry. The next two terms are evaluated as discussed in the previous section, while the last two terms are trivial to calculate. It should be noted that at $q = Q_{TS} : W = 1.0$ and $\frac{\partial W}{\partial q} = 0.0$, because of which simplifications arise in the above equation.

2.4.4 Self-consistent solution for all parameters

While the optimal parameters for the off-diagonal elements capture the transition state and the nearby regions around it accurately, it invariably disturbs the minima region in the process. A simple example depicting this scenario has been discussed in one of the previous sections. In order to solve this issue, an iterative procedure is employed where the parameters for one element of the vibronic model are determined at a time, and after each such step the model is checked at all the critical points for correctness (whether it is able to reproduce the ab initio data at that geometry or not). This process is repeated until convergence, or self-consistency, is reached. A window function with small width achieves convergence faster, while on the the other hand, convergence can not be guaranteed in general for an arbitrarily large width of the window. This is due to possible oscillations in the iterative procedure, as we solve for one set of parameters at a time. There is no convergence issue in 2×2 vibronic model if one does not demand correctness of the model at the minima.

2.5 Choice of Coordinates

A potential energy surface by its very definition depends on the interatomic distances of the constituting elements, and therefore is described using the $3N - 6$ internal nuclear degrees of freedom for nonlinear polyatomic molecules ($3N - 5$ for linear molecules) consisting of N atoms. The overall location of the molecule in space as well its orientation does not make a difference in the total electronic energy for a given set of relative atomic positions, in the absence of any external forces. In general, quantum chemistry programs use internal coordinates to describe the PES as it naturally leads to translational and rotational invariance of the PES. In case of EVB based approaches, the situation is somewhat complex. For example, in the proposed scheme in

this chapter, reactant, product, and transition state can have their own set of internal coordinates (such as defined by a Z -matrix), i.e. each diabatic matrix element can have its own coordinate system. However, one needs a common set of coordinates to describe the lower adiabatic surface, the real quantity of interest. One possibility is to use a set of *generalized internal coordinates* such that each local region, and therefore the entire PES is described using same set of coordinates throughout. It is a viable scheme, one that has also been recently explored in the context of vibronic spectroscopy. That being said, the implementation and usage of such generalized internal coordinates lacks ease and simplicity. The focus in this work is on developing a scheme which can be readily adapted for implementation and easy to comprehend.

With this goal in mind, the next best choice for internal degrees of freedom is the normal coordinates. Since it is assumed that the ab initio energies and its derivatives up to second order are known at the critical points, the local potential energy surface corresponding to minima and transition state can be easily expressed in their own normal modes. This stage simply corresponds to performing a harmonic vibrational analysis for individual critical points, a routine procedure in quantum chemistry calculations. The normal modes of transition state are then chosen as *reference state normal modes*, and all the ab initio quantities of minima are expressed in terms of transition state normal modes, providing a common set of coordinates. In this work, $3N - 3$ rovibrational normal coordinates are employed such that the coordinate transformation is always carried out by a unitary matrix, preserving the character of each local region, i.e. the frequencies of any local region remains the same in the new coordinates. The $3N - 3$ normal coordinates are used in conjunction with Eckart frame, which is the norm. This is done in order to use a consistent Body Frame (molecule fixed coordinate system) and an optimal separation of rotations from vibrations. [52]

The rotational degrees of freedom can be explicitly projected out (details later) nullifying any contribution from rotations to the potential energy. An exception to this general rule will be made in places for transition state search, letting the vibrations and rotations mix freely, as it makes the optimization process more efficient. It is to be noted with great emphasis that our objective is *not* to describe rovibrational spectra or any other *dynamical* process where the kinetic energy operator (KEO) must be included in the description. The separation of rotation and vibration in such a situation becomes extremely important for various reasons, whether for assignment of transitions, or increase of computation efficiency, or employing approximate but intuitive models. For locating saddle points on a given PES, these concerns do not play any role and the use of rotation-vibration coordinates simplify matters, instead of complicating it. The use of Eckart frame is still important so that the coordinate system, i.e. the x, y and z axes associated with the molecule does not switch its orientation while exploring the PES during the optimization process, and the changes in geometry are continuous and smooth, without any jumps.

The determination of Eckart frame, though not trivial, is a solved problem. It is equivalent to finding an optimal superposition of two molecular structures, a fact well established in the literature, [53] which is an easier problem to solve and think about in an intuitive manner. The superposition will be referred to as *alignment* of geometries hereafter. The target geometry will be aligned by performing a rotation such that the residual distance between alike atoms is minimized with respect to the reference geometry. The goal is then to determine this rotation matrix, which will be referred to as the Eckart rotation matrix. A recently proposed scheme based on the use of quaternion algebra [53] is employed in order to obtain the Eckart rotation matrix, and thus the Eckart frame. It is a numerically stable scheme, applicable to any general system. Alignment will play a vital role in the vibronic model based construction of PES and transition state search. Every geometry in nuclear configuration space will always be aligned with respect to the reference state geometry. In addition, the rotational degrees of freedom will be projected out from the corresponding gradient and hessian whenever necessary.

Harmonic Vibrational Analysis

Here, a brief overview of the well-established normal mode analysis is presented for a given nuclear configuration. The description is valid at a stationary as well as a non-stationary point. The approach to project out translational and rotational degrees of freedom closely follows the procedure used in Gaussian program, as discussed by Page and McIver. [54] One starts with the Cartesian force constant matrix (FCM) obtained from Gaussian (or any other ab initio program):

$$F_{ij} = \frac{\partial^2 V}{\partial X_i \partial X_j} \quad i, j = 1, \dots, 3N \quad (2.31)$$

Next, the FCM is mass-weighted as follows:

$$\mathbb{H} = \mathbb{M}^{-1/2} \mathbb{F} \mathbb{M}^{-1/2} \quad (2.32)$$

Where,

$$\mathbb{M} = \begin{pmatrix} m_1 & 0 & \dots & 0 \\ 0 & m_2 & \dots & 0 \\ \vdots & \vdots & \ddots & \vdots \\ 0 & 0 & \dots & m_{3n} \end{pmatrix} \quad (2.33)$$

The translational and rotational vectors are constructed in mass-weighted coordinates following the procedure described in Gaussian. [54] After orthonormalizing these vectors, the translation-rotation subspace is projected out from the mass-weighted FCM:

$$\mathbb{H}_{proj} = (\mathbb{I} - \mathbb{P})\mathbb{H}(\mathbb{I} - \mathbb{P}) \quad (2.34)$$

The projected hessian is diagonalized, which gives exactly six zero eigenvalues corresponding to overall translation and rotation of the molecule.

$$\mathbb{H}_{proj}\mathbb{L} = \mathbb{L}\Lambda \quad (2.35)$$

The six eigenvectors corresponding to the overall translation and rotation of the molecule are removed from the eigenvector matrix \mathbb{L} , to which the three rotational vectors are added *manually*, thus defining the $3N - 3$ normal modes of vibration and rotation. This analysis is performed for each critical point, though at the end only the reference state normal modes (transition state here) will be used in practice. The transformation between normal coordinates and Cartesian coordinates is then defined as follows:

$$\begin{aligned} Q &= \mathbb{L}^T \mathbb{M}^{1/2} X \\ X &= \mathbb{M}^{-1/2} \mathbb{L} Q \end{aligned} \quad (2.36)$$

Where \mathbb{L} is $(3N, 3N - 3)$ rectangular array defining normal modes of vibration-rotation.

Coordinate Transformation

Once the ab initio data has been processed for each critical point individually, it all needs to be re-expressed in terms of reference state coordinates. This transformation, as mentioned earlier, follows the procedure used in theoretical computation of Franck-Condon spectra. Following steps are performed to carry out this analysis:

1. First the Cartesian geometry is aligned with respect to the transition state, which is the reference state, Cartesian geometry. This procedure yields a rotation matrix, known as Eckart rotation matrix, \mathbb{R} .
2. The modified Duschinsky matrix is calculated as follows:

$$\mathbb{J} = \mathbb{L}_{target}^T \cdot \mathbb{R}_b^T \cdot \mathbb{L}_{reference} \quad (2.37)$$

Where \mathbb{R}_b is the block diagonal form of the Eckart rotation matrix.

3. Displacement vector is calculated as follows:

$$\mathbf{K} = \mathbb{L}_{reference}^T \mathbb{M}^{1/2} (\mathbb{R} \mathbb{X}_{target} - \mathbb{X}_{reference}) \quad (2.38)$$

4. New coordinates are defined as:

$$\mathbf{Q}' = \mathbb{J} \mathbf{Q} + \mathbf{K} \quad (2.39)$$

5. The quadratic potential defined in Equation 2.1 is expressed in terms of transformed coordinates as follows:

$$V(\mathbf{Q}) = E_A + \mathbf{g}^T \cdot \mathbb{J}\mathbf{Q} + \frac{1}{2}\mathbf{Q}^T \cdot \mathbb{J}^T\mathbb{H}\mathbb{J} \cdot \mathbf{Q} \quad (2.40)$$

Such that the new gradient and hessian become:

$$\begin{aligned} \mathbf{g}' &= \mathbb{J}^T\mathbf{g} \\ \mathbb{H}' &= \mathbb{J}^T\mathbb{H}\mathbb{J} \end{aligned} \quad (2.41)$$

This analysis is performed for all critical points and at the end one has all ab initio data in reference state normal mode coordinates. This becomes the starting point for determination of vibronic model parameters, which has been discussed previously.

Projecting out rotational degree of freedom at a random geometry

As discussed above, a vibronic model will be represented in terms of $3N - 3$ normal coordinates, \mathbf{q} . Any geometry in the \mathbf{q} space can be transformed to Cartesian coordinates by the means of Equation 2.36. When one walks on the vibronic model PES away from critical point geometries, such as during a transition state search, the molecule would in general rotate away from the Eckart frame. Moreover, the gradient and hessian would have non-zero components along rotational modes at a particular geometry. On the vibronic model PES, a rotating molecule costs (or gains) energy, which is undesirable. Therefore, the rotational degrees of freedom can be explicitly projected out.

Consider a geometry \mathbf{q} in the $3N - 3$ space. The corresponding Cartesian geometry X can be aligned with the reference Cartesian geometry X_0 by determining the corresponding Eckart rotation matrix, \mathbb{R} . This gives the new aligned Cartesian geometry: $X' = \mathbb{R}X$. The corresponding normal coordinate, denoted as $\mathbb{R}\mathbf{q}$ can be evaluated using Equation 2.36. The points $\mathbb{R}\mathbf{q}$ represent a manifold of geometries, in which the molecule always stays aligned with the reference geometry.

The quantities of interest on the vibronic model, i.e. the energy, gradient and hessian are then evaluated on the point $\mathbb{R}\mathbf{q}$. The gradient and hessian obtained from the model are quantities of dimension $3N - 3$ and $(3N - 3, 3N - 3)$ respectively. The goal is to project out rotational contribution from these quantities, which can be done in the following way: Compute the rotational vectors in (mass-weighted) Cartesian coordinates at the geometry $\mathbb{R}X$, as discussed earlier in the context of harmonic vibrational analysis. [54] Transform these vectors to normal mode coordinates. Project out the rotational degrees of freedom from gradient and hessian as follows:

$$\begin{aligned} \mathbf{g}^P &= (\mathbb{I} - \sum_i |L_i^R\rangle\langle L_i^R|)\mathbf{g} \\ \mathbb{H}^P &= (\mathbb{I} - \sum_i |L_i^R\rangle\langle L_i^R|)\mathbb{H}(\mathbb{I} - \sum_i |L_i^R\rangle\langle L_i^R|) \end{aligned} \quad (2.42)$$

Where L^R are the rotational normal mode vectors. The projected gradient \mathbf{g}^P should have three zero components and the projected hessian \mathbb{H}^P should have three zero eigenvalues along the rotational modes.

Discussion of Rotational Projection

A comparison between numerical and analytical gradient and hessian can shed some light on the complications due to rotations. To check the correctness of analytical gradients and hessian for the model one would do the following finite difference calculation:

1. Take a starting geometry \mathbf{q} and align this with the reference geometry.
2. Make small displacements along the $3N - 3$ coordinates and calculate gradient and hessian using numerical differentiation (see section 2.3.3).

From such a test one should get excellent (i.e. up to 7 significant digits) agreement between numerical and analytical derivatives. The components of the gradient and hessian along rotational displacements are non-zero, because the PES is being represented in terms of vibronic model. This reflects the fact that the vibronic model is rotationally invariant. One can conduct the procedure in a slightly different way and realign each displaced q-coordinate with the reference geometry, after each small displacement. Now the numerical gradient does not have a component along rotational degrees of freedom, as such small displaced geometries upon re-alignment are no longer displaced.

This numerical gradient coincides with the projected analytical gradient. However, the numerical hessian does not necessarily agree with the projected hessian. They do agree at stationary points (where the gradient is zero) but not at non-stationary points. The numerical hessian exhibits rotational invariance because it essentially contains cross derivatives of the gradient and alignment derivatives. These are not included in the projected analytical hessian. The above analysis can also be used to compare the vibronic model which is constructed at a non-stationary reference geometry (to be done later for transition state search) and the data from ab initio calculations. There are two choices:

1. The vibronic coupling parameters are obtained by matching the unprojected analytical results to ab initio data before projection.
2. The vibronic coupling parameters are obtained after rotational projection.

2.6 Results & Discussions

In this section, the methodology discussed in the previous sections will be applied to a test set of Unimolecular reactions. Most of these reactions are taken from a benchmark test set of locating transition state structures [Baker]. The goal here is to investigate the validity and accuracy of the vibronic model in representing the ground state reactive PES.

2.6.1 Scans of Potential Energy Surface

The comparison with ab initio data will be performed along three different pathways connecting the reactant and product via the transition state. These paths are described below briefly:

- **Intrinsic Reaction Coordinate (IRC):** An IRC is a minimum energy path (MEP) connecting the transition state to the reactant on one side and to the product on the other. It is defined as the steepest descent path in mass-weighted coordinates. Computing IRC is a standard black-box technique in most modern quantum chemical programs, for example in Gaussian09, the program of choice in this work. Careful calculations were performed to obtain a converged IRC for all the reactions considered here.
- **Quadratic Transit Path (QTP):** In the absence of IRC, or even as a complimentary pathway, the quadratic transit path is the simplest path connecting the two minima and a transition state. The path can be parameterized in terms of a reaction coordinate variable s as follows:

$$\mathbf{Q}(s) = \mathbf{Q}_0 + s\mathbf{Q}_1 + \frac{1}{2}s^2\mathbf{Q}_2 \quad (2.43)$$

The endpoints of the path ($s = +1$ and $s = -1$) are represented as the minima geometries, while the center point ($s = 0$) is assigned to the transition state geometry. With this parameterization scheme, the variables \mathbf{Q}_0 , \mathbf{Q}_1 , and \mathbf{Q}_2 are obtained as follows:

$$\begin{aligned} \mathbf{Q}(-1) &= \mathbf{Q}_A = \mathbf{Q}_0 - \mathbf{Q}_1 + \frac{1}{2}\mathbf{Q}_2 \\ \mathbf{Q}(0) &= \mathbf{Q}_{TS} = \mathbf{Q}_0 \\ \mathbf{Q}(1) &= \mathbf{Q}_B = \mathbf{Q}_0 + \mathbf{Q}_1 + \frac{1}{2}\mathbf{Q}_2 \end{aligned} \quad (2.44)$$

Such that,

$$\begin{aligned} \mathbf{Q}_0 &= \mathbf{Q}_{TS} \\ \mathbf{Q}_1 &= (\mathbf{Q}_B - \mathbf{Q}_A)/2 \\ \mathbf{Q}_2 &= \mathbf{Q}_A + \mathbf{Q}_B - 2\mathbf{Q}_{TS} \end{aligned} \quad (2.45)$$

- **Cubic Transit Path (CTP)**: The cubic transit path is similar to its quadratic analog, except that it is modeled differently around the TS region. The tangent to the path at the TS geometry is now equal to the direction of eigenvector of TS hessian associated with its 1 negative eigenvalue. In this regard, the CTP is equivalent to IRC in the close proximity of TS region (note that in IRC algorithms, since the gradient is zero at the TS geometry, in order to descend down the eigenvector corresponding to negative eigenvalue of the hessian is chosen as the starting point). It is also interesting to note that if the aforementioned eigenvector is close to $\mathbf{Q}_B - \mathbf{Q}_A$, all three paths around the TS region will become equivalent. The equation for parameterized path can be written as follows:

$$\mathbf{Q}(s) = \mathbf{Q}_0 + s\mathbf{Q}_1 + s^2\mathbf{Q}_2 + s^3\mathbf{Q}_3 \quad (2.46)$$

The endpoints and midpoint is characterized as before, in addition there is one new equation for the tangent. The variables are then obtained as follows:

$$\begin{aligned} \mathbf{Q}(-1) &= \mathbf{Q}_A = \mathbf{Q}_0 - \mathbf{Q}_1 + \mathbf{Q}_2 - \mathbf{Q}_3 \\ \mathbf{Q}(1) &= \mathbf{Q}_B = \mathbf{Q}_0 + \mathbf{Q}_1 + \mathbf{Q}_2 + \mathbf{Q}_3 \\ \mathbf{Q}(0) &= \mathbf{Q}_{TS} = \mathbf{Q}_0 \\ \frac{\partial \mathbf{Q}}{\partial s} &= \vec{P} = \mathbf{Q}_1 \end{aligned} \quad (2.47)$$

Such that,

$$\begin{aligned} \mathbf{Q}_0 &= \mathbf{Q}_{TS} \\ \mathbf{Q}_1 &= \vec{P} \\ \mathbf{Q}_2 &= (\mathbf{Q}_A + \mathbf{Q}_B - 2\mathbf{Q}_{TS})/2 \\ \mathbf{Q}_3 &= (\mathbf{Q}_B - \mathbf{Q}_A - 2\vec{P})/2 \end{aligned} \quad (2.48)$$

The ab initio data was computed for the QTP and CTP along a set of grid points between $s = -1$ and $s = 1$. Although the comparison between ab initio results and vibronic model results is performed along the entire path starting at one minima geometry and ending at the other, the focus will largely remain around the TS region as this will be the most important part for the transition state searches. It is also important to note that both QTP and CTP can be easily computed even for a guess TS geometry, as will be the case for later chapters, though if the guess contains more than one negative eigenvalue for the hessian, the tangent to the path will be determined using the eigenvector having maximum overlap with the $\mathbf{Q}_B - \mathbf{Q}_A$ vector.

Along the three paths discussed above, the energies and norm of the gradient will be compared at each geometry. Another quantitative measure for the accuracy of gradient will be assessed in terms of the angle between vibronic model gradient and ab initio gradient. In addition, in order

to gain some insight into the modeling process, the off-diagonal element of the vibronic model Hamiltonian will also be analyzed along these paths, in conjunction with the effect of the window function for a couple of reactions. A comparison of diabatic and adiabatic surfaces, including the (artificial) upper surface, will also be made in order to understand the underlying ideas of the modeling. Before moving on, a brief description of the ab initio calculations is presented below.

2.6.2 A note on quantum chemical calculations

Two different types of ab initio data is used in the construction of vibronic model (and transition state searches) in this work. The first is a lower level of theory using a small basis set - the Hartree-Fock method with the 3-21G basis set (HF/3-21G) and the second is a DFT method using B3LYP functional with the cc-pVTZ basis set (B3LYP/cc-pVTZ). The HF/3-21G calculations serve as a quick development tool along with providing a starting point for more accurate calculations. The Hartree-Fock method being a mean field approach does not account for electron correlation effects. Therefore, the results obtained at this level are not quantitatively accurate. The B3LYP/cc-pVTZ approach provides a much better estimate of activation energies, for example, and includes electron correlation, mostly at the cost of Hartree-Fock calculations. It is representative of a method that is widely used by practicing chemists. That being said, the past couple of decades have seen tremendous progress in the field of electronic structure theory, for both single reference and multi reference methods. For the former, approaches such as MP2 and CCSD(T) have become routine, while for the latter accurate methods such as MRCI and CASPT2 have become quite popular as well. The applicability of these methods has also been on the rise due to an exponential growth in computing power. It is important to emphasize in the context of vibronic model construction that by using a higher level of theory / basis set, the critical points will become more accurate. However, the quality of the PES at intermediate geometries might still not be satisfactory. Additional discussion concerning quantum chemical calculations will follow in later chapters in the context of locating transition states.

2.6.3 Reaction Test Set

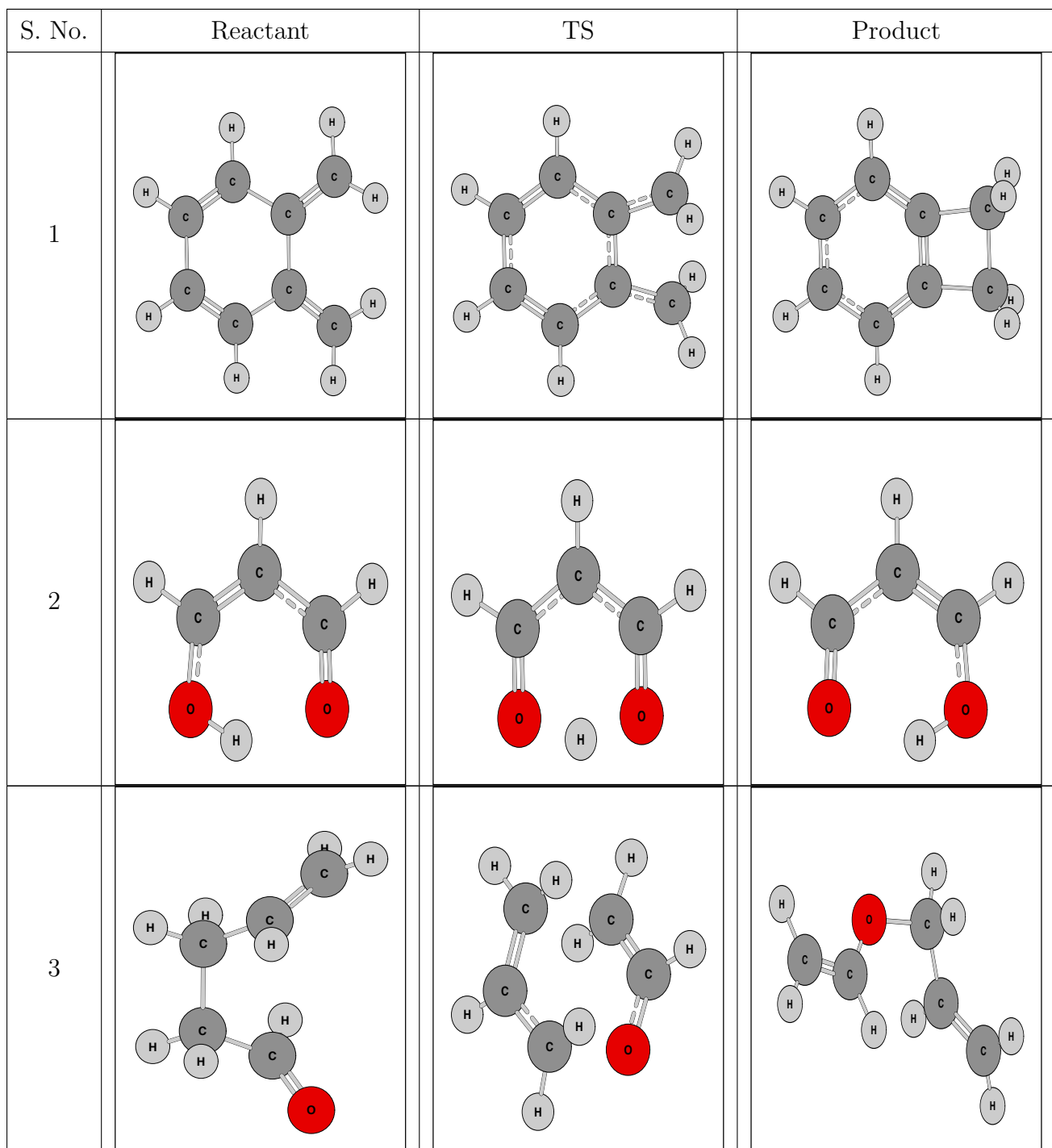
The Unimolecular reactions used for the construction of vibronic model are presented in Table 2.2. As mentioned earlier, most of these reactions are adopted from the Baker test set for transition state search. The test set contains different kinds of Unimolecular reactions such as ring opening, hydrogen shift, cis-trans isomerization and a TS corresponding to change of conformation. This test set is a subset of a bigger suite of tests to be used later for transition state search in the forthcoming chapters. In order to illustrate the methodology being discussed in this chapter, and to emphasize important points pertaining to the modeling process, the following three

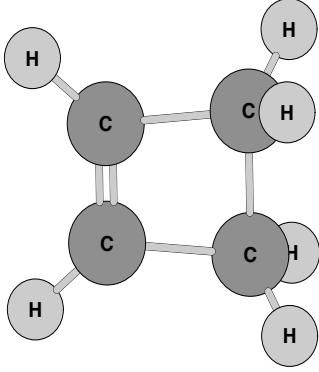
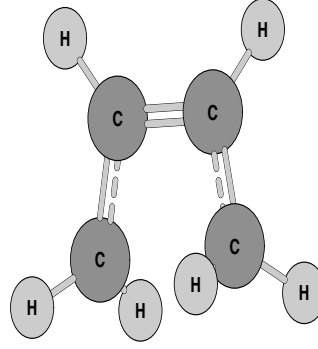
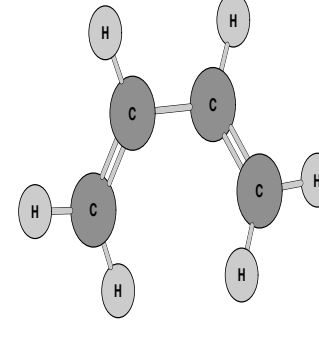
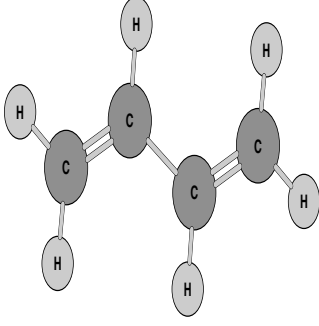
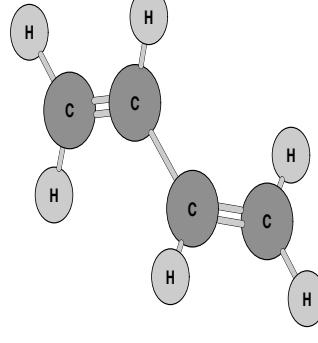
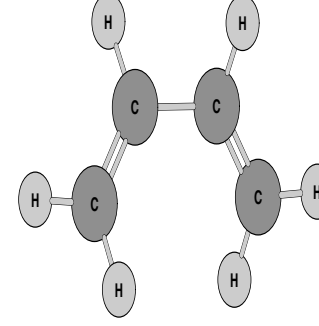
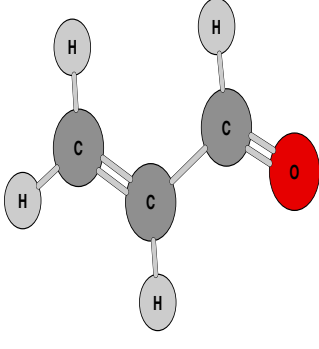
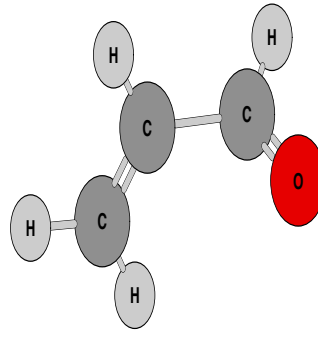
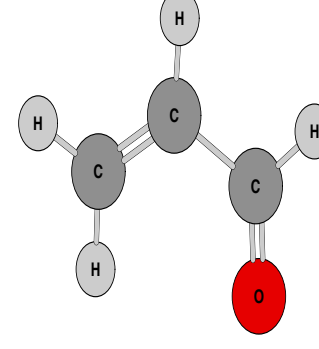
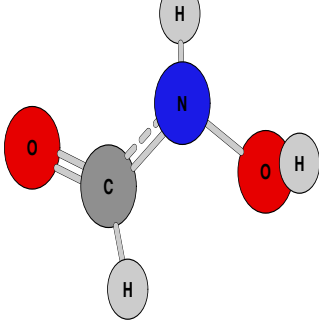
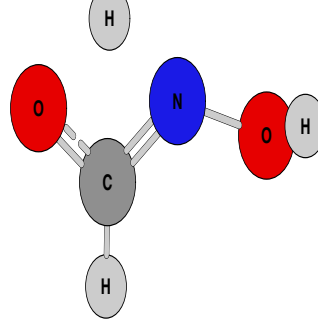
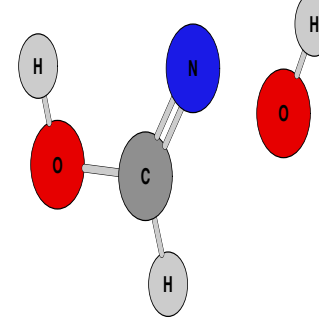
reactions will be discussed in significant detail: 1, 3, and 9, which correspond to ring opening, Claisen rearrangement and a simple Hydrogen shift reaction respectively.

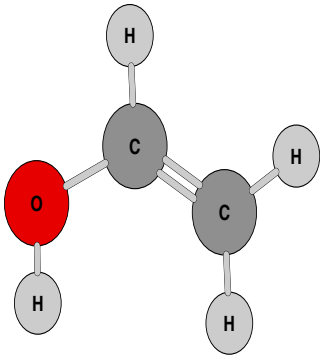
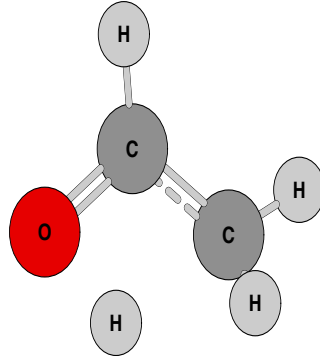
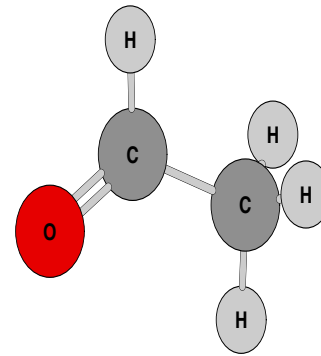
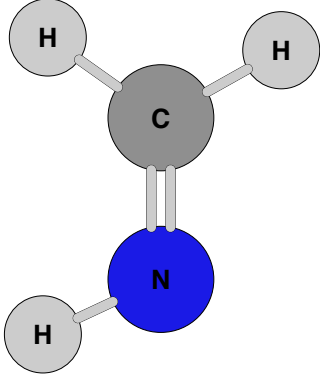
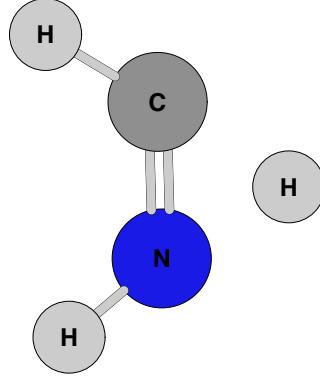
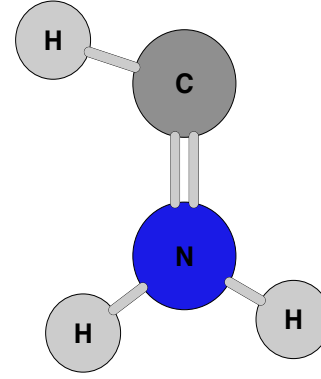
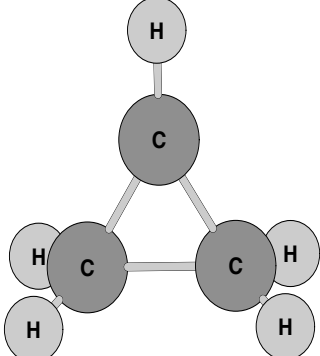
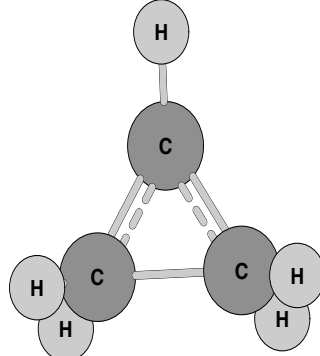
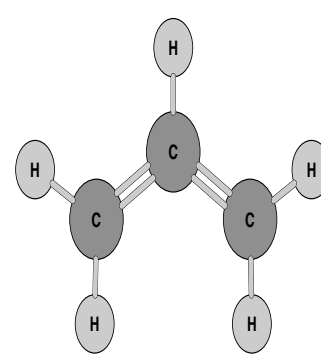
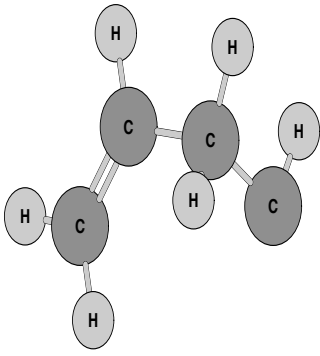
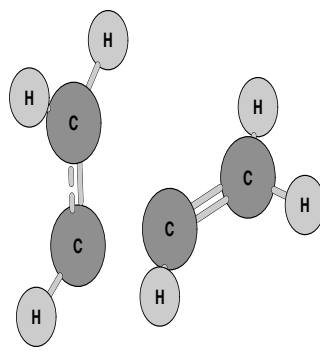
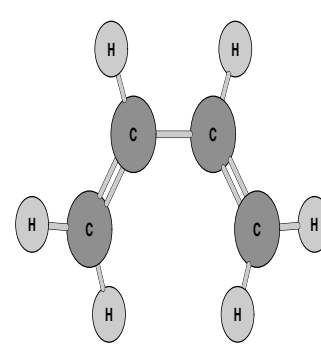
Computational steps for constructing a vibronic model

To summarize, the following steps are performed in order to construct a vibronic model as discussed in this chapter

1. Compute required ab initio data - Energy, Gradient, and Hessian - for reactant, product and transition state optimized geometries at a desired level of theory (*Gaussian09*)
2. Perform an IRC calculation in Gaussian, and obtain transit path scan data (QTP, CTP) using the custom program provided by author (which calls *Gaussian09* internally)
3. Perform construction of vibronic model and analysis of fit (comparison along IRC, QTP, CTP) for the model using the custom program provided by author



4			
5			
6			
7			

8			
9			
10			
11			

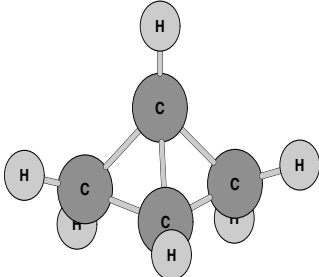
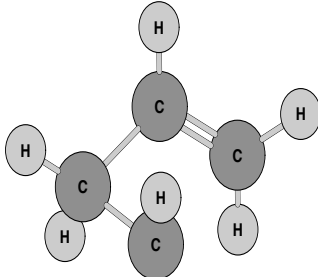
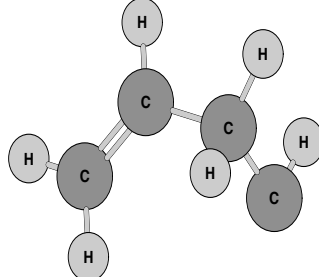
12			
----	---	--	---

Table 2.2: Unimolecular Reactions

2.6.4 Results for HF/3-21G: A detailed discussions of three reactions

In order to determine the accuracy of a vibronic model in regards to how well it is able to reproduce the true ground state PES, the following three quantities will be compared along the three paths discussed earlier: i) Energy, ii) Norm of the gradient vector, iii) Angle between vibronic model gradient vector and ab initio gradient vector (both normalized) for the three selected reactions. The primary figures are organized into two panels for each reaction:

- Energies: Lower (ground) state on the left, all adiabatic and diabatic energies on the right
- Gradients: Norm on the left, angle between ab initio and vibronic model gradient on the right

A visual inspection of these figures will immediately reveal the quality of the vibronic model. In addition, in order to gain insight into the modeling process, the exact form of the off-diagonal element V_{ab} as well as that predicted by the vibronic model alone will be compared for a couple of reactions. The importance of window function will also be discussed in this context.

Reaction 9: Hydrogen shift

The first example to discuss the accuracy and validity of the vibronic model is a relatively simple hydrogen transfer reaction. The lower state energies computed from vibronic model follows the true ab initio energies quite well, along all the three paths, namely the IRC, CTP and QTP, as seen in Figure Table 2.3. Alongside, the cuts of upper adiabatic surface as well as the two diagonal diabatic surfaces are shown as well. As one moves from the transition state region towards (any of the) minima, the lower energy curve approaches and overlaps the respective diabatic curve, as one would expect. These are the quadratic minima regions as computed by ab initio calculation in the harmonic approximation. The upper surface, an artifact of the modeling process with no associated physical meaning, lies quite high in energy.

The comparison of gradients also fairs well in this case. The norm of the gradient follows corresponding ab initio data for most parts. This is also reflected in the angle between vibronic model gradient and ab initio gradient, which is always close to unity. Away from the transition state region, the quality of gradient does deteriorate a little, as is noted in the IRC and QTP figures in Figure Table 2.4. However, the CTP in this respect differs, as most of the geometrical structures along this path are very close to the TS structure, as noted in the distance plot. The distance variable is essentially the norm of the normal coordinate vector. It is important to emphasize that this is the region most relevant for locating transition states, thus reassuring their use of this model in transition state search.

Reaction 1: Ring Opening

For the second example, a ring opening reaction, the comparison of energies is good along all paths (Figure Table 2.5), though it leaves a little to be desired in certain regions, mostly away from the transition state. The comparison of gradient, however, leaves a lot to be desired. Although the comparison close to the TS region remains reasonable, as is most clearly visible in the CTP curve, away from it the quality of gradient diminishes severely. This is reflected both in the norm of the gradient as well as the angle between the vibronic model and ab initio gradient along the QTP and IRC, in particular the latter.

This example indicates that the vibronic model is only accurate in limited regions around the stationary points. The cubic transit path has many points within about 1 unit of distance and the results in this region are quite satisfactory. The other paths have most points on the curve quite far removed from the critical points, in particular from the reference geometry. While the energies from the vibronic model are adequate, this is not true for the gradient. It is likely that the gradient contribution from the window function is at play here.

Reaction 3: Claisen Rearrangement

The results of third reaction considered here has quite some interesting features. Firstly, one of the minimum located by IRC in Gaussian09 is different than the optimized minimum geometry, thus making the vibronic model completely invalid in that region. This can be seen in the comparison of energy along IRC in Figure Table 2.7, and in the comparison of gradient along IRC in Figure Table 2.8. Moreover, for the QTP and CTP, the paths curve in a weird way, featuring a very high energy peak during the descent towards one of the minimum. The comparison of gradient is equally bad as the comparison of energies. However, it is to be noted that even for such a vibronic model, the comparison for both energies and gradients remain reasonable close to the TS region (by design), which is the most relevant region for TS search.

2.6.5 Results for B3LYP/cc-pVTZ

The general pattern of DFT results more or less follows the HF results. Some differences demand attention nonetheless. The activation energies (barrier heights) are less than their HF counterparts, as expected. The other major difference is for the Claisen Rearrangement IRC as it finds the correct minimum on both sides, albeit the high energy "horn" for the vibronic model seems to persist in this case as well, as seen in Figure Table 2.13. With gradient comparison not being up to the mark, it does not seem to be the case that at this level of modeling, the vibronic model can be very useful for applications such as the computation of reaction rates. More sophis-

ticated schemes, such as those mentioned in Chapter 1, seem to be more suitable for such applications. It is evident that many such schemes already exist and are being pursued by other groups, as noted earlier also. As such, the EVB based approaches are used frequently for studying condensed phase chemical dynamics with a mixed QM/MM methodology. That being said, the focus of this work, as mentioned earlier, is two-fold: a) simplicity and ease of implementation, such as the use of Cartesian and normal coordinates, and b) on transition state search using EVB based vibronic model scheme, which, although touched upon in the literature, has not been explored exhaustively.

Comment on the behavior of V_{ab} and window function

The exact form of V_{ab} as well as that predicted by the vibronic model alone has been compared for a couple of reactions along the IRC path, with and without the presence of window function. Exact V_{ab} can be calculated along a given reaction path analytically as the ab initio energies are known, and for a given geometry the diabatic potentials can be easily evaluated. For Reaction 9, the simple hydrogen transfer reaction, the exact V_{ab} approaches zero as it gets closer to minima geometries, which is the expected behavior. This is not true for the V_{ab} predicted by the model, which increases rapidly in both the minima directions. A window function is thus necessary to push this term downwards. A product of V_{ab} and the window function is able to imitate the exact V_{ab} quite accurately in this case, resulting in a good vibronic model.

2.6.6 Conclusions

While it can be concluded from the examples discussed above that the vibronic model is not globally accurate, it is a fairly faithful representation of the PES in the vicinity of the transition state (within a hyper-sphere of radius 1 unit approximately). This is most clearly illustrated by the cubic transit path, which tends to circle around the transition state. If it is true that in general the vibronic models are accurate in a significantly large region around the reference geometry this would indicate the models can be used in transition state searches.

The cubic transit results show another interesting feature. The diabatic potentials weave around each other in the TS regions considered here. The diabatic potentials are close to each other and in diagonalization of the vibronic model there is significant mixing in the electronic state vector (c_1, c_2) . This is considered to be a desirable feature of a good vibronic model around the transition state. It means both diabatic states contribute to the formation of the final adiabatic surface. This is the rationale behind using such a vibronic model in the first place. This feature will be further discussed in the next chapter, in which a modified definition of vibronic model will be discussed, which will be more suitable for transition state searches.

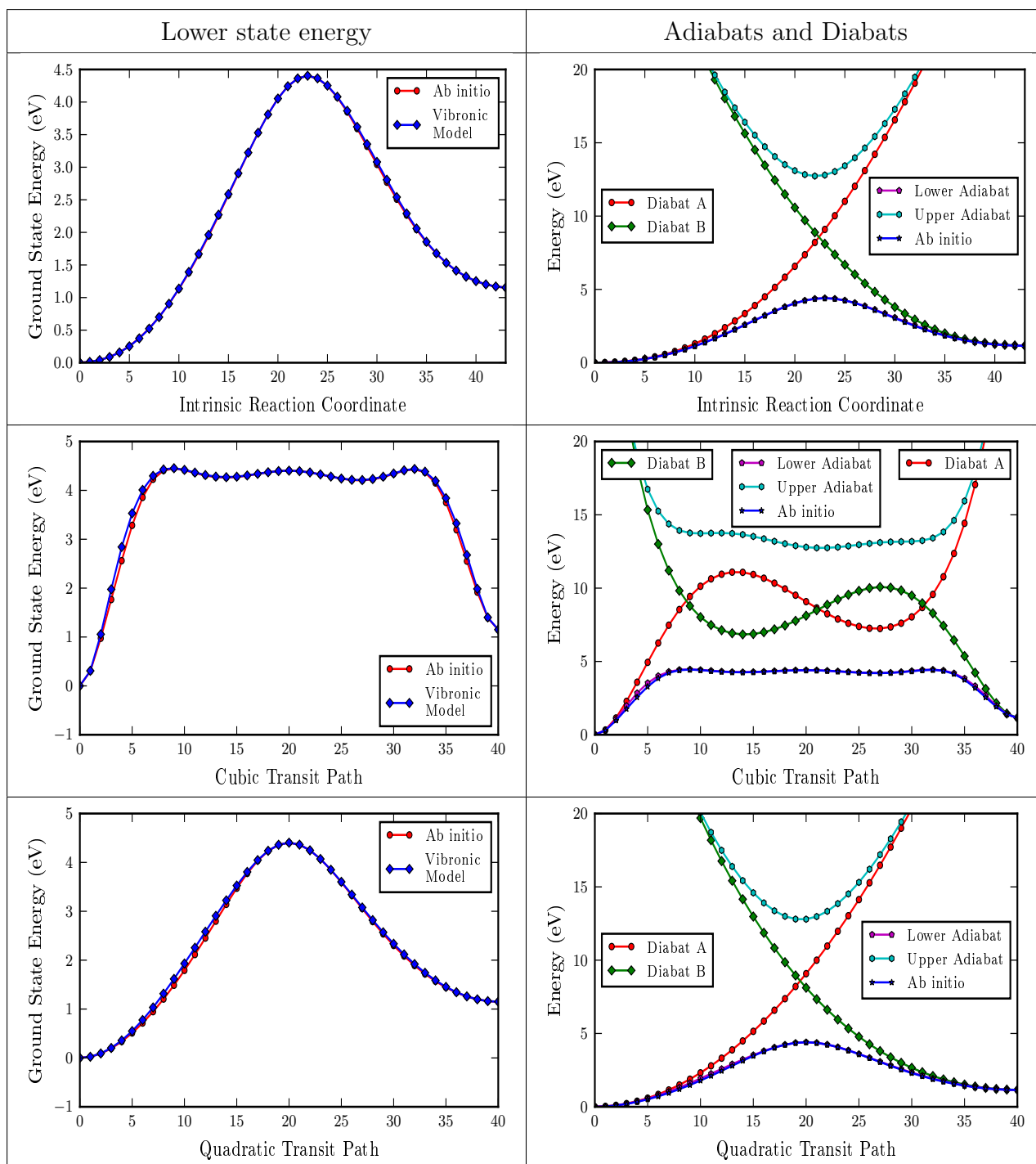


Table 2.3: Comparison of Energies for Reaction-9: H-shift [HF/3-21G]

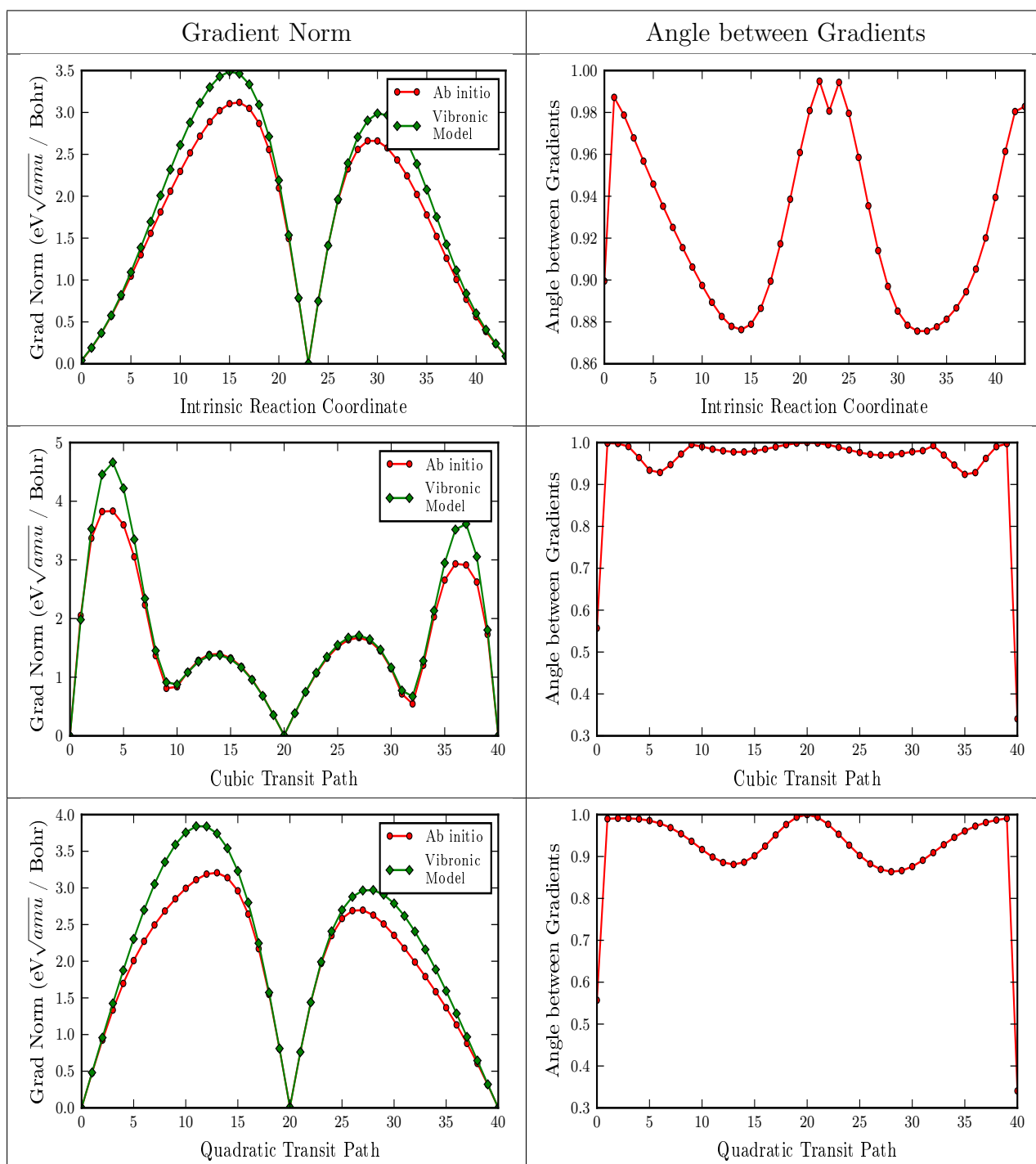


Table 2.4: Comparison of Gradients for Reaction-9: H-shift [HF/3-21G]

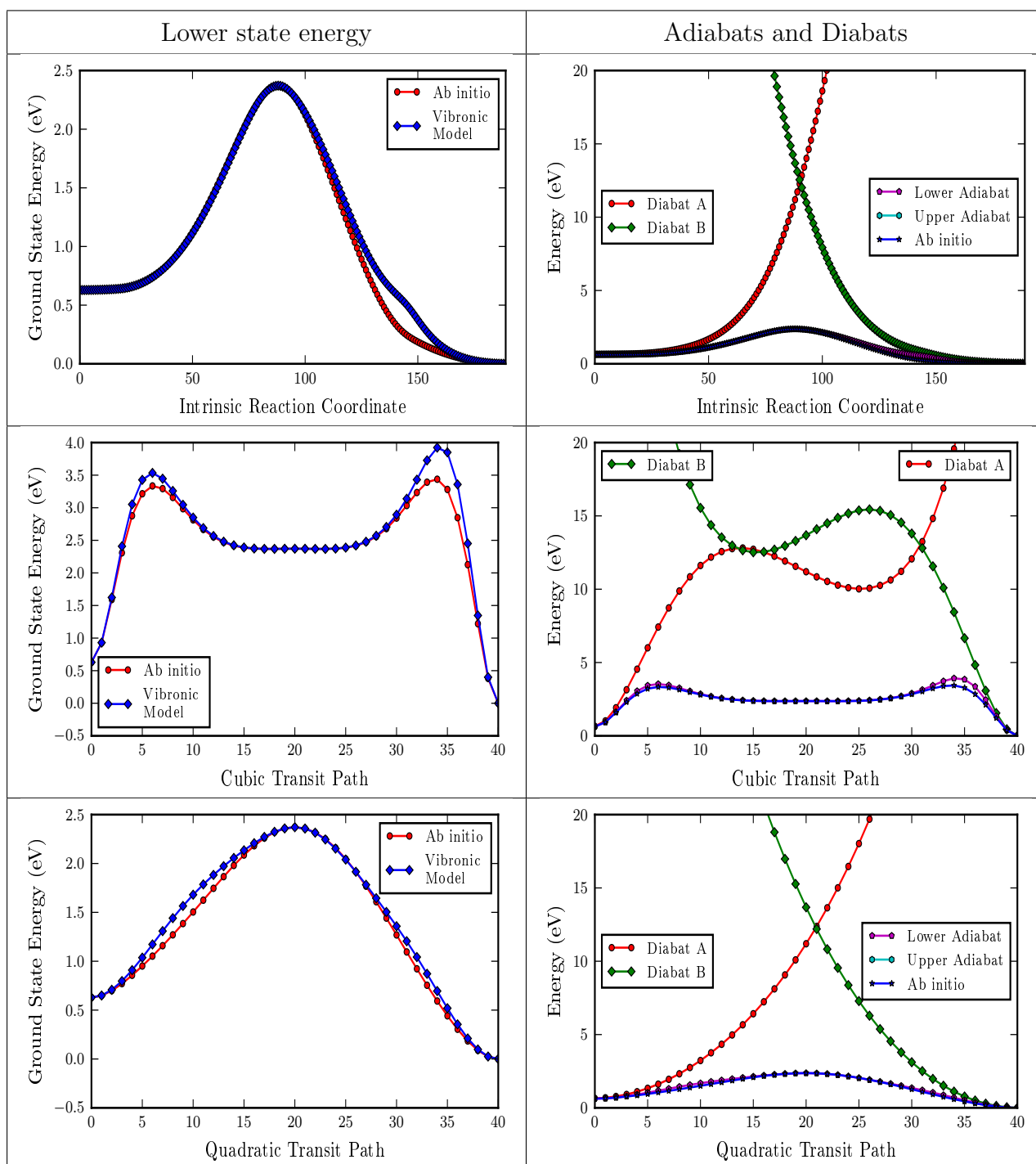


Table 2.5: Comparison of Energies for Reaction-1: Ring Opening [HF/3-21G]

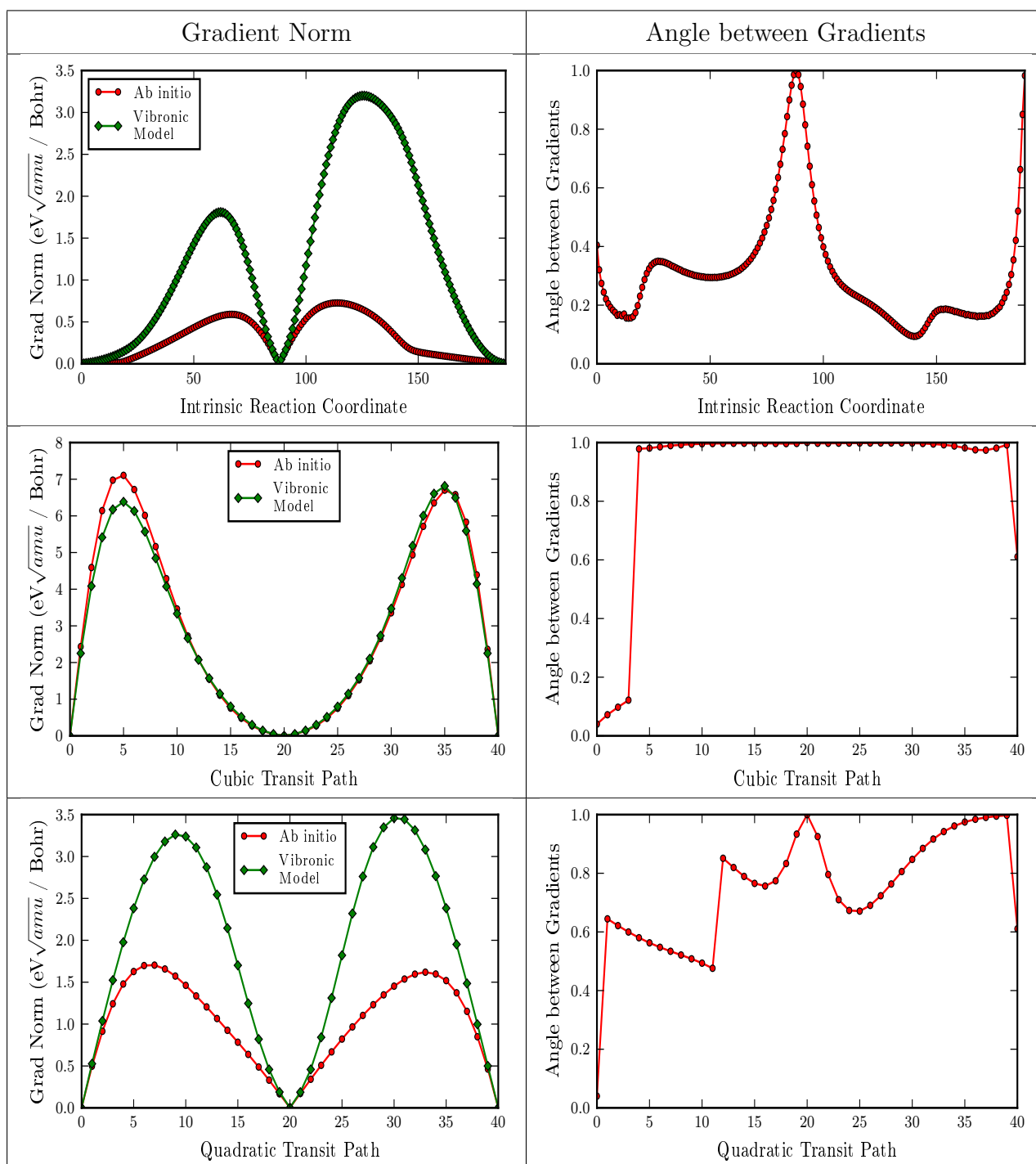


Table 2.6: Comparison of Gradients for Reaction-1: Ring Opening [HF/3-21G]

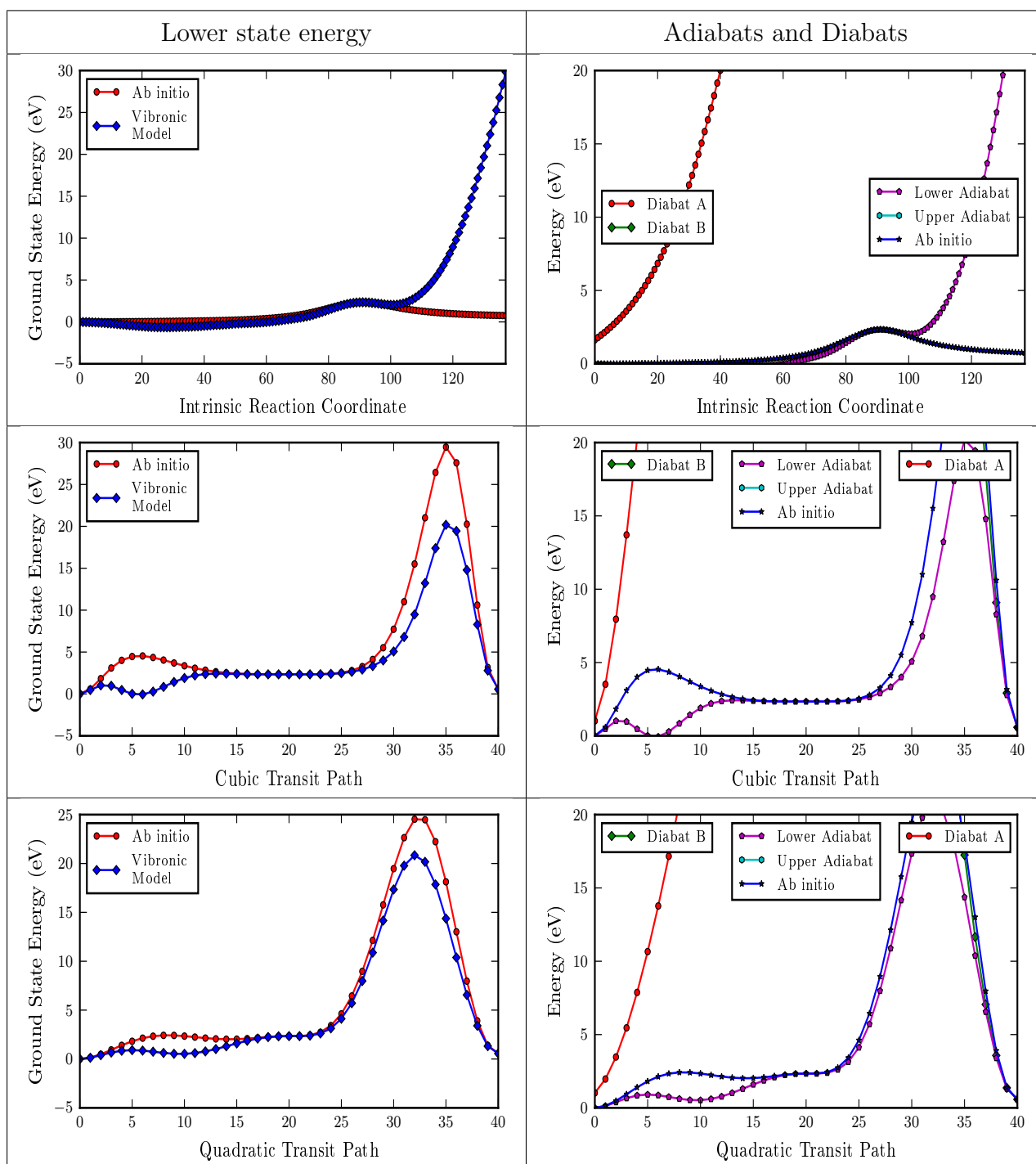


Table 2.7: Comparison of Energies for Reaction-3: Claisen Rearrangement [HF/3-21G]

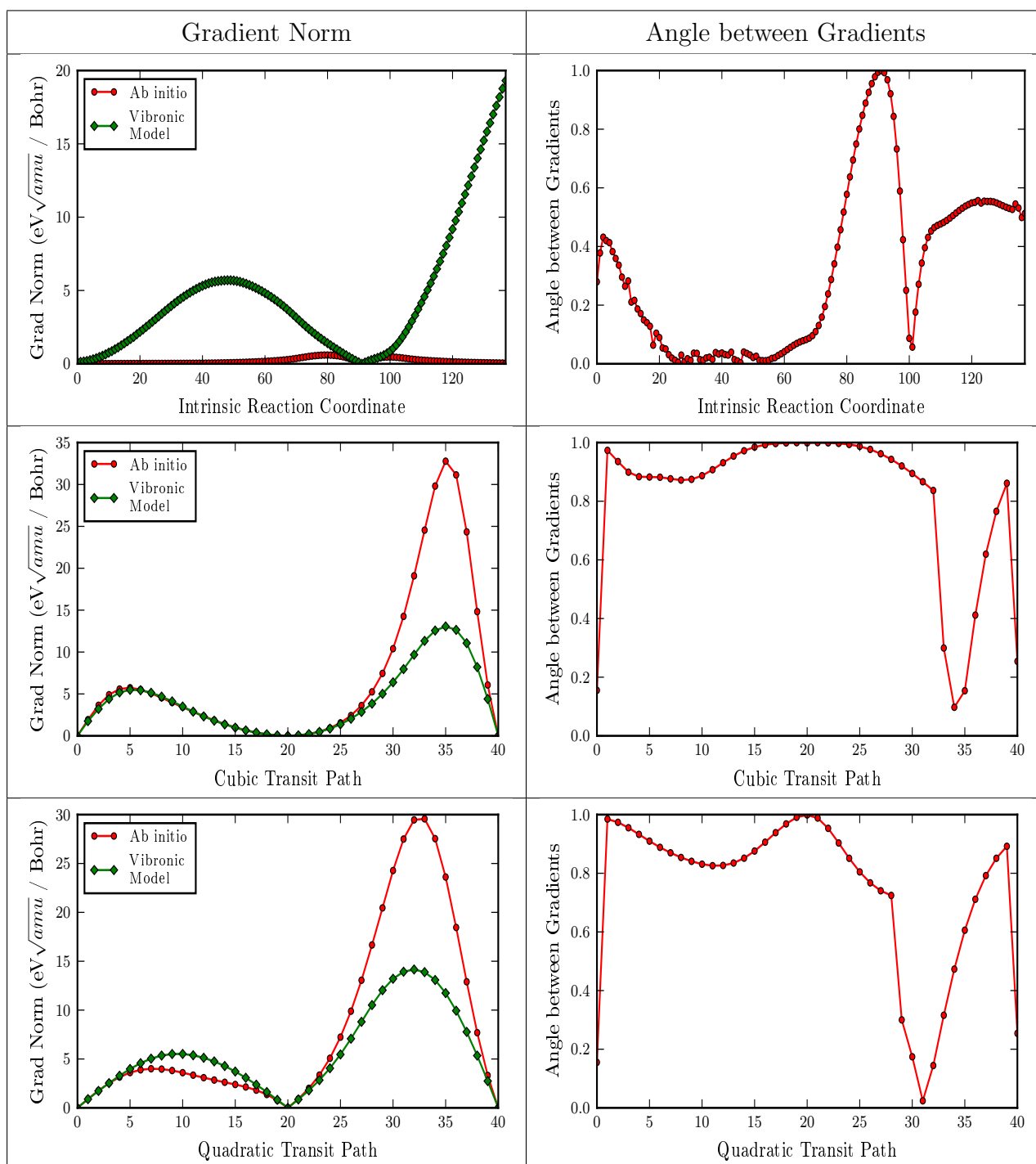


Table 2.8: Comparison of Gradients for Reaction-3: Claisen Rearrangement [HF/3-21G]

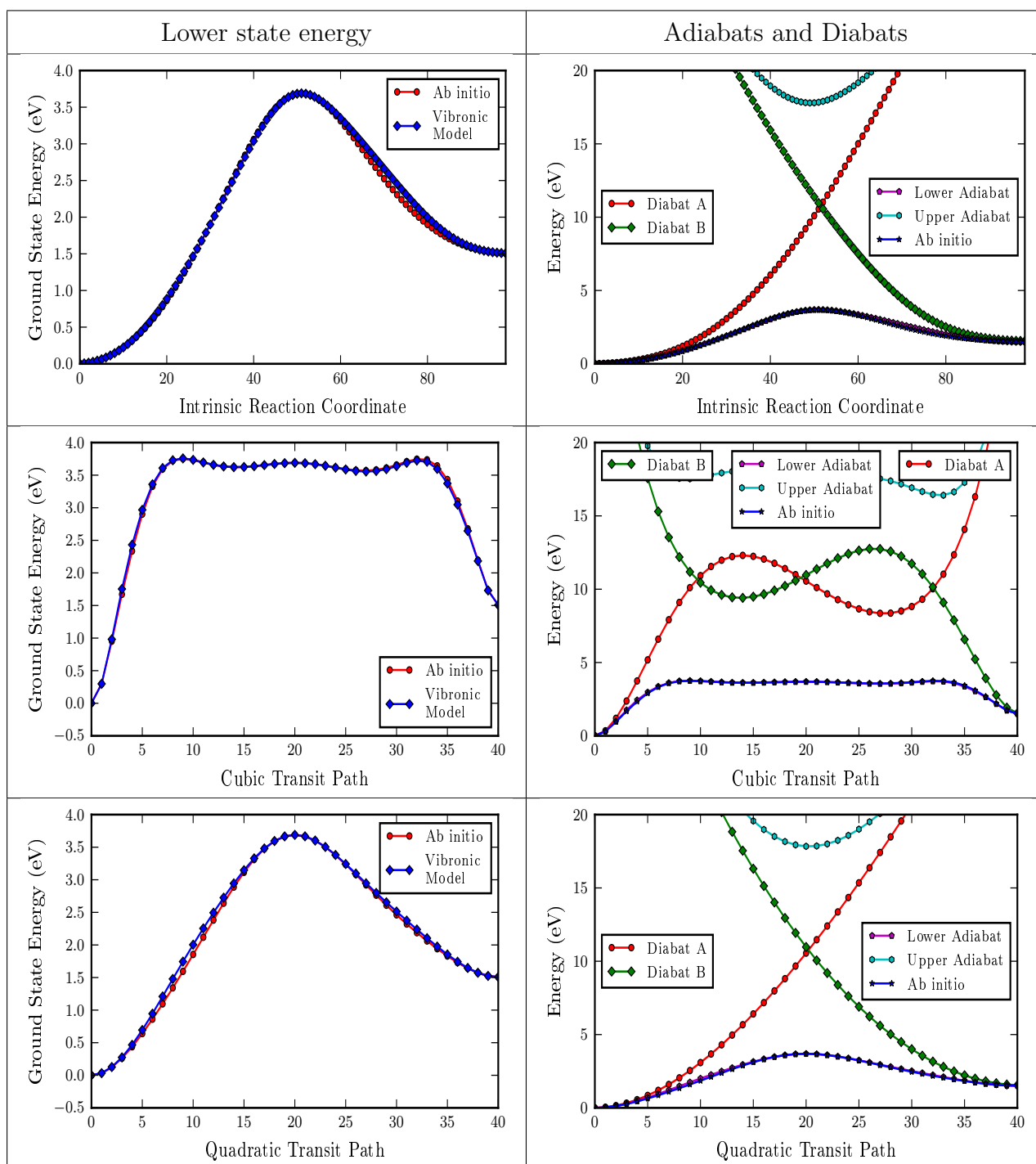


Table 2.9: Comparison of Energies for Reaction-9: H-shift [B3LYP/cc-pVTZ]

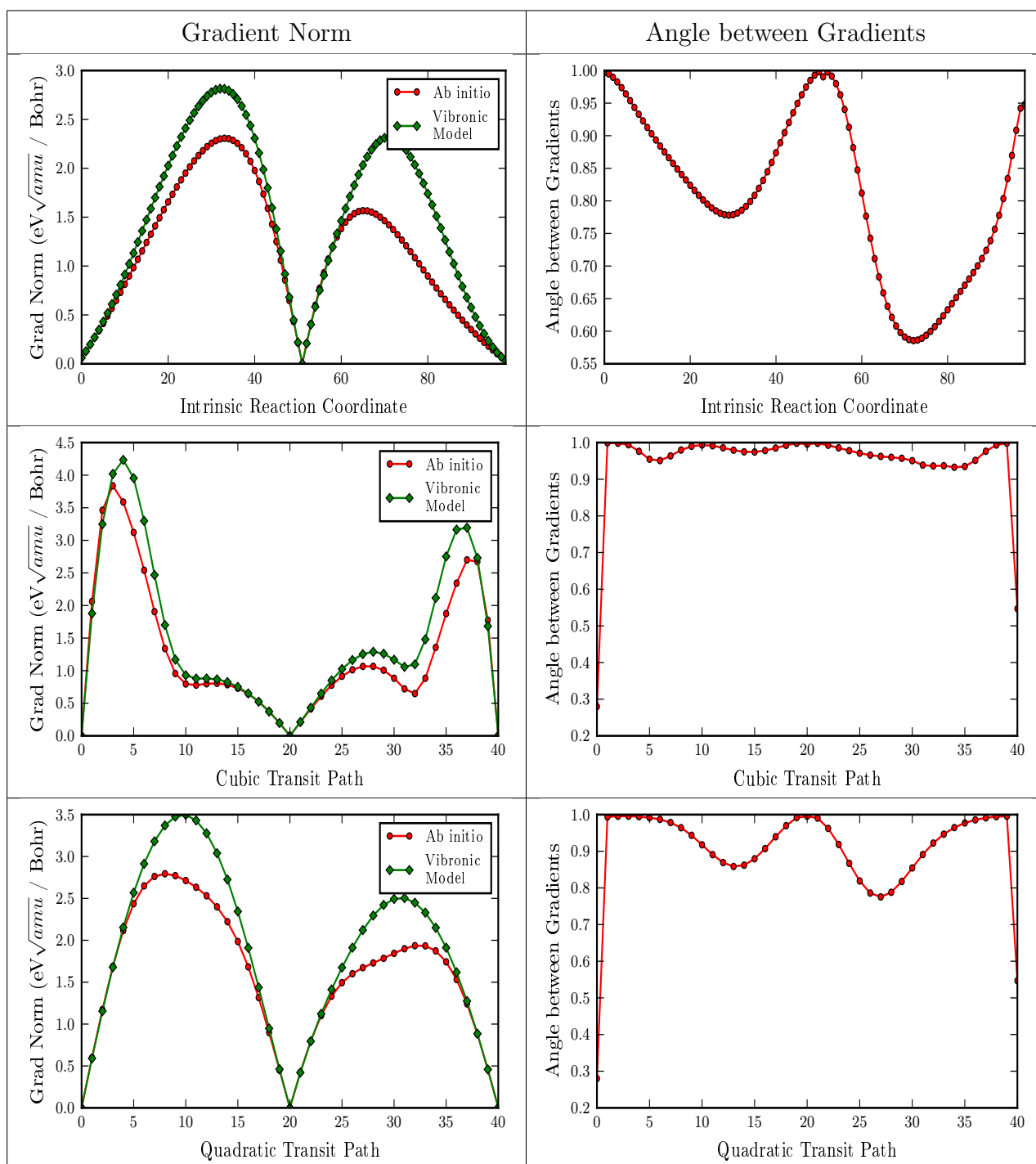


Table 2.10: Comparison of Gradients for Reaction-9: H-shift [B3LYP/cc-pVTZ]

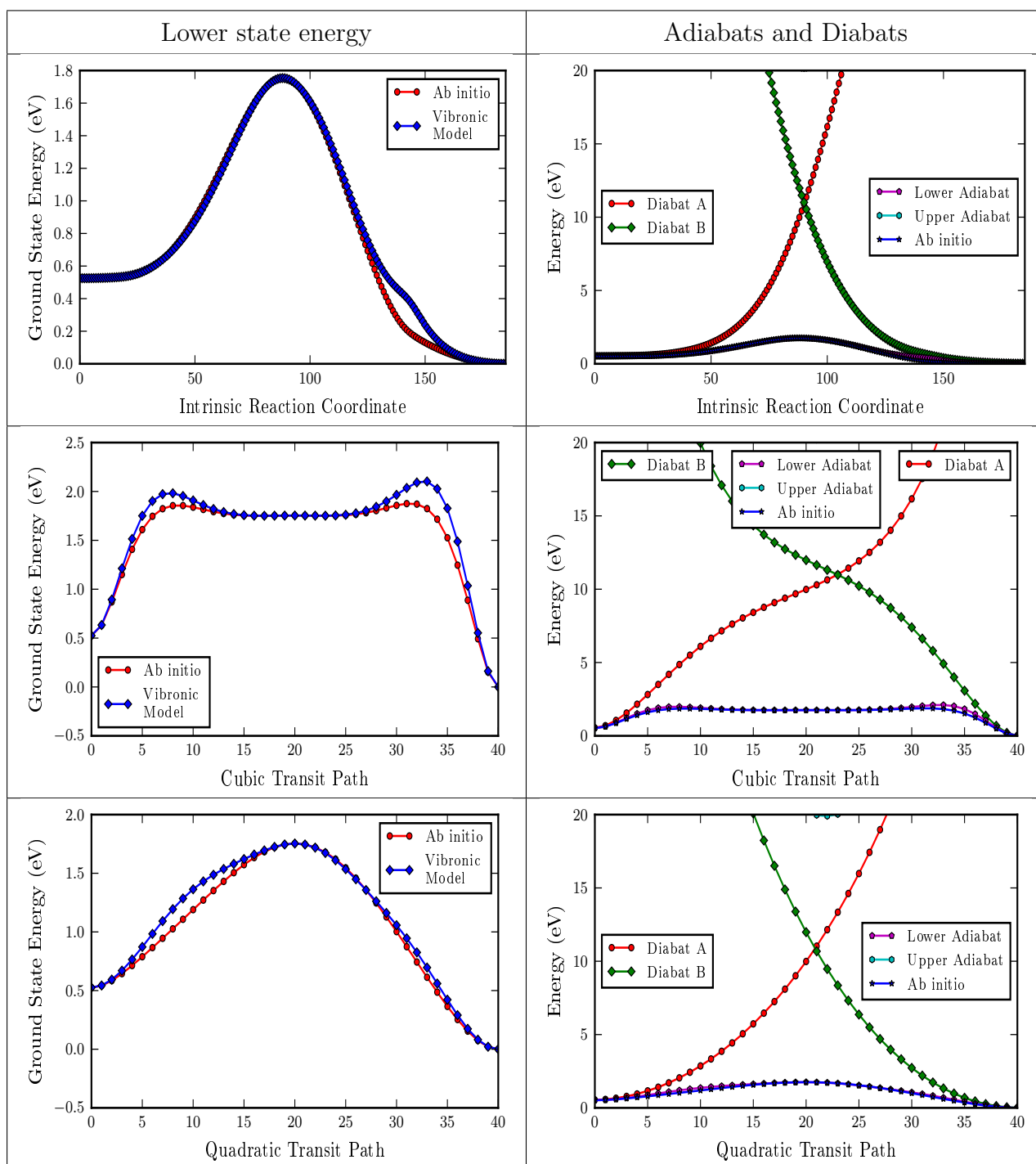


Table 2.11: Comparison of Energies for Reaction-1: Ring Opening [B3LYP/cc-pVTZ]

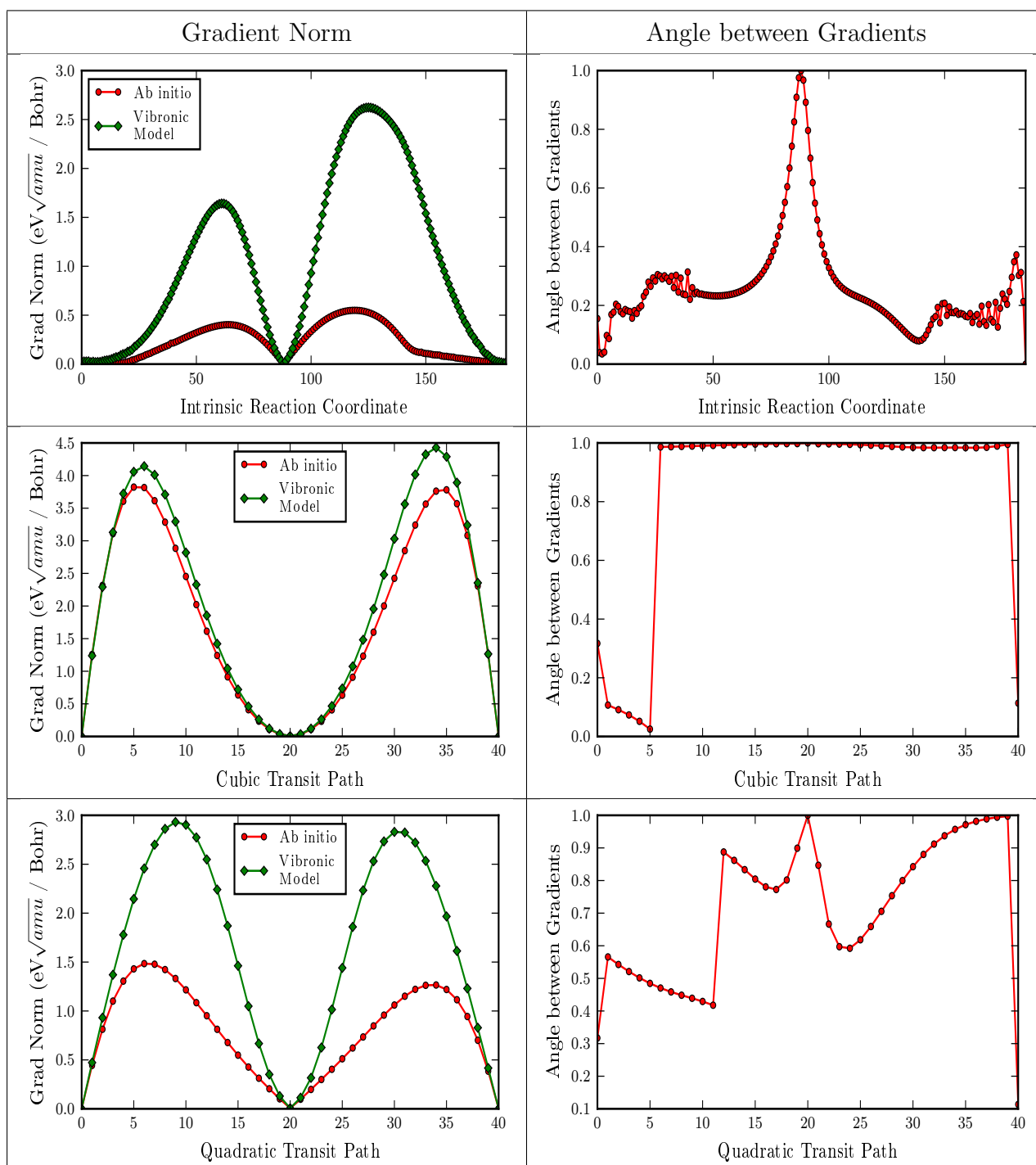


Table 2.12: Comparison of Gradients for Reaction-1: Ring Opening [B3LYP/cc-pVTZ]

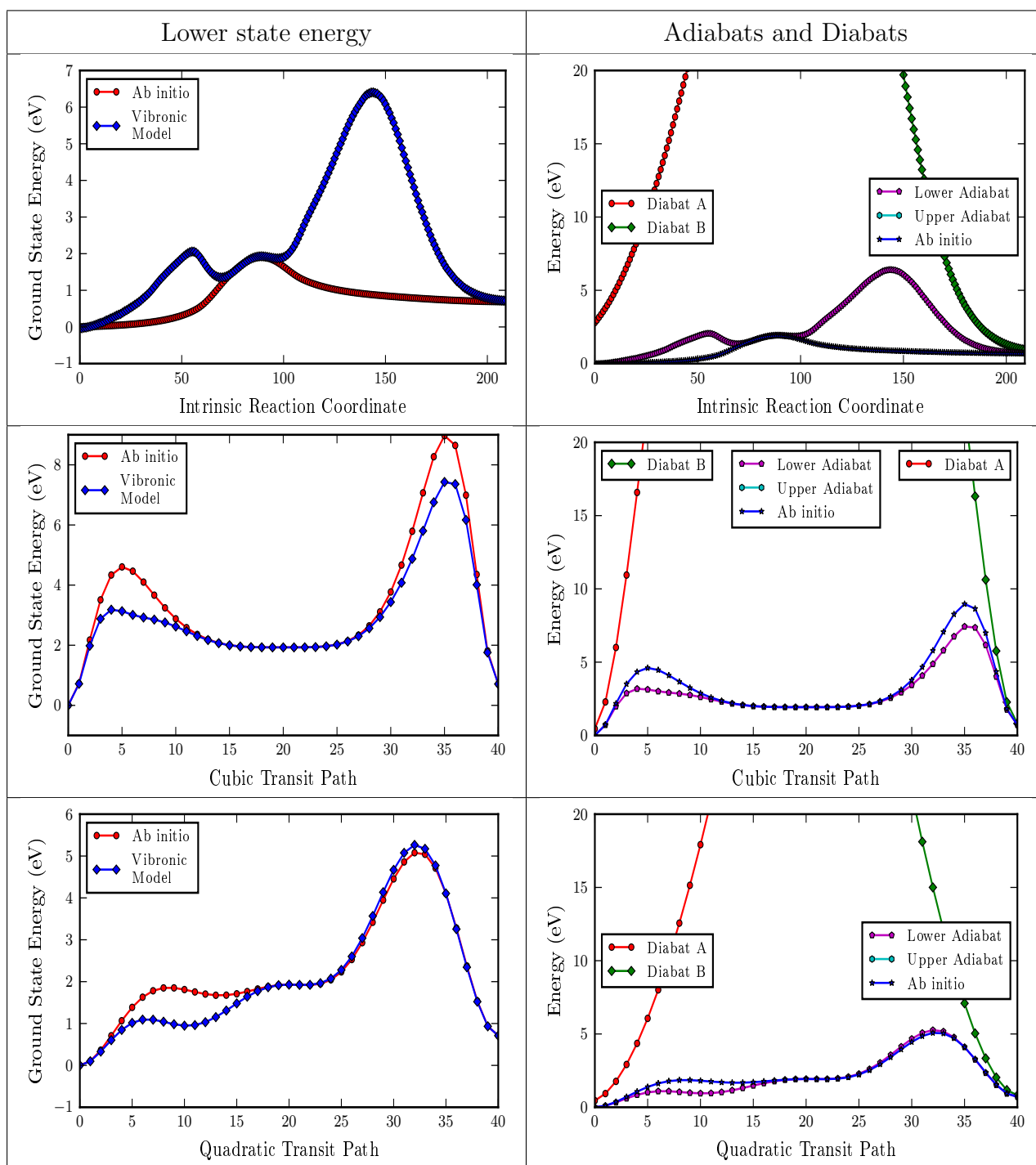


Table 2.13: Comparison of Energies for Reaction-3: Claisen Rearrangement [B3LYP/cc-pVTZ]

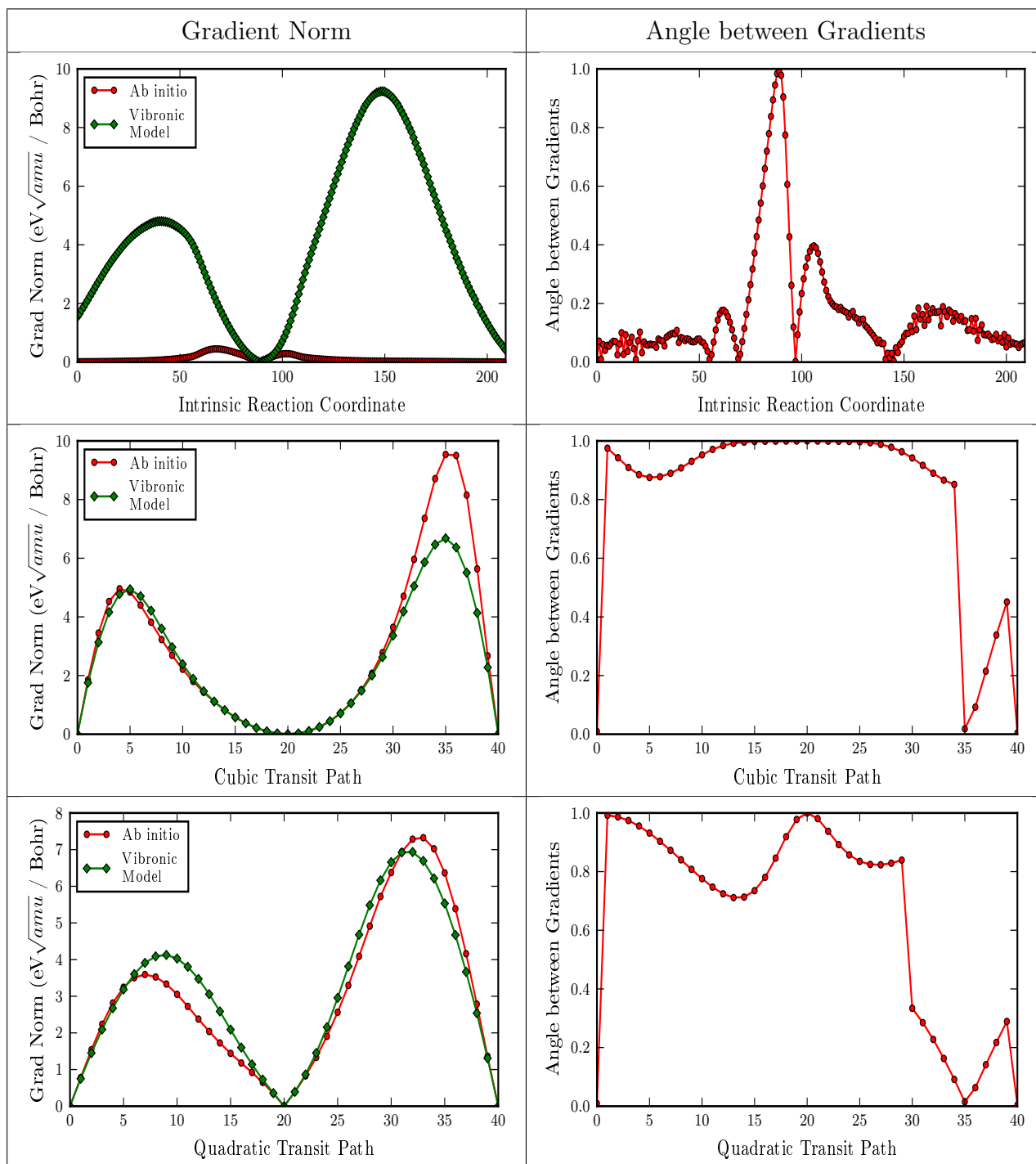


Table 2.14: Comparison of Gradients for Reaction-3: Claisen Rearrangement [B3LYP/cc-pVTZ]

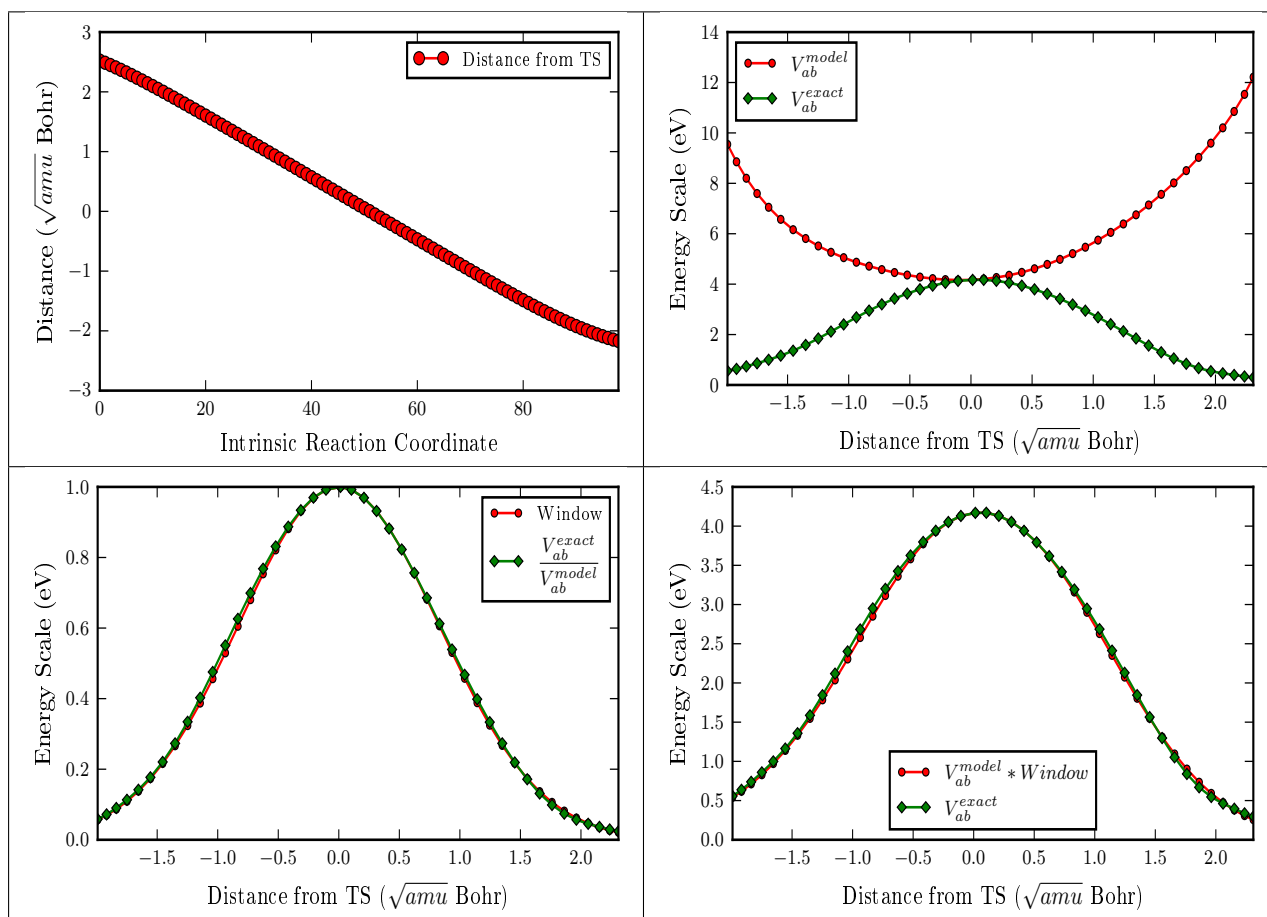


Table 2.15: Comparison of V_{ab} and Window function for Reaction 9

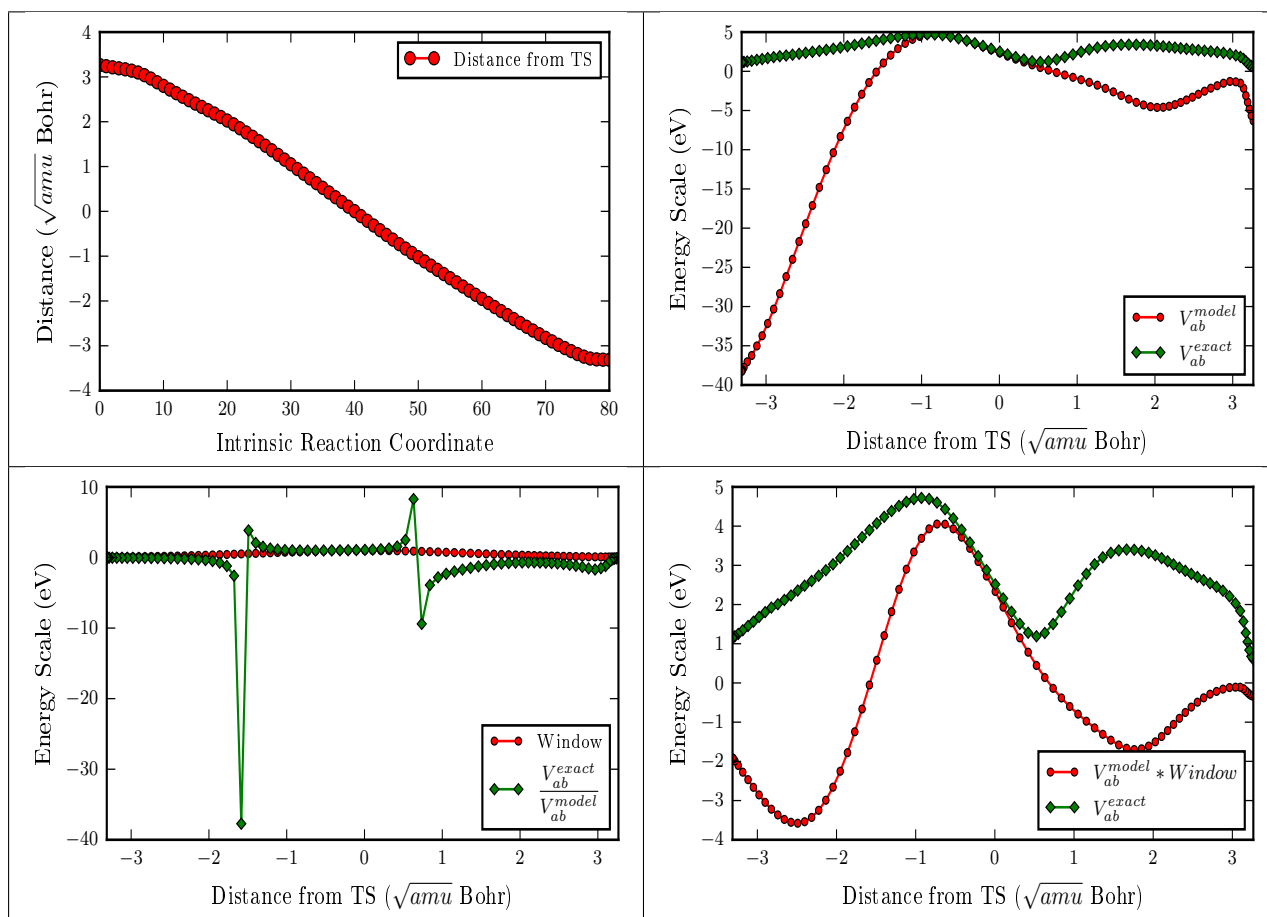


Table 2.16: Comparison of V_{ab} and Window function for Reaction 10

Chapter 3

Alternative Vibronic Model

Construction for Transition State

Search: VMTS-c

In the previous chapter the construction of vibronic models was discussed in which the models were designed to be accurate in the vicinity of minima geometries and around a reference point, which was taken to be the transition state geometry. After comparing to the corresponding ab initio data it became clear that the vibronic models are often accurate in a basin around the reference point (and minima), which can have a substantial radius, around $1 \sqrt{amu} \times Bohr$. However, at geometries further away from the critical points used in the construction of the model, the energies and in particular the gradients tend to be less accurate. Therefore, it was concluded that the models thus constructed cannot be assumed to be globally accurate, not even along a path connecting the points of interest in many cases. In addition, there are cases where even in the proximity of critical points, certain artificial features can arise, making the validity of the model questionable in those regions as well.

In this chapter, a number of modifications in the construction of the vibronic model will be presented, which aim towards making the model robust and accurate around a reference geometry, often a guess geometry for the transition state search. The range of the validity of the model will be limited to 1-2 units of distance ($\sqrt{amu} \times Bohr$), the target range for locating transition states. Given this new aim, the design of the vibronic models will be adjusted such that the models exhibit following features:

- The two diabatic states will have significant mixing throughout the search region around the guess geometry for TS. This implies that the diabatic energies at the guess geometry should be similar and the off-diagonal matrix element is *large*.
- The contribution of the window function will be minimized, as it can introduce artificial

components to gradient and hessian.

- The self-consistent criteria for the construction of vibronic model will be lifted, which means the minima regions will not be accurately represented, but this is not expected to affect the transition state search algorithm as these regions are not part of the *trust region*. The term trust region will be used to describe the region of validity for the vibronic model in an analogous way to how it is used in the field of Mathematical Optimization. [55] When the mathematical model describing an objective function (that needs to be minimized, most often) is adequate inside the trust region, the region is expanded, otherwise it is contracted. The same philosophy will be used for the vibronic model, where the objective function would be the difference in quantities calculated by the model and by using ab initio methods.
- The shape of diabatic potentials near their respective minima will be preserved (original harmonic potential).

Below, the recipe to create models which exhibit the above mentioned features will be presented, followed by examples illustrating the importance of these changes in the definition of the models.

3.0.1 Recipe for construction of new vibronic model

The following recipe is employed to create the newly defined vibronic models:

- The diabatic potentials V_A and V_B are shifted such that at the reference geometry Q_{ref} the absolute difference in energy, i.e. $|V_A - V_B|$ is $2 eV$. This will be referred to as $E_{shift} = 2 eV$.
- The constant part (E_{ab}) of the off-diagonal term in the vibronic model will be set to a large number ($E_{ab} = 10 eV$).
- The linear and quadratic coupling terms for the off-diagonal terms will be determined to reproduce ab initio data at the reference (guess) geometry, using the methods discussed in the previous chapter, but no self-consistent solution will be found, leaving the minima potential in the quadratic form of original ab initio data.
- The threshold for the window function is set in the range of $0.95 - 0.99$ virtually making the window nonexistent in the trust region.

Regarding the last point, it is also important to mention that a slightly modified form of the window function is employed here. Instead of quadratic exponent, now a quartic exponent is used. The quartic window is more shallow and decays slowly compared to the older quadratic window. Another feature is that the vibronic model parameters do not depend on the window function, unlike the previous case.

3.0.2 Illustrative and Representative Example

Since many of the issues associated with the original definition of the vibronic model appear during transition state search, at reference geometries away from the true TS geometry, it is imperative that an example should be discussed from that scenario. In one of the forthcoming chapters, the new definition of vibronic model will be employed to locate transition states, in which the transition state on the vibronic model is located in a particular cycle, and a new vibronic model is then constructed taking this new geometry as the reference. This process is repeated until the new geometry converges to the true transition state. In order to illustrate the problems associated with the original definition of the vibronic model to be applicable for such a process, a set of all such intermediate geometries are taken for transition state search corresponding to a particular reaction, using the original vibronic model. Based on the relative values of V_A and V_B , and the mixing of the diabatic states, a couple of geometries will be selected for which the detailed original model as well as the modified models will be presented and discussed. The goal is simple: to illustrate that the original definition can be problematic, and the modifications proposed here resolve the issues.

Reaction 8, a hydrogen shift reaction from the reaction data set in the previous chapter is selected for the above purpose. Starting from the first guess for transition state search, $\frac{Q_A+Q_B}{2}$, after 4 cycles into the search process, a vibronic model cannot be constructed anymore. The data at all geometries until this point is presented in Table 3.1 below.

Geometry	E_{guess}	V_A	V_B	$ V_A - V_B $	V_{AB}^{cons}	$\frac{V_{AB}^{cons}}{ V_A - V_B }$	%A	%B
1	8.9855	12.8854	11.1056	1.7798	2.8753	1.6155	0.3489	0.6510
2	3.8148	11.0479	6.6629	4.3850	4.5388	1.03507	0.2823	0.7176
3	4.3172	5.5419	9.6078	4.0658	2.5455	0.6261	0.8177	0.1822
4	3.4722	4.4873	8.1114	3.6240	2.1700	0.5984	0.8205	0.1794
5	4.5724	7.9233	4.3965	3.5268	-	-	-	-

Table 3.1: Data for Reaction-8 during TS search using original definition of the vibronic model

First the starting geometry will be examined in some detail. The data at this point is not problematic, with V_A and V_B being close in energy, and the adiabatic character at this geometry has significant mixing of A and B diabatic states. The diabatic and adiabatic surfaces, as well as energies and gradients for the lower adiabatic surface are presented along the CTP and QTP in Table 3.3. These figures look similar to the ones presented in previous chapter for the known transition states. There are deviations from ab initio data away from the critical regions, as has been the case for some cases before. However, the gradient norm comparison is especially poor, a manifestation of the presence of window function. The new models created at the same geometry are

shown in Table 3.4. The main differences between the two definitions of model appear in the form of diabatic potential shifted upwards in energy in the new model, resulting in minima region not being captured accurately. More importantly, since the window function is quite large now, the transition state region is captured more accurately, without any artificial features. It shows that although including a window (small enough, dropping off to zero near the minima) is important in order to achieve self-consistency, it can really introduce undesirable features on the adiabatic surface, such as artificial stationary points.

A more difficult situation arises at geometry #5. One of the diabatic surface lies below the true ab initio surface at this point ($V_B < E_{guess}$). In such situations, Equation 23 of the previous chapter has no real solution for E_{ab} , thus bringing the TS search process to a halt. In such a circumstance, it is essential to shift the diabatic surfaces upwards in energy in order to create a vibronic model. The curves for CTP and QTP for the new definition of model at this geometry are shown in Figure Table 3.5. These curves are shown in the vicinity of the reference geometry only. The comparison of energies and gradient norm within this range is satisfactory.

In addition to the above scans for new model, the data at all intermediate geometries is also presented for the new definition of the model in Table 3.2, to illustrate the features of the new model explicitly. It is evident that for all geometries $|V_A - V_B| = 2 eV$ and $V_{AB}^{cons} = 10 eV$, which is fixed by design. Also interesting to note feature is that now the mixing of states is always of the order of 0.5 for both diabatic states.

Geometry	E_{guess}	V_A	V_B	$ V_A - V_B $	V_{AB}^{cons}	$\frac{V_{AB}^{cons}}{ V_A - V_B }$	%A	%B
1	8.9855	13.0469	11.0469	2.0	10.0	0.2	0.4502	0.5498
2	3.8148	8.6604	6.6604	2.0	10.0	0.2	0.4502	0.5498
3	4.3172	5.4962	7.4962	2.0	10.0	0.2	0.5498	0.4502
4	3.4722	4.4869	6.4869	2.0	10.0	0.2	0.5498	0.4502
5	4.5724	6.3965	4.3965	2.0	10.0	0.2	0.4502	0.5498

Table 3.2: Data for Reaction-8 for new definition of the model at geometries during TS search using original definition of the vibronic model

3.0.3 Conclusions

It can be concluded from the above discussion that the modifications presented for the construction of vibronic model in this chapter are essential in order to implement a working algorithm for transition state search. It is also evident, as has been iterated before, that such potentials are not globally accurate and are tailor made to suit the needs of locating transition states.

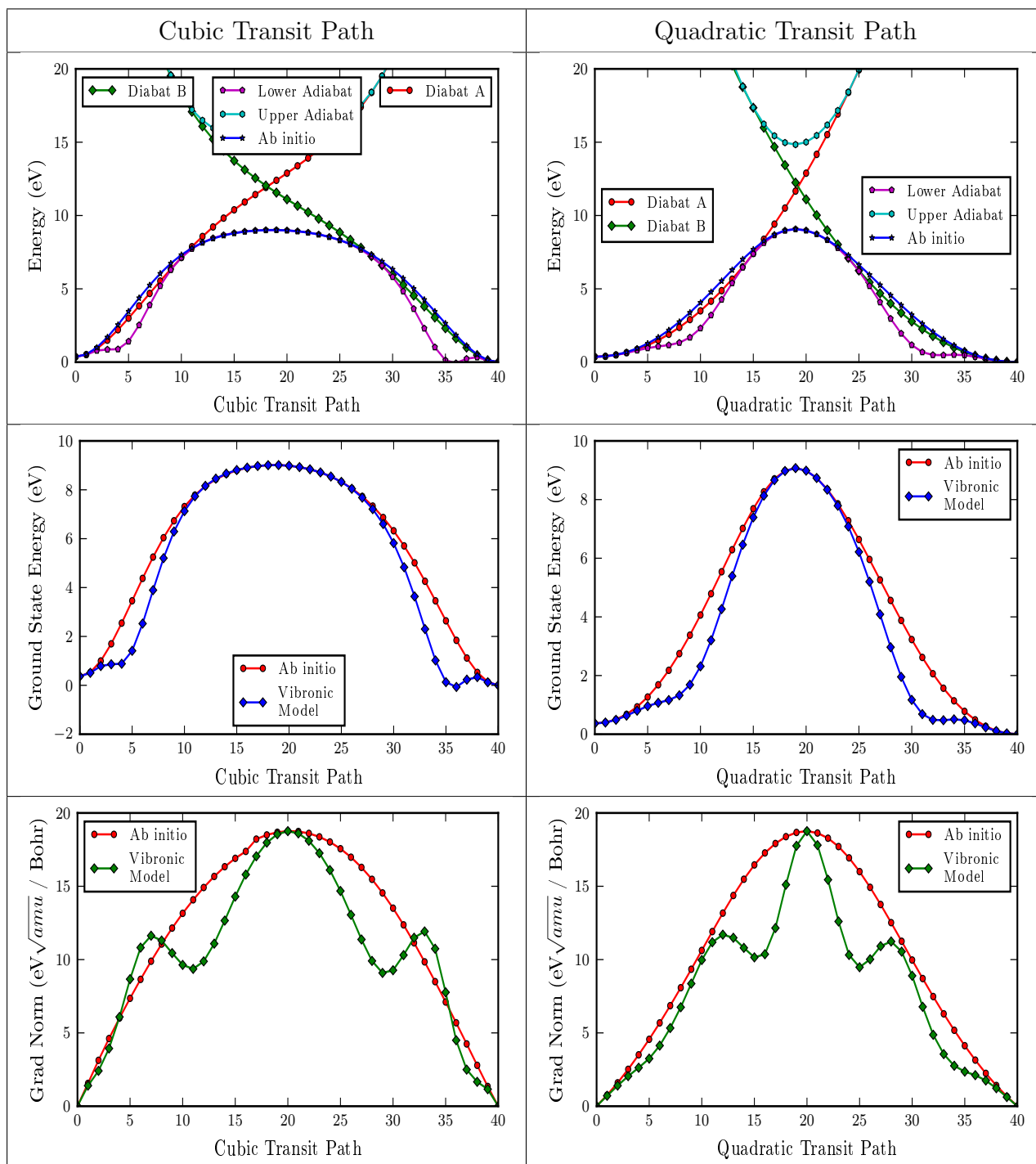


Table 3.3: Energy and Gradient Norm Comparison for Reaction 8 at first guess geometry ($\frac{Q_A+Q_B}{2}$) using the original definition of the vibronic model

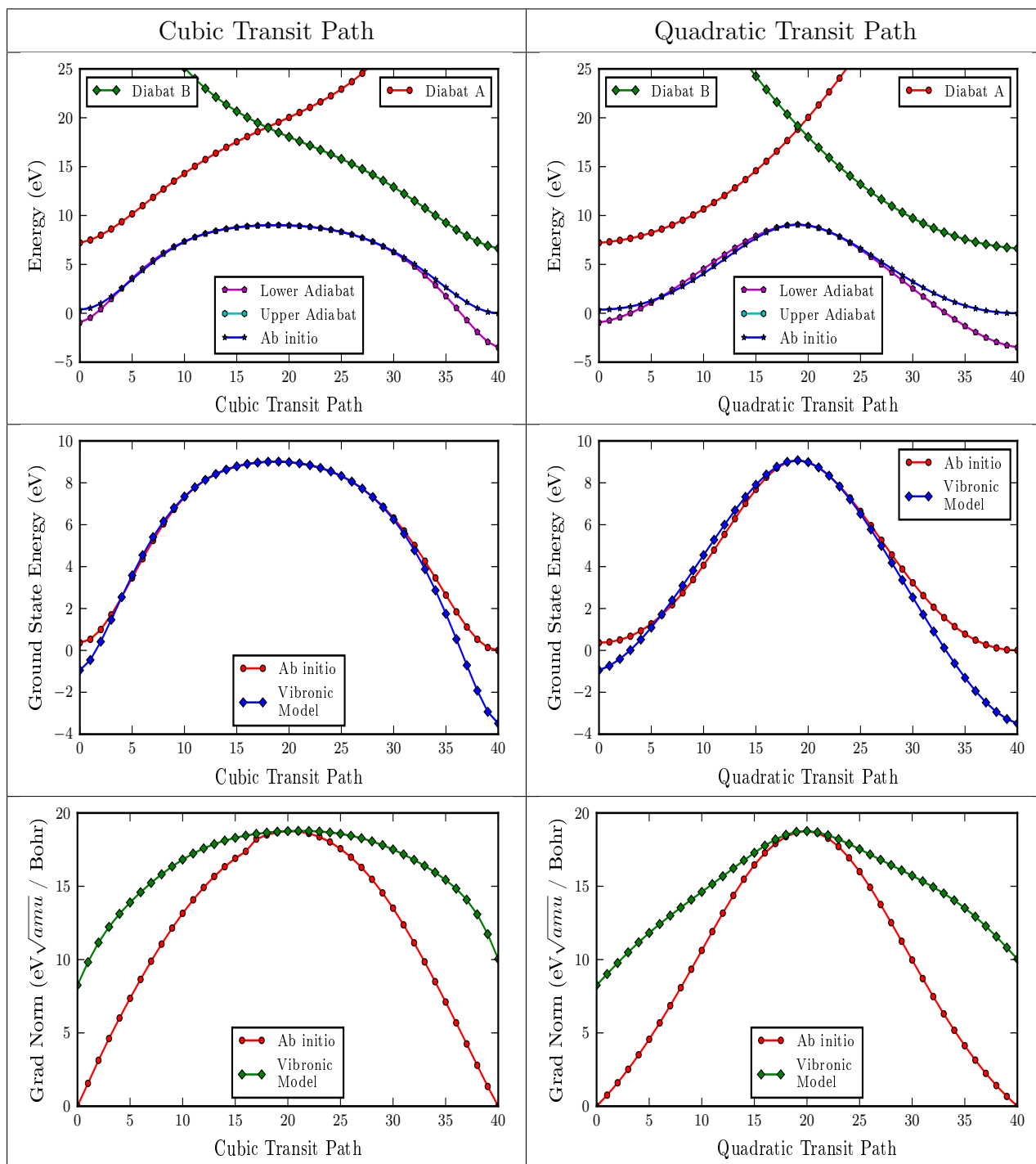


Table 3.4: Energy and Gradient Norm Comparison for Reaction 8 at first guess geometry ($\frac{Q_A+Q_B}{2}$) using the modified definition of the vibronic model

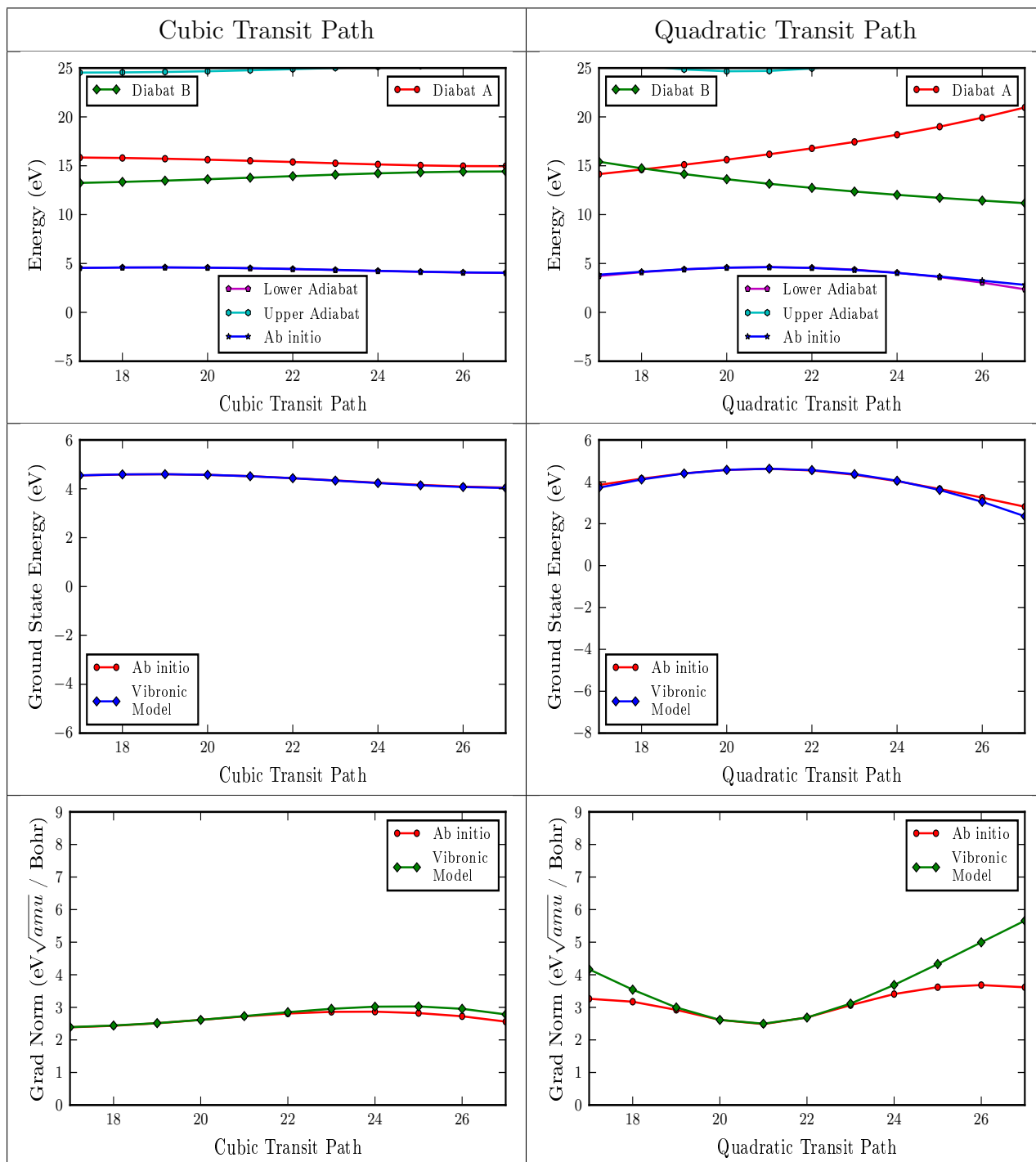


Table 3.5: Energy and Gradient Norm Comparison for Reaction 8 at an intermediate geometry using the modified definition of the vibronic model, where original model can not be constructed

Chapter 4

Transition State Optimization on Vibronic Model: VMTS-o

In this chapter we will discuss the location of transition states on vibronic models that are constructed as discussed in Chapters 2 and 3. The current algorithm and program, VMTS-o, to do transition state searches has its clear limitations, and can no doubt be improved. It is not the focus of the thesis, but it is vital to demonstrate the potential for using vibronic models in transition state searches. The current implementation is mostly suitable for fairly small molecules (less than about 30 atoms). Let us start with some general considerations, before we get into specific details.

4.1 Characterization of Transition States

Assume one has found two minima on the potential energy surface (PES) and the corresponding geometries can be characterized as reactant and product (R and P). One can traverse a continuous path between R and P, and find the highest energy point on such a connecting path. The geometry corresponding to the *lowest possible* highest energy point on any continuous path connecting R and P is what we would refer to as the transition state (TS). This is the most relevant energy and geometry in simplified rate theories. Such a point will be a first-order saddle point on the PES (One negative frequency in the force constant matrix). Finding the TS is in general a very hard problem. One might start from a guessed path and then continuously deform the path to find the lowest high-energy point on such a path. However, this is not necessarily the lowest possible high-energy point.

Another metaphor might be suitable to characterize the TS. Consider the mental imagery in which one puts the potential energy surface in a (3N-dimensional) bucket that can be filled with water. One drills holes in the PES at the location of the minima (just R and P suffices). Now

one fills the bucket with water up to some (energy) level and lets the water freeze, putting flags in the ice at the positions of the minima. If a skater can skate over the horizontal ice between R and P the ice level is higher than the energy of the TS. One can lower the level of the water / ice until the skater can no longer make trip between R and P, and at the level where it is just no longer possible the ice gets separated into different lakes that touch each other: the location of the transition state. The virtue of this metaphor is that one can easily visualize the existence of the transition state, and a powerful mental strategy to locate it. Note that even if the ice is at the proper level it is not trivial for the skater to locate the transition state, the pass between the two "lakes". A better way would be to pour a liquid (that does not stick to the ice) and see if a fierce wind would blow the liquid from one flag to the other. It would allow one to find the energy of the transition state. Even with this mental equipment in place it is still non-trivial to actually locate the transition state, and this perhaps illustrates the complexity of the question in general. Let us note that there could be multiple geometries that are all transition states with exactly the same energy (narrow strips of ice that get blocked at the same critical energy level). The presence of multiple equivalent transition states would usually reflect molecular symmetry. The only requirement for a TS to exist is a continuous PES (a function of nuclear coordinates), that is bounded from below. It does not even have to be differentiable. The vibronic model provides such a PES (which at conical intersections is not differentiable). Therefore one can identify the concept of TS associated with a vibronic model. This is a major reason to be interested in vibronic model type of construct in TS searches: It provides a simple construction for a global potential energy surface that supports the notion of a transition state.

If a TS associated as defined above with reactant and product has been located, one can define a suitable minimum energy path (MEP) that connects R-TS-P on a continuous path. One could start constructing a Reaction Path (such as an IRC) starting from the TS. Such IRCs end up in other stationary points (usually either minima or transition states). One can then construct paths all the way down, and the energy along the path would never exceed the energy of TS. It will be clear that such a definition of piece-wise paths connecting stationary points on the PES is cumbersome. The skater on ice metaphor is more intuitive. It does not need a characterization of additional stationary points along a continuous path, or the path itself.

4.2 Potential Advantages of Vibronic Model Transition State Optimization (VMTS-o)

As explained above vibronic models support the notion of a TS associated with two minima R and P on the lowest energy surface defined by the vibronic model. One can also construct continuous paths that traverse R, P and TS, such that the highest energy point on the path is located

at TS. A second key advantage is the fact that it is computationally inexpensive to calculate energy, gradient, hessian or even higher derivatives. These derivatives exist at all points at which the energies of the vibronic model are non-degenerate. In practice we have never experienced any issues with possible degeneracies, indicating that geometries during the search tend to be removed from conical intersections. Therefore, if the representation of the true PES by the vibronic model is faithful one can use powerful algorithms to find transition states that are not limited for example by the number of times the hessian on the model is calculated. In practice we currently might perform a 1000 hessian calculations during a VMTS-o optimization, while the computational expense of such a complete VMTS-o call is typically much smaller (taking on the order of seconds) than the computational expense of an electronic structure calculation of the analytical gradient at a single geometry. Currently we employ straightforward search algorithms, that are similar to the ones used in conventional electronic structure calculations. However, the vibronic model leaves open the possibility of very different search strategies, e.g. the Jacobi type algorithms explored by Dey and Ayers (*et al.*). [56] We wish therefore to emphasize the open-ended nature of VMTS-o in principle.

4.3 Limitation of Vibronic Model Transition State Optimization (VMTS-o)

The most serious limitation of the vibronic model is that it has a somewhat limited range of validity, as discussed in previous chapters. It tends to be accurate within a radius of about $1 \text{ Bohr} \sqrt{amu}$ (or 1 'unit'). Therefore, even if it is in principle possible to locate a TS in the above sense for the vibronic model, it may really be an artifact of the model, meaning that the TS on the model is far removed from the true transition state. The vibronic model may also have additional artificial minima. In such a situation it is not unlikely that a first-order saddle point exists on the model, that is much closer to the true transition state, but is not the highest point on a continuous path. In practice therefore we have decided to locate the first-order saddle point on the VM that is close to the reference point (the current best guess for the transition state geometry). For this reason more conventional search algorithms are used that are based on local quadratic models, using gradients and Hessians defined by the vibronic model. These gradients and Hessians are easily evaluated, and this remains a major advantage of vibronic models. However, this feature of limited validity of the VM means that we shy away from powerful TS search algorithms like nudged elastic band, which would be potentially very useful. Even if we restrict the search to finding a first-order saddle point close to the reference point, it may be that such a point is outside the range of validity of the VM. For this reason the VMTS-o algorithm always yields a "best" guess for the TS that lies within a user defined radius in mass weighted Cartesian met-

ric denoted as "MaxD" (maximum distance). This defines the trust region associate with the vibronic model, which was briefly noted in the previous Chapter. This means the algorithm tries to locate the transition state, and the algorithm simply exits if the last geometry determined by the iterative algorithm exceeds this radius, and returns the previous penultimate geometry, which would still satisfy the trust basin criterion.

There is another serious issue that can arise due to the limited accuracy of vibronic models. It is possible that there are no problems finding a TS on the model in the vicinity of the reference point, Ref-1 say. In the next cycle of VMTS-o a new model is launched at the converged geometry Ref-2, and again a transition state is found on the model, but this might bring us back close to the original reference point Ref-1. This can lead to oscillations in the search procedure while in every step the VMTS-o optimization itself experiences no difficulties whatsoever. Such a repetitive cycle can arise over multiple steps, and one would observe a more or less cyclic pattern in subsequent iterations that never converges. At this point in time we do not have a solution for this problem. Let us emphasize that this constitutes a potential flaw in the VMTS-o approach that needs an additional fix. The search algorithm for a given vibronic model would work optimally (locating the transition state at every step), but the overall procedure does not converge. A possible solution might be to use extrapolation of geometries from different VMTS-o searches, in the spirit of DIIS [57], but now for a sequence of geometries.

There are other, more mundane, reasons that VMTS-o may experience troubles, and these are simply due to the difficulty of locating transition states. The PES from the vibronic model in principle has the same richness as the true PES, and it may be hard to find transition states for the same reason that it may be hard in other strategies based on local update procedures. Hence the current version of VMTS-o may simply be unable to locate a transition state, even if it would appear one is present within the trust region. The fact that one can calculate the hessian easily and exactly (on the model) means one can use advanced search strategies, without the cost of the search increasing rapidly. However, more sophisticated search strategies may need to be developed, explicitly exploiting that the hessian can be calculated at little cost, or one could potentially exploit the fairly large trust basin of the model to use more global VMTS-o strategies, rather than local updates based on gradient and hessian. This avenue of research is left for the future.

There are some other subtle issues as the current vibronic models are defined in terms of $3N - 3$ normal modes with respect to the reference geometry. The energy of the vibronic model is not invariant under rotations of the molecular geometry, which is unphysical. Therefore, whenever a geometry is accessed in VMTS-o it is first aligned with the reference geometry. Moreover, when a gradient or hessian is calculated, the rotational degrees of freedom are projected out from the VM gradient and hessian. Hence the hessian has always at least 3 zero eigenvalues. The current

version of the code is not tested for linear geometries. The program will terminate when there are less than 3 zeros for the hessian at any time during the optimization. Whenever we mention geometries, gradients or Hessians below they will also be aligned and projected quantities to reflect the rotational invariance of the true problem.

Before we describe some more of the details it is useful to identify modes of termination for an individual VMTS-o run on a given vibronic model.

- **0.** The program has located a transition state (gradient below convergence threshold and one negative eigenvalue of the hessian).
- **1.** The program has obtained a geometry during the search that is outside the trust region for the model $|q - q_{ref}| > MaxD$.
- **2.** The program has found a stable point ($|\Delta q| < \tau_{conv}$) within its algorithm, but this point is actually not a transition state. It could be a hill-top (two negative eigenvalues), or a minimum on the model. Most often the issue arises in conjunction with an inflection degree of freedom, which is characterized by a zero second derivative, but non-zero gradient along this degree of freedom. These are attraction points for second-order Newton procedures and the algorithm can get stuck in these situations.
- **3.** VMTS-o runs out of cycles (currently 200). The program exits and simply returns its best guess for the TS geometry.

The main program VMTS that does geometry optimization and obtains a new vibronic model when required, does not check for the status of the VMTS-o step but simply continues. It is a frequent occurrence that VMTS-o does not terminate satisfactorily (i.e. status 0 or 1), but the problem disappears as the vibronic model is updated and the program continues to converge, eventually. As mentioned before, it is possible that VMTS-o repeatedly terminates in its ideals status, 0, and still the overall optimization runs in circles and does not converge. This is an issue that is unrelated to VMTS-o, as indicated before. In the following, the current TS search algorithm on the vibronic model is described in some detail.

4.4 Basic algorithmic steps employed in VMTS-o

1. *Augmented_Hessian_Update*

The hessian is diagonalized. If the hessian has at least one negative eigenvalue, one eigenvector with negative eigenvalue is selected which has the maximum (absolute) overlap with a path direction (usually $\mathbf{q}_P - \mathbf{q}_R$). For all other negative eigenvalues the sign of the eigenvalue is reversed. The gradient is transformed to the eigenvector basis and a Newton step is

taken $\Delta q_\lambda = \frac{g_\lambda}{\omega_\lambda}$ (for non-zero eigenvalues). The step $\Delta \mathbf{q}$ in the eigenvector basis is transformed back to the original basis. The augmentation aspect comes in by restricting the maximum value of Δq_λ (in the hessian eigenvector basis) to a fairly small `max_step` ($0.05 \sqrt{amu} \text{ Bohr}$), for each Δq_λ . In the literature the restriction of the stepsize while approximately taking a Newton step is often done a bit differently. Here `max_step` is small, and we simply recalculate and diagonalize the hessian more frequently than usual. It can happen that in subsequent augmented hessian steps the step $\Delta \mathbf{q}$ oscillates. This is monitored by calculating the inner product between subsequent normalized steps. If this inner product is close to -1 (< -0.9 in practice), the `max_step` is reduced by a factor of 2. It is a clear sign that the step size is too large, and we simply reduce `max_step` as long as oscillation is present (until an absolute minimum of $1e-4$) is reached). `max_step` can also be increased upto an absolute maximum (0.2), by factors of 2 if the inner product between subsequent normalized updates is close to 1 (> 0.9 in practice). This indicates we are making small steps in the same direction, and we can move more aggressively. The dynamic `max_step` is primarily helpful to get through some difficult regions.

If the hessian in this procedure has no negative eigenvalues a different branch is taken altogether.

2. *TS_line_search*

If the hessian has exactly one negative eigenvalue VMTS-o climbs uphill in this direction until a maximum has been found (gradient in the search direction vanishes) or until a maximum stepsize ($0.2 \text{ Bohr} \sqrt{amu}$) is encountered. This maximum stepsize is in regard to the initial geometry in the subroutine. Because it is cheap to calculate the hessian in VMTS the negative eigenvector is updated in every small uphill step and the path can be somewhat curved. It is found to be beneficial to climb up fast in the direction of the "reaction coordinate" and to maintain the maximum in this direction while moving more slowly in the orthogonal directions towards the minimum, which is done in the *Augmented_Hessian_Update* procedure.

3. *Transit_path_climb*

If the hessian does not have negative eigenvalues, a quadratic transit path, $\mathbf{q}(s)$, (see Chapter 2) is constructed that goes through R, P and current \mathbf{q}_c . The path is partitioned in typically 25 small steps in s , and a geometry $\mathbf{q}(s_i)$ is determined along the path at which the hessian has exactly one negative eigenvalue, while $|\mathbf{q}(s_i) - \mathbf{q}_{ref}| < \frac{MaxD}{2}$. We try to be removed from the full *MaxD* and stay well in the trust region, such that there is sufficient room to optimize the geometry away from the transit path. The subroutine selects among the valid points that specific point that has the *most negative*, among negative eigenvalues. It may be that two values of s_i along the path can be found (on either side of \mathbf{q}_c).

The algorithm then selects one of the points according to this "most negative eigenvalue" criterion. After this it proceeds with *Augmented_Hessian_Update* steps and subsequent *Transit_path_climb* steps as it often loses the negative frequency in the process. As it goes through this procedure it switches to using a cubic transit path (see Chapter 2) using path direction from a previous negative frequency eigenvector.

4. *Minimize_Subspace_Determinant*

A complicated situation for TS searching based on locally quadratic approaches is the occurrence of inflection points. At such a point the eigenvalue of the hessian goes through zero and changes sign, while the gradient along the corresponding eigenvector is non-zero. These situations can occur for the climbing direction of interest, meaning that one loses the negative eigenvalue of interest as one climbs up hill. We do not have a good practical solution for this particular situation at this stage, and more discussion on this follows below. Another situation that arises quite frequently is that one obtains a second (small) negative frequency during the iterations. This also indicates an inflection point, but here the frequency changes from positive to negative. We can refer to it as a secondary inflection point as the climbing frequency remains clearly negative throughout. Again, it can be hard to move away from such a point as the Newton procedure tends to oscillate around such a point (gradient is more or less the same, while frequency changes sign in the eigenvector basis of the hessian, giving rise to +/- `max_step` in the update step since frequency is small). For this situation it appears one can often get away from the troublesome geometry by minimizing the determinant (d) of the hessian projected on the subspace of interest (usually two-dimensional: the negative climbing vector and the eigenvector with small (non-zero) eigenvalue). In this procedure one uses a finite difference technique to calculate

$$d_0, \frac{\partial d}{\partial q_i}, \frac{\partial^2 d}{\partial q_i^2}$$

$$d(\Delta q_1, \Delta q_2) \approx d_0 + \sum_{i=1}^2 \left[\frac{\partial d}{\partial q_i} \Delta q_i + \frac{1}{2} \frac{\partial^2 d}{\partial q_i^2} (\Delta q_i)^2 \right] \quad (4.1)$$

At the initial geometry one has $d > 0$ as there are two negative eigenvalues. The procedure then minimizes the determinant, attempting to make it negative, and maximizing the saddle point character (product of negative and positive frequency which constitutes the determinant). If the second derivative of the determinant is negative one limits the size of the step to some maximum value (0.2 currently). In the above formula we neglected the off-diagonal quadratic coupling, and this simplifies the procedure. It should be noted that in effect one calculates the second derivative of the subspace determinant, which involves really a fourth order derivative of the energy. In practice we recalculate and diagonalize the (projected) hessian in a set of slightly displaced geometries to construct the determinant.

This procedure is often quite efficient to move away from "secondary" inflection points, and the change in both q_1 and q_2 is crucial. Let us note the advantage of the vibronic model in this respect. The procedure could be implemented in electronic structure calculations, but it would take substantial effort and computation time. In the context of VMTS-o there is negligible effort involved.

The above procedure might also be effective to switch between the climbing direction and the small frequency direction. This would indicate the presence of a Valley Ridge Inflection (VRI). [58] This however can only be achieved if both climbing and inflection frequency are small. We do not seem to have encountered such situations in practice yet.

5. *Locate_Inflection_Point*

As discussed above, a cumbersome situation occurs if the climbing frequency of interest changes sign, while climbing up hill. One loses the negative frequency while climbing up hill. In VMTS-o an attempt is made to make a quartic approximation to the energy (cubic approximation for the gradient) along the climbing direction, and to locate the true (real valued) maximum. Often this geometry is far away, and the procedure does not seem to work well in conjunction with geometry optimizations for the other degrees of freedom. It is possible the code has a bug at this time. In practice the decision is made to optimize for the inflection point itself and zoom in on a point with an additional zero frequency (besides the 3 zero frequencies due to rotation). This is fairly easy to accommodate as part of the *TS_line_search* procedure. We repeatedly encounter a change of frequency and have to climb up hill in the search direction, to regain the negative frequency. However, one keeps falling back to the inflection point. At some point the decision is made to optimize the inflection point instead. The gradient upon convergence is non-zero, but the frequency of interest is, and the change in geometry is close to zero. Then in the main subroutine in VMTS a new hessian is constructed, and a new call to VMTS-o is made. It is not infrequent that during this optimization process by accident we move away from the inflection point, and after some hurdle VMTS overall converges to a first-order saddle point. There is no design to this and of course one is not always so lucky. It appears the occurrence of "primary" inflection points is a major remaining issue for which a more satisfactory solution is needed.

4.5 Main VMTS-o Algorithm

In general the VMTS algorithm proceeds as follows:

- Initially we usually have more than one negative eigenvalue. VMTS-o makes calls to *Augmented_Hessian_Update* and makes small updates in geometries. Usually this work well,

and either MaxD is reached (status 1), or one reaches the region with one negative eigenvalue.

- Alternatively, initially there is no negative eigenvalue, and VMTS-o makes calls to *Transit_path_climb* and *Augmented_Hessian_Update* to reach a stable region with one negative eigenvalue. Also this strategy usually works fairly well.
- If the gradient is considered to be small enough and the hessian has one negative eigenvalue, VMTS-o uses a sequence of calls to *TS_line_search* and *Augmented_Hessian_Update*. If an additional negative eigenvalue is encountered the procedure *Minimize_Subspace_Determinant* may be invoked. This is the common mode of operation in a smooth convergence in VMTS-o.
- On occasion we encounter the dreaded primary inflection point. VMTS-o then proceeds to locate the inflection point. Upon convergence to the inflection point (gradient is zero in all other directions), it makes a second attempt using *Transit_path_climb* and a cubic transit path to find a region with one negative frequency. Often VMTS-o then finds its way back to the original inflection point. At that stage VMTS-o gives up and returns command to VMTS. Sometimes a new vibronic model resolves the issue, but at other times it does not and VMTS fails to converge. In any case primary inflection points are a known issue for VMTS-o, but one expects a solution for this problem to exist.

In the next chapter we will discuss results of the procedure. Let us mention here that it is felt that VMTS-o can be substantially improved. However, it is not the focus of this thesis. The VMTS-o procedure has been developed by M. Nooijen for usage with VMTS, and it is used as more or less of a black box procedure in the context of the thesis. More systematic investigations are needed to clearly delineate the problems. The project has certainly led to a deeper appreciation of the difficulties in locating transition states.

Chapter 5

Vibronic Model Transition State Search: Results

5.1 Introduction

In previous chapters, the idea of using a vibronic model in order to find transition states (VMTS) has been encountered on multiple occasions. In Chapter-3, the construction of such a model was discussed, which was based on the original definition of Chapter-2 but with certain modifications. In Chapter-4, the methods used in the actual search engine were discussed, along with a detailed discussion of pros and cons of using a vibronic model in order to locate transition states. Therefore, the underlying theory and the necessary tools are now established to start applying this idea to real systems. In this chapter, a test suite of 36 Unimolecular reactions will be benchmarked for locating transition states against the algorithms implemented in Gaussian09. While most results will be of statistical nature, looking at overall performance for all the reactions together, a handful of reactions will be discussed in detail, primarily to highlight interesting and / or important features of VMTS approach, in particular to highlight its failure for certain cases and what can be done to prevent such scenarios and improve the algorithm.

The basic outline of a VMTS algorithm can be understood as follows: a vibronic model is constructed at a starting guess geometry for the transition state, which is also the reference geometry, using the methods discussed in Chapter 3. This vibronic model has a transition state of its own (or the highest point on the relaxed path, as discussed in the previous chapter), which is found using methods discussed in previous chapter, i.e. using VMTS-o. This new geometry is then checked for convergence by evaluating the ab initio gradient. If it is a true transition state, i.e. if all the components of the gradient are zero (less than a threshold) the job is done. If not, a new model is constructed at this geometry and the process is repeated until the true transition state is found. There are two main aspects of this process based on which there will be a few

variants of this approach, which will be discussed next. A primary issue is the evaluation of ab initio hessian at a geometry given by VMTS-o at a particular cycle. As hessian computations can be computationally very expensive for most ab initio methods, one has to make a choice on the nature of hessian update. Another issue that most commonly arises in locating transition states is the choice of starting guess geometry. A good guess can significantly speed up the search process, but figuring out a "good" guess can be a nontrivial task and a couple of variations in this context will be discussed. Based on these two criteria - hessian update and starting guess geometry - variants of VMTS approach are discussed below.

5.2 Potpourri of VMTS Schemes

Several variations of VMTS are presented below based on how the hessian is updated during each cycle.

1. **Small:** In this version, the ab initio data including the *exact* hessian at each new cycle is computed at the same level of theory as energy and gradient. This implies that at every cycle one has access to *full* ab initio data. A lower level of theory and basis set, such as HF/3-21G, is usually employed for this scheme as hessian computation can be very expensive for a higher level of theory and a bigger basis set, a major bottleneck of geometry optimization approaches. An algorithmic flow chart for this scheme can be found in Figure 5.1.
2. **Large:** In this version of VMTS, the goal is to find a transition state at a higher level of theory in conjunction with a large basis set, such as B3LYP/cc-pVTZ, therefore computing the exact ab initio hessian at every cycle is not a practical possibility. This motivates the use an approximate hessian, which opens up many possibilities leading to the following sub-schemes in this category:
 - **A:** The first scheme in this category employs the use of ab initio hessian at a lower level of theory, in conjunction with energy and gradient at the (desired) higher level of theory. In this work, the former is always used at a HF/3-21G level, but one could exercise other choices. In the results section, it will be noted that this approach can work quite well for many systems, but not always. An algorithmic flow chart for this scheme can be found in Figure 5.2.
 - **B:** The second scheme makes use of multiple Hessians, each employed at an optimal stage during the search process. The algorithm is started with the use of a lower level hessian, same as scheme **A** discussed above, however, now the convergence criteria is kept loose so that this stage is converged quickly. This will be denoted as Stage 1.0. Immediately after this stage is completed, a full ab initio calculation is performed at

the desired higher level of theory and larger basis set. This is only done once, in order to obtain an accurate hessian before proceeding further. This stage is denoted as 1.5. After this step, the remaining cycles (if convergence is not already achieved) always use the hessian from vibronic model itself, never launching any ab initio hessian calculation. This last stage is referred to as 2.0, and is referred to as "bootstrapping". The idea behind this mixed approach is to reach a region in which vibronic model hessian is reasonably accurate and can be trusted. This approach, in principle, can reduce computational expense significantly, as even a lower level ab initio hessian will become quite expensive for a large molecule. Computing the vibronic model hessian is dirt cheap, and even if this final stage takes more than usual number of cycles, it would still be affordable. One could ask then why the vibronic model hessian is not employed throughout the search? The reason is simple: the quality of vibronic model will deteriorate as one moves away from the (guess) transition state region, and could lead to "unphysical" regions of the PES. Therefore, it is not a reliable choice. An algorithmic flow chart for this scheme can be found in Figure 5.3.

- **C:** The third and last scheme in this category would be to calculate the full hessian in the first step, and subsequently use hessian updating schemes, such as Bofill, to update the hessian using gradients. This is also closest to what is used in Gaussian09, for example, so it would also allow the comparison with Gaussian09 to be more like "apples-to-apples". Another variant along this line would be to use the bootstrapping idea to update the hessian using the vibronic model, but in addition use the information on gradients at previous geometries to adjust the vibronic model in the spirit of a Bofill hessian update scheme, which may prove to be the optimal choice. Both of these schemes are actively being pursued currently but they are not yet ready at an operational level.

A summary of all the schemes is presented in Table 5.1 below:

VMTS Scheme	Starting Guess	Hessian Update	Ab initio method
Small	$\frac{Q_A+Q_B}{2}$, $\frac{Q_A+2Q_B}{3}$, QST2(1)	Full ab initio hessian at each cycle	HF/3-21G
Large-2A	VMTS small or QST2 result	Ab initio hessian at a lower level	HF/6-31G* B3LYP/cc-pVTZ
Large-2B	VMTS small or QST2 result	Lower level hessian (1.0) + Vibronic model hessian (2.0)	HF/6-31G* B3LYP/cc-pVTZ
Large-2C	VMTS small or QST2 result	Bofill Update	N/A

Table 5.1: A summary of schemes used for TS search using Vibronic Models (VMTS)

A custom program has been written by the author to drive VMTS calculations, which is inter-

faced with Gaussian09, VMTS-o, and VMTS-c. The driver calls these programs as and when necessary. Before discussing the results, small comments regarding the starting guess geometry and analogous schemes for TS search in Gaussian are made below.

5.2.1 Note on the starting guess geometry

For the *small* scheme variant of VMTS approach discussed above, three different starting guess geometries have been tested:

- $Q = \frac{Q_A+Q_B}{2}$: This guess is a mid-point of a linear synchronous transit path between the two minima, and for many reactions this works quite well using (essentially) Cartesian coordinates. However, there are a few cases where this starting geometry might not be a good choice. One such example is that it may have small interatomic distances, which will force the method to fail in the beginning itself. In such situations, an alternative guess will need to be supplied.
- QST2(1): In this case, Gaussian's QST2 program is only run for one cycle (by setting max-cycles=1) and the resulting geometry is then used as the starting point for the VMTS small scheme. Not only is this a good guess for a useful comparison between VMTS and Gaussian, it can also be used when the first choice mentioned above fails.
- $Q = \frac{Q_A+2Q_B}{3}$: As a test of the importance of a good starting guess geometry, the VMTS results for the small scheme have also been obtained with this guess, which will be compared to the results obtained with the above two cases. It can also serve as an alternative choice for starting guess geometry when $\frac{Q_A+Q_B}{2}$ fails.

For all the schemes in *large* category, the starting guess is taken as the converged result of *small* scheme. If for a particular reaction, the VMTS small scheme fails and the corresponding *small* Gaussian09 is successful, the latter result can be the starting point for any of the large schemes. It is also possible to start from $Q = \frac{Q_A+Q_B}{2}$ for the large schemes, where Q_A and Q_B would be the optimized minima geometries at the desired higher level of theory, in particular for cases where a starting guess from previous *small* calculation is not available.

5.2.2 Note on the analogous schemes in Gaussian09

For the *small* scheme, the equivalent Gaussian09 calculation is the QST2 method with the `calcall` keyword on for optimization, which implies that a full hessian is calculated at all stages of optimization, as is the case for corresponding VMTS *small* scheme. The QST2 method also starts with optimized minima geometries as input, and builds a quadratic synchronous transit path

going from A to B. This allows for a direct, "apples-to-apples" comparison of VMTS and Gaussian09.

For all the schemes in *large* category, the equivalent Gaussian09 calculation is the QST3 method with the `calcfc` keyword on, which implies that a full hessian be calculated only once, at the beginning of the optimization process. In addition, like VMTS, it requires a starting guess for the transition state geometry, which is taken to be the geometry obtained as the QST2 (or VMTS *small*) result. In this regard, Gaussian09 and VMTS large schemes are equivalent. However, as pointed out earlier, the hessian update schemes in **2A** and **2B** differ from that of QST3, and a more suitable equivalent scheme would be **2C**, where the hessian update would be the similar as that of QST3. However, as of now, QST3 results will be compared to those obtained with VMTS-2A and VMTS-2B.

5.2.3 Reaction Data Set: Unimolecular reactions

A data set of 36 Unimolecular reactions is employed to test the VMTS method and compare its results to those obtained with Gaussian09. These reactions have been taken from the PhD thesis of Dr. Sandra Rabi in the Ayers' group at the McMaster University. A number of these reactions coincide with Baker's testsuite, as discussed in Chapter 2. Both Ayers' and Baker's test set was designed to benchmark transition state search methods. In this respect, it is a good set of reactions to investigate transition state searches. In addition, the reactions themselves, although all belonging to Unimolecular category, vary significantly from a chemical point of view. The list of reactions including the Lewis structure of reactants and products are presented in Table Figure 5.4. In addition to the chronological reaction number, each reaction is also labeled according to the original reaction number in Dr. Rabi's thesis.

In this first test set we consider Unimolecular reactions $A \leftrightarrow B$. All of the test cases for vibronic model up to this point are constructed for Unimolecular reactions as the vibronic model for the minima A and B are unambiguous then. In the case of bimolecular reactions, $A + B \rightarrow C$, the minimum structure of $A + B$ is not unambiguous, as one has to decide on the relative orientation of A and B , and on the distance between the moieties A and B . The VMTS strategy would be applicable, but at this point we will investigate and benchmark VMTS without this additional complexity.

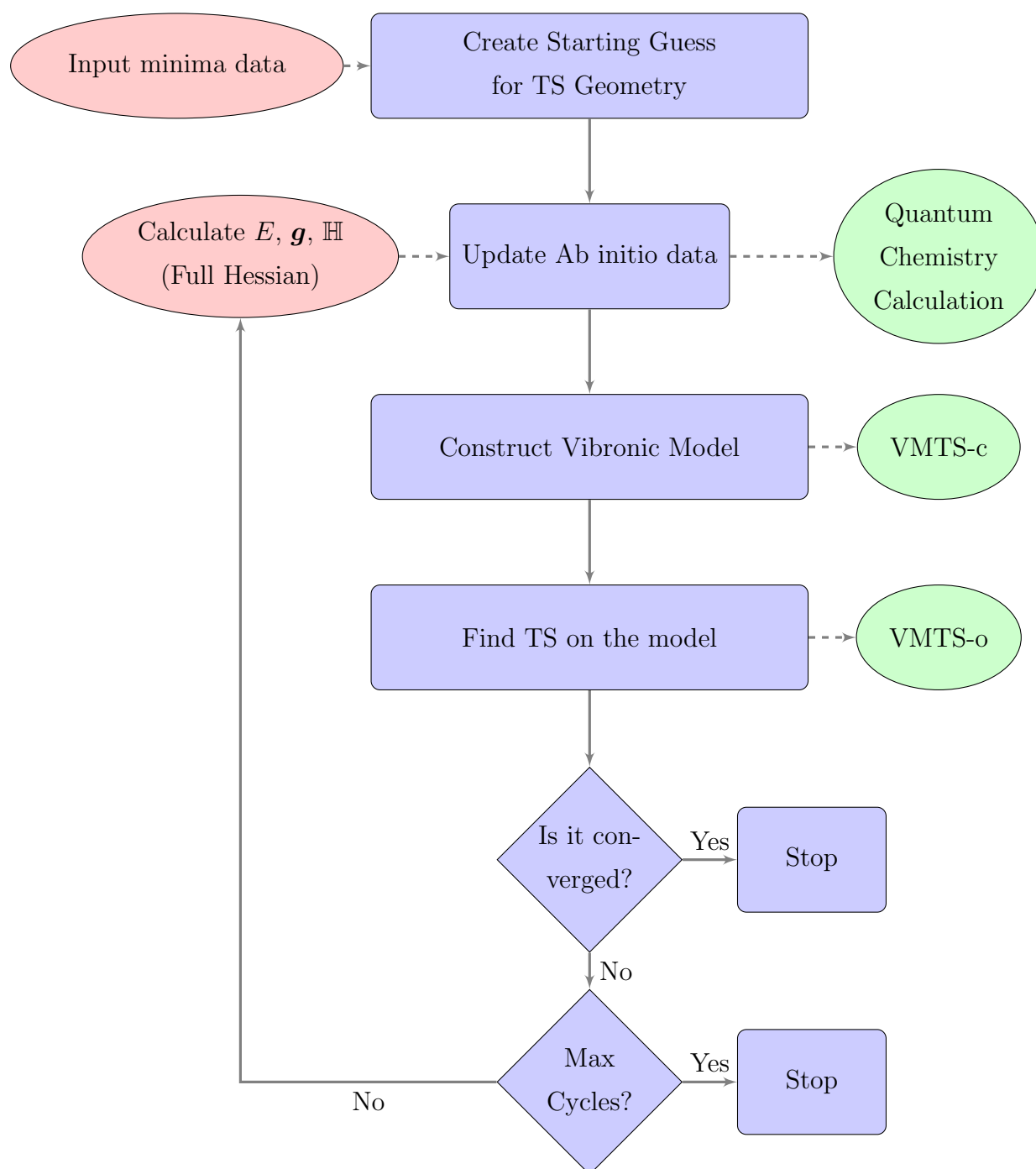


Figure 5.1: Algorithm employed in VMTS small scheme using full ab initio hessian at each cycle

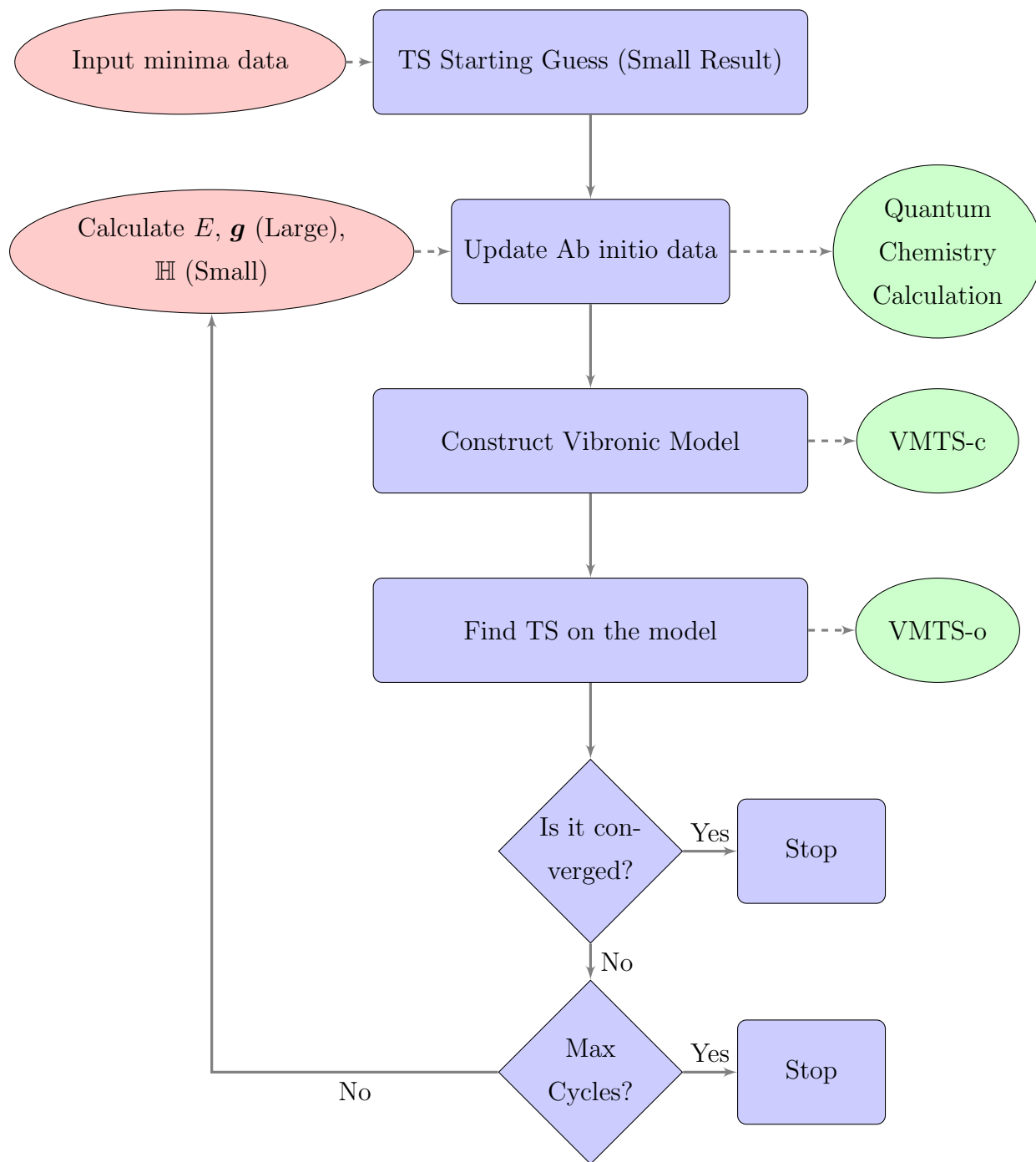


Figure 5.2: Algorithm employed in VMTS **2A** scheme using ab initio hessian at a lower level of theory

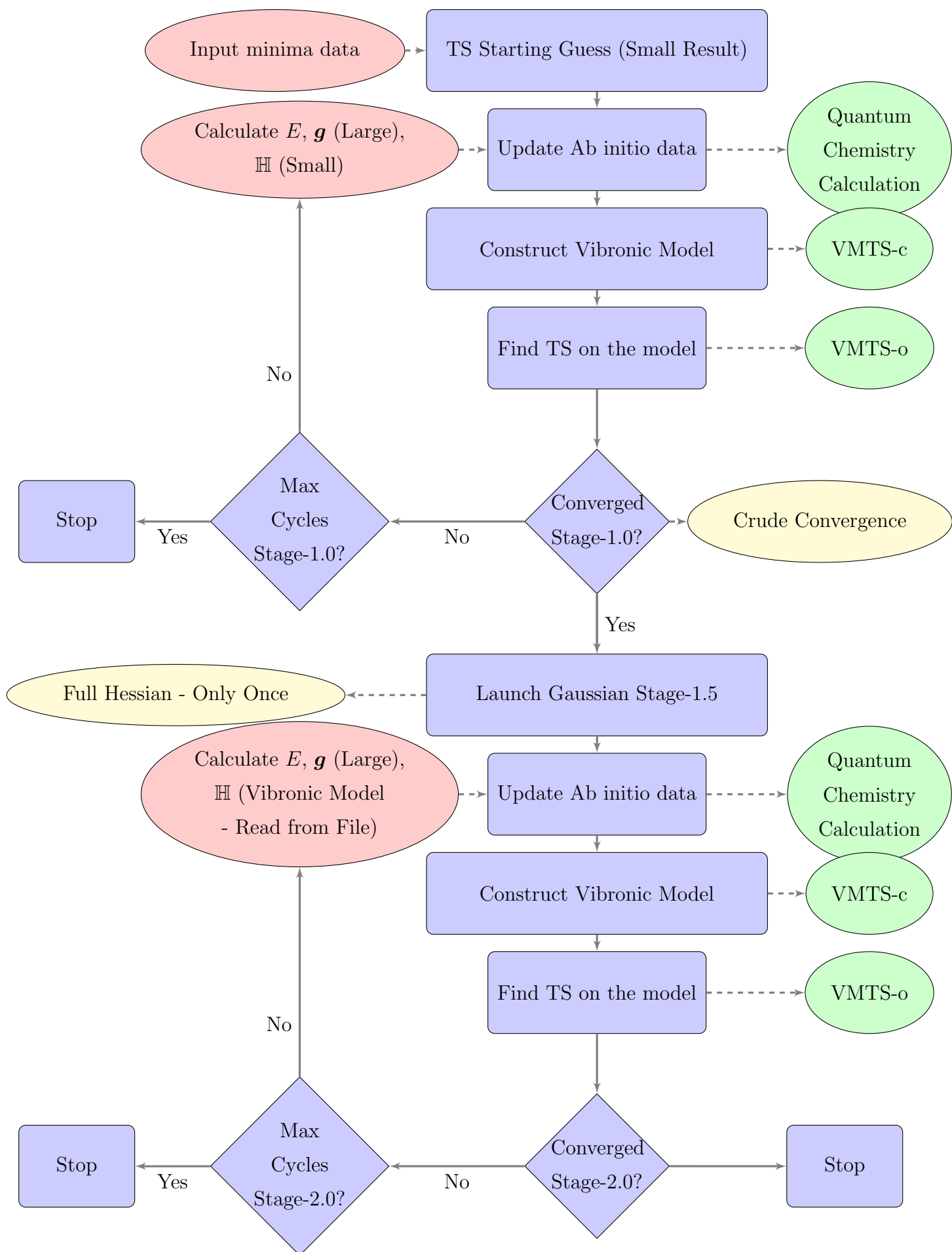

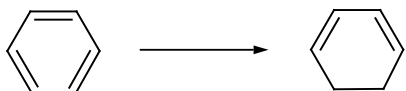
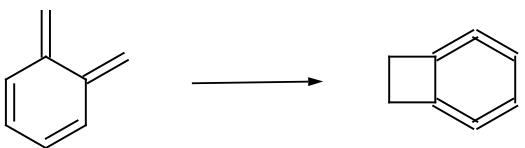


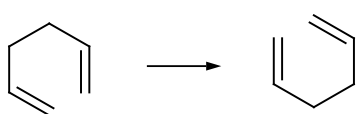
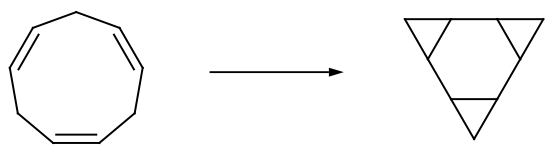
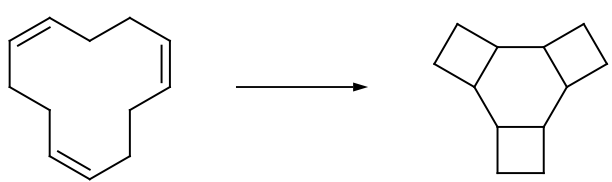
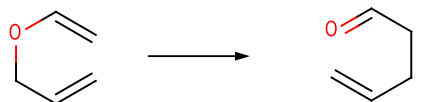
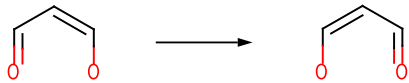
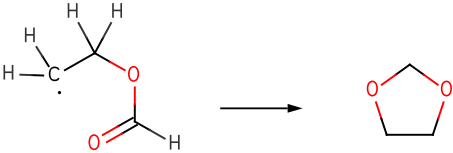


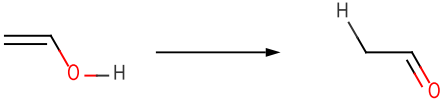
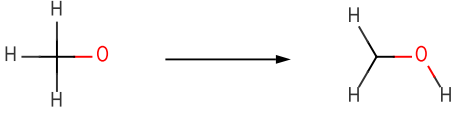
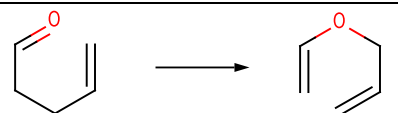
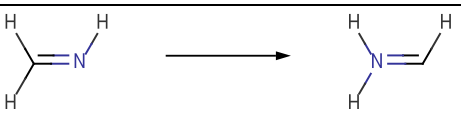
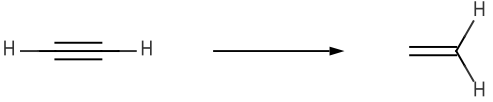



Figure 5.3: Algorithm employed in VMTS **2B** scheme using mixed hessian update strategy

Reaction Number	Sandra's Thesis	Reactant and Product Lewis Structures
1	6	
2	10	
3	11	
4	12	
5	13	
6	14	
7	17	
8	18	
9	27	

10	28	
11	29	
12	30	
13	31	
14	32	
15	35	
16	36	
17	37	
18	40	
19	44	

20	47	
21	48 (just a rotation)	
22	49 (just a rotation)	
23	52	
24	54	
25	55	
26	56	
27	57	
28	58	
29	59	

30	60	
31	63	
32	82	
33	84	
34	103	
35	104	
36	105	

Figure 5.4: Reaction Test Set for VMTS: 36 Unimolecular Reactions

5.3 Results and Discussions

5.3.1 Results for VMTS *small* scheme

Below, the results for the VMTS *small* scheme will be discussed based on three different counts: i) Comparison with Gaussian’s QST method when the starting geometry for VMTS comes from the QST2’s first cycle geometry, ii) Comparison of three different starting geometries for VMTS, and iii) Comparison of ”max distance” parameter (importance of *trust region*) on VMTS. In addition, a summary of statistical average for all the different cases will be presented at the end to have a quantitative measure of comparison. Reactions for which there are problems with any of the minima geometry optimization (20, 25, 30) are omitted from the primary tables and figures.

- **Comparison with Gaussian:** First, the VMTS results starting from the first cycle of Gaussian’s QST2 geometry, labeled as QST2(1) are compared with those of full Gaussian QST2 results. Since the starting geometry and the hessian update schemes are equivalent in this case, it is a good way to benchmark the VMTS scheme against a popular method like QST2. The comparison can be visualized in Figure 5.5 where the number of cycles needed to converge are shown for all the reactions (note that the figure spans across two tableaus). The comparison in general is satisfactory here, with VMTS often requiring less number of cycles than Gaussian’s QST2 method. There are few reactions where VMTS fails to locate the transition state. These cases are indicated by shaded bar in Figure 5.5. The specific reasons for failures are discussed below:
 - For **Reaction 16**, VMTS fails to find a TS and stops after hitting maximum number of cycles. Many instances of VMTS-o run have no negative eigenvalues of the hessian, while some also tend to go outside the trust region, where the validity of the vibronic model starts to become questionable. As a result, VMTS-o is often unable to locate a TS even on a vibronic model for a single run. During many cycles of VMTS-o, the hessian has zero (or near zero) frequency making it singular. It is also indicative of the presence of an inflection point. Many of these issues can be potentially resolved with an improved VMTS-o code.
 - For **Reaction 29**, the VMTS finds a transition state, but not the desired one.
 - **Reaction 36** also hits the maximum number of cycles without finding a TS. The issues here seem to be of more subtle nature, as the VMTS-o always remains inside the trust region as well as there is always one negative frequency for the hessian, which does not change much after a point. This appears to be a more serious issue with VMTS.

Gaussian’s QST2 also runs into its own issues sometimes, such as for **Reaction 11**, SCF does not converge. For **Reaction 32**, it finds a transition state, but not the desired one.

- **Effect of starting guess geometry:** Next up, the effect of starting guess geometry is tested for VMTS. As discussed earlier, three different starting geometries are employed for this purpose. The behavior of each guess can be seen in Figure 5.6. In VMTS, the following cases do not work for $\frac{Q_A+Q_B}{2}$ starting geometry:
 - **Reaction 22:** The starting geometry has small interatomic distances and thus is not physical. Therefore, VMTS can not proceed further.
 - **Reaction 35:** VMTS-o has issues of small, close to zero, eigenvalues as well as it tends to go outside the trust region also couple of times. Potentially resolvable issues, as mentioned above for the QST2(1) case.
 - **Reaction 36:** Same issues as discussed above for starting geometry QST2(1).

Amongst the three guesses, the QST2(1) guess works best, as noted in Figure 5.6. This is because Gaussian’s first guess from QST2 method is often already in the regime where hessian has only 1 negative eigenvalue. For the other two guess geometries considered here, $\frac{Q_A+Q_B}{2}$ performs much better than $\frac{Q_A+2Q_B}{3}$. This could be considered a potential weakness of the VMTS scheme, since ideally a method to locate transition states should not depend so strongly on the starting guess of TS geometry. The failures of $\frac{Q_A+2Q_B}{3}$ starting geometry are similar to the above two cases, facing problems because of SCF convergence during a Gaussian run, VMTS-o specific issues, hitting maximum number of cycles or the guess simply not being physical (small interatomic distances).

- **Effect of "max distance" parameter:** The dependence of VMTS, and in particular VMTS-o on the `max_distance` parameter was discussed in detail in the previous chapter. Here, results are shown for three values of max distance: 0.5, 1.0, 2.0 in Figure 5.7. The best results are obtained for the 1.0 case, which is a sweet spot between 0.5, a too tight criterion for trust region, and 2.0 being too large of a radius to trust the validity of the vibronic model hessian. The problems for reactions that do not converge, in particular for case `max_distance = 2.0`, are same as the ones discussed above.
- Another interesting feature of VMTS scheme is that for a starting geometry of $\frac{Q_A+Q_B}{2}$, it very quickly reaches the region where the hessian has only 1 negative eigenvalue. The numbers for many reactions can be seen in Table 5.5. Except for a handful of reactions, where it takes 6 cycles to reach the 1 negative eigenvalue regime, most other reaction take 1 or 2 cycles to achieve this. Explicit geometry panels for all the intermediate geometries indicating the in and out number of negative eigenvalues of hessian during a VMTS-o cycle are shown for Reaction 3 and 17 in Figure 5.8 and 5.9 respectively.
- Finally, the convergence of VMTS small scheme is shown for three reactions (3, 17, 16) with respect to change in energy and gradient as a function of cycle in Figure 5.6. For reaction

16, it takes 29 cycles. While the initial drop in the gradient is satisfactory for this reaction, the VMTS-o continually hits the boundaries of trust region, i.e. tends to cross the set `max_distance` limit (1.0), the recovery from which results in overall poor convergence. The other two reactions have very smooth convergence, for them the transition state is located in less than 10 cycles.

One must note that **Reaction 20, 25, and 30** are not part of the Figures 5.5, 5.6, and 5.7. These are the reactions for which one of the minima, i.e. either the reactant or the product could not be correctly optimized in Gaussian at the level of HF/3-21G. Below, a summary of all different cases are presented in the form of average number of cycles taken for all the reactions that worked successfully. It's a good quantitative indication towards selecting the best method.

Description / Scheme	Gaussian09	VMTS <i>Small</i>			VMTS <i>Small</i>		
	QST2	Starting Geometry			"Max Distance"		
		QST2 1-cycle	(A+B)/2	(A+2B)/3	0.5	1.0	2.0
Average # of iterations	10.26	10.10	10.72	21.76	9.93	10.10	8.56
Maximum # of iterations	24	36	34	58	33	36	23
# of correct TS located	31	30	29	25	29	30	25
# of incorrect TS located	1	1	1	1	1	1	1
# of TS not found	1	2	5	7	3	2	7

Table 5.2: A statistical summary of VMTS small (HF/3-21G) results

5.3.2 Results for VMTS *large* schemes

The VMTS large schemes have been tested for two sets of ab initio methods: HF/6-31G* and B3LYP/cc-pVTZ. Recall that for all the variation of large schemes, the starting guess is always taken as the result of a small calculation, whether VMTS or QST2. The comparison here then is mainly focused on performance against Gaussian, and the variation between schemes due to the difference in hessian update. Below, the results for two sets of ab initio data will be discussed individually.

HF/6-31G*: Scheme 2A

First, the results of VMTS **2A** scheme, in which the hessian is always calculated at a lower level of theory (HF/3-21G), are compared to Gaussian's QST3 result. As noted in Figure 5.10, for most reactions, VMTS outperforms Gaussian in terms of number of cycles needed for convergence.

However, similar to the VMTS small case discussed above, there are a number of reactions where VMTS fails to converge. These cases are listed and discussed below:

- **Reaction 9, 16:** VMTS hits maximum number of cycles. Since VMTS-o mostly remains inside the trust region, one possible explanation of failure would be the lack of accuracy in the hessian being used at the HF/3-21G level.
- **Reaction 11:** VMTS hits maximum number of cycles. The analysis of energy and gradient behavior during the search is indicative of oscillations being present for this case. Which implies that the geometries located on the vibronic model in two subsequent cycles start to repeat themselves in a loop. This problem can be fixed potentially by improving the VMTS code. This is an interesting case to test further developments.
- **Reaction 19:** VMTS hits maximum number of cycles. It tends to violate the trust region for some intermediate geometries, as well as there is some indication of the oscillatory behavior as well, as discussed above for Reaction 11.
- **Reaction 25, 26:** VMTS hits maximum number of cycles. For many cycles of VMTS-o, there are no negative eigenvalue of hessian, some being close to zero. This can cause potential issues, as discussed earlier also.
- **Reaction 35:** VMTS hits maximum number of cycles, but seems to have gotten stuck at a particular geometry close to the TS.
- **Reaction 20:** VMTS locates a transition state, but not the one desired.

For **Reaction 29 and 30**, either the reactant or product has trouble during optimization, therefore no VMTS or Gaussian's QST3 calculation could be performed, which is the reason these are omitted from Figure 5.10. Therefore, these should not be taken as a direct failure of VMTS, at least in the current state of affairs. Additionally, Gaussian's QST3 also fails for **Reaction 11** and can not locate a transition state before reaching the maximum number of cycles.

HF/6-31G*: Scheme 2B

The VMTS scheme **2B**, which uses the mixed hessian update (refer to the flow diagram in Figure 5.3) performs better than the Scheme **2A** overall. The tricolor VMTS bars in Figure 5.11 indicate the contribution of each stage (of hessian update) to the overall convergence. While for most cases, the contribution of vibronic model hessian (stage 2.0) appears only towards the end, there are exceptions to this pattern, such as Reaction 19, 26, 27, and 35, as noted in the Figure 5.11. The following reactions for VMTS do not converge:

- **Reaction 20:** VMTS converges but not to the desired TS.

- **Reaction 25:** VMTS calculation fails during Stage 1.0. itself, most likely due to the lack of accuracy of HF/3-21G* hessian.
- **Reaction 29, 30:** Complete data not available, as discussed above in the context of scheme **2A**.

In addition to the problems related to minima optimization for Reaction 29 and 30, Gaussian’s QST3 also fails for **Reaction 11** and **18**, due to technical difficulties in optimization algorithm. Note that for the latter two reactions, VMTS is successful. Reaction 29 and 30 are not part of Figure 5.11 because of incompleteness of the data, similar to the case **2A** above.

Below, a summary of statistical average is presented for both schemes **2A** and **2B**. Even though the average number of cycles for **2A** is much less than to that of **2B**, the latter is able to find a TS for more reactions, indicating that it is a more reliable scheme than **2A**. Overall, the results are encouraging for scheme **2B** to use this scheme for more accurate level of theories with a larger basis set.

Description	Gaussian QST3	VMTS-2A	VMTS-2B
Average # of iterations	11.29	5.96	11.94
Maximum # of iterations	43	20	74
# of correct TS located	31	26	31
# of incorrect TS located	0	1	1
# of TS not found	3	7	2

Table 5.3: A statistical summary of VMTS large (HF/6-31G*) results

B3LYP/cc-pVTZ

For this ab initio method, only the VMTS **2B** results will be compared to Gaussian’s QST3 results. The VMTS results here leave a lot to be desired, as seen in Figure 5.12, which is bit of a disappointment. However, it should be noted that this is still a work in progress at the time of writing this thesis, and there are currently more developments in sight, therefore one can expect improvements for these results in near future. Below, the reactions which fail in VMTS are discussed in groups according to the stage at which they terminate.

- **Stage 1.0 Failures:** Reactions **13, 21, 25, 29, 30**, and **31** fall into this category. Reactions 13, 21, 29 hit maximum number of cycles with similar reasons as has been discussed for previous level of theories (many near-zero hessian eigenvalues, for example, or the HF/3-21G hessian lacking accuracy), while the other three reactions stop during a particular VMTS-

o before hitting maximum number of cycles. These problems can be addressed with improvements in VMTS-o as well as hessian updating schemes, as discussed in Chapter 1 (using Bofill update for example).

- **Stage 2.0 Failures:** Reactions **6**, **7**, **17**, and **18** fall into this category. Similar considerations arise here as above, most important being the apparent lack of accuracy of vibronic model hessian. We anticipate that this issue can be addressed by improved hessian update, which is being implemented currently.
- For **Reactions 28**, VMTS converges, but to the wrong TS.
- For **Reaction 32**, Gaussian’s QST3 fails for technical reasons.
- For **Reaction 8**, the minima optimization has issues, therefore both Gaussian and VMTS can not be attempted.

One should note that since for Reactions 7, 8, 18, 30, and 31 both Gaussian and VMTS do not work, these are not part of the Figure 5.12. Below, a summary of statistical average is presented similar to the previous cases for a quantitative assessment.

Description	Gaussian QST3	VMTS-2B
Average # of iterations	8.63	11.27
Maximum # of iterations	17	33
# of correct TS located	30	22
# of incorrect TS located	0	1
# of TS not found	1	8

Table 5.4: A statistical summary of VMTS large (B3LYP/cc-pVTZ) results

5.4 Conclusions and Perspective on VMTS Future Work

Below, a discussion of current status and further improvements for VMTS approach will be presented. Along with it, some scrutiny and criticism also demands attention, which will be briefly discussed as well. This essentially leads to the conclusion of Part-A of the thesis.

5.4.1 VMTS: A positive outlook and the road ahead

The basic idea underlying the VMTS approach is quite promising as it provides with an analytic, albeit approximate, representation of a ground state potential energy surface, on which the computation of gradient and hessian becomes extremely cheap compared to ab initio methods. To

use such a model for geometry optimization in order to locate stationary points, in particular the transition state, becomes an exciting avenue. The results presented in this chapter, though not perfect, hold promise. Two major issues stand out from the failures: a) accuracy of the hessian update at each cycle, and b) the algorithmic limitations of VMTS-o at present. Regarding the former problem, it is likely that a HF/3-21G hessian is perhaps not a suitable choice for a B3LYP/cc-pVTZ optimization. One could use a lower accuracy hessian by using a smaller basis set, but keeping the level of theory the same, such as B3LYP/6-31G* for B3LYP/cc-pVTZ. The overall computational effort is unlikely to change in a significant manner. This argument can also be supported by looking at the results of HF/6-31G*, for which the VMTS scheme **2B** works well. Along the same line, the vibronic model hessian used in Stage 2.0 of scheme **2B** can also be improved significantly by using a hessian update scheme in the spirit of Bofill update, as discussed in Chapter 1. These developments are actively being pursued currently, and we anticipate that many failed cases will eventually become successful. The VMTS-o code is also evolving and has not reached a mature stage yet. The exact nature of improvements for VMTS-o has already been discussed in the previous chapter.

A subtle issue arises in the context of above discussion during the hessian update. The point at which one should switch between Stage 1.0 and Stage 2.0 remains a delicate affair. One might also want to relaunch a full hessian calculation (Stage 1.5) when things start to become desperate, i.e. the approximate hessian has lost too much accuracy. Automation of such decision-making steps is important for a robust black-box technique, which requires minimal interference of the user, and the efforts to achieve this are also part of the near future outlook.

Another aspect of the VMTS that demands attention is the choice of coordinates. The performance of Cartesian / Normal coordinates is surprisingly good. Nonetheless, it is well known that the issues associated with large amplitude motion, for flexible molecules, are not described appropriately in these coordinates. One then turns towards curvilinear internal coordinates, which are most suitable to describe these type of nuclear motions. One can expect that will make the VMTS scheme more robust and reliable. This can also be considered one of the main components of future work.

In summary, the improvements of VMTS on many fronts are either in active development or in sight for near future. We anticipate that this will lead to a robust and reliable black-box tool to locate transition states.

5.4.2 VMTS: A critical outlook

In spite of all the good things that VMTS has to offer, there are certain aspects that must be looked with a critical eye. First and foremost, the failure to obtain a "globally" accurate PES, as

seen in Chapter 2, is a bit disappointing as one can not utilize the powerful interpolation schemes to find transition states, such as the String based methods, for example the Nudge Elastic Band (NEB) or the Growing String Method (GSM). Such methods often bypass the critical step of using a good starting guess geometry, an important step of the local methods, such as the (quasi)-Newton approaches, and are designed to find the minimum point on a path connecting the minima.

There is also the issue of performance, in addition to robustness, compared to the many methods available in the literature for transition state searches. It would need an extensive benchmark to establish where VMTS would stand amongst the plethora of TS search methods, even with its ability to calculate gradient and hessian in a very efficient manner. One must note that the implementation of string based methods, such as NEB, is highly parallel, as the computation on each image can be performed at the same time. Even if one looks at the currently available comparison, Gaussian's QST3 method seems to provide a tough competition to VMTS. However, much of these performance comparison issues with other methods will become more relevant once we have a stable, and reliable code.

It must be emphasized that the the discussion of virtues of VMTS is based on the test suite of Unimolecular reactions. In principle, the VMTS strategy is applicable in the same manner to Bimolecular reactions, and in fact has already been tested successfully for a few reactions. The initial results on this front have shown promise but they are not included in the thesis since the complete results are not yet available. One reason for this is the ambiguity in defining the alignment of reactants/products during the construction of vibronic model, as mentioned earlier, which needs to be automated. This is under active development. One must also recall from the discussion in Chapter 4 that VMTS-o is not the focus of this thesis, but the goal of VMTS in the context of this thesis is rather to demonstrate that this could potentially be an interesting strategy to locate transition states. The Unimolecular test set achieves this goal. A comprehensive set of results, including Bimolecular reactions is a work in progress.

Reaction	Cycles
1	1
2	1
3	2
4	1
5	1
6	2
7	0
8	0
9	6
10	0
11	2
12	2
13	1
14	2
15	0
16	6
17	1
18	1
19	1
21	3
23	2
24	0
25	2
26	1
27	1
28	1
30	0

Table 5.5: Number of cycles it takes to reach 1 negative eigenvalue regime starting from $\frac{Q_A+Q_B}{2}$ guess for VMTS small scheme

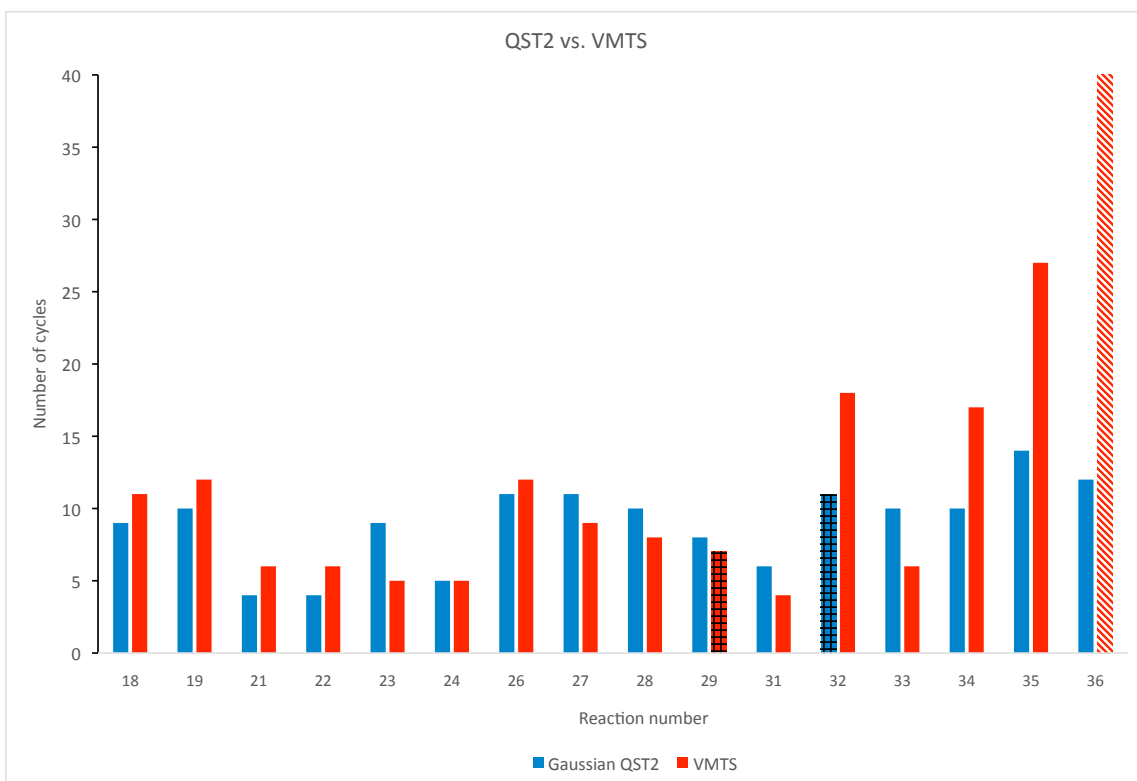
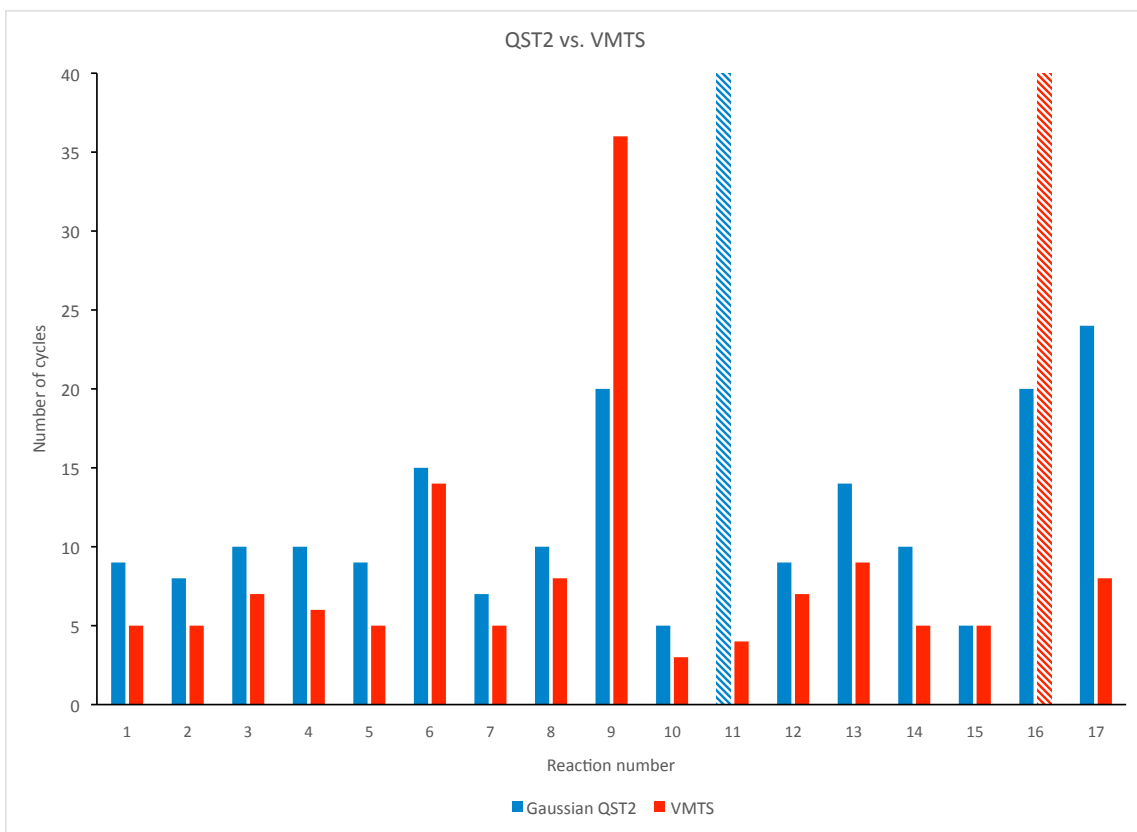


Figure 5.5: VMTS small scheme with starting geometry QST2(1) vs. Gaussian's QST2

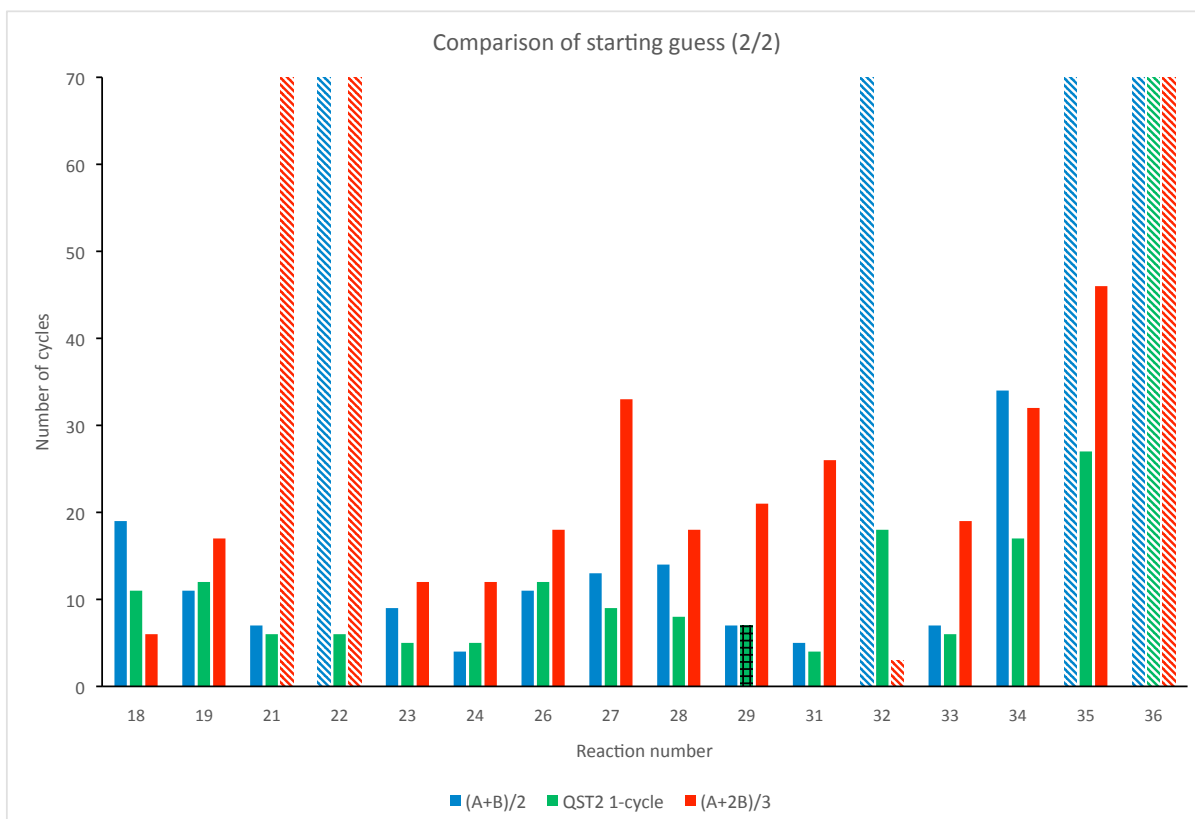
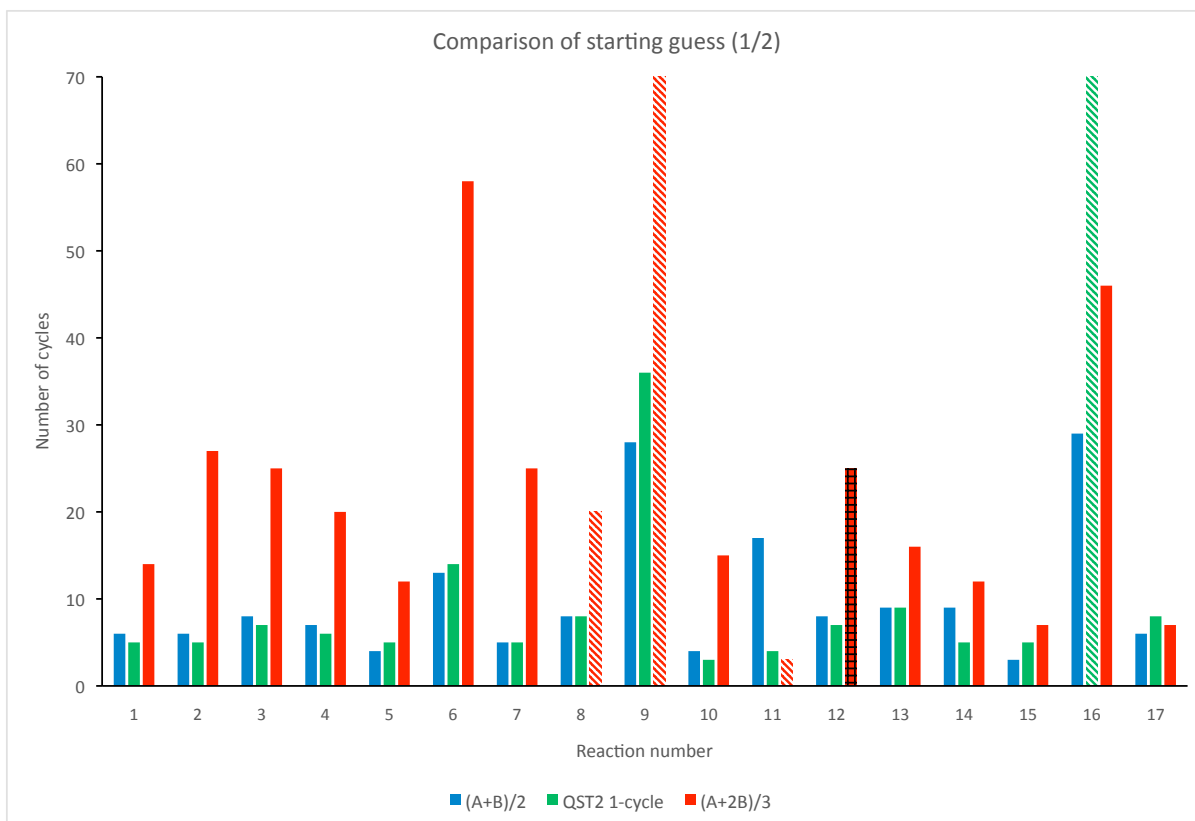


Figure 5.6: VMTS small scheme: comparison of starting guess geometries

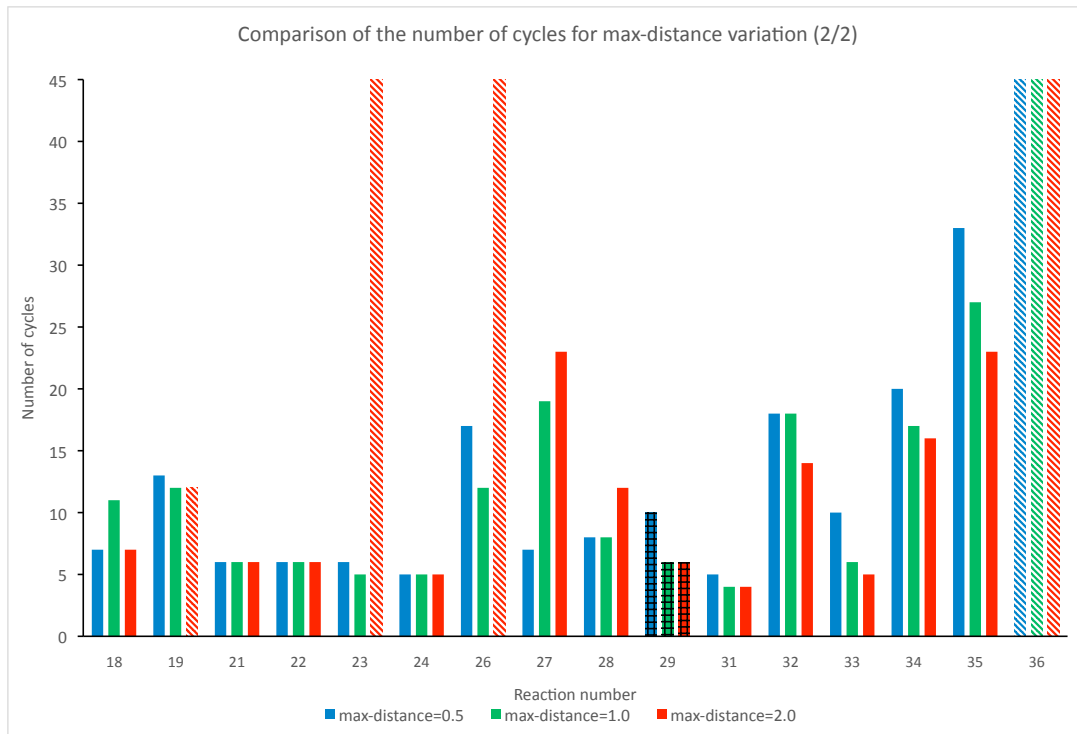
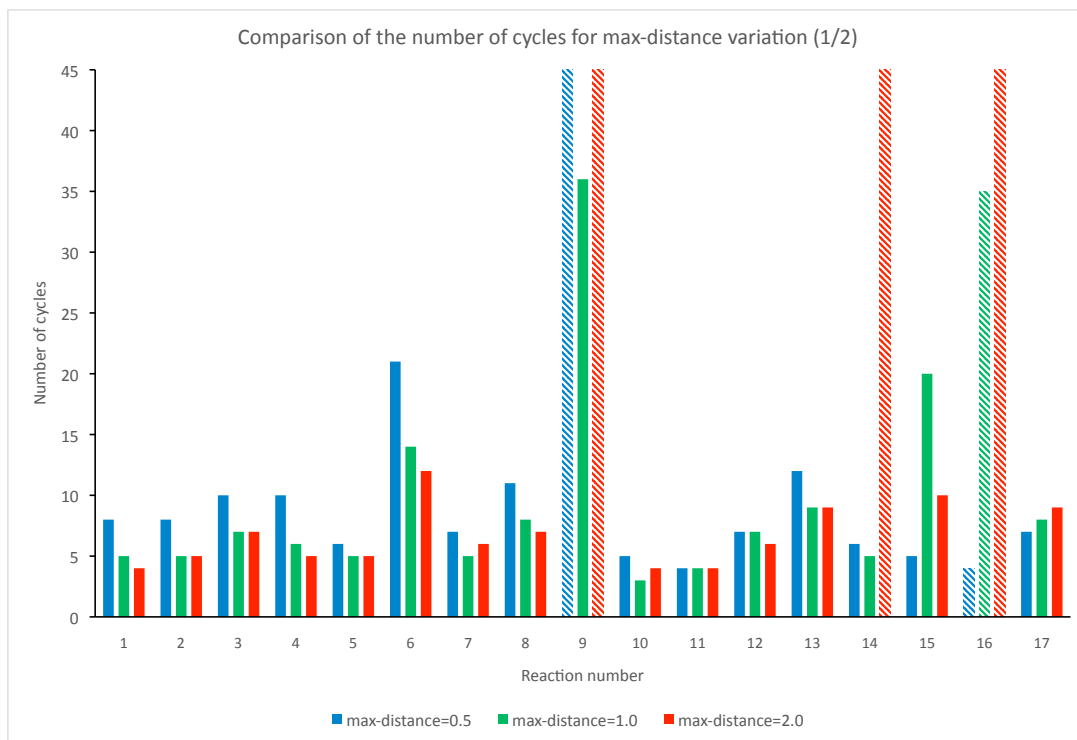


Figure 5.7: VMTS small scheme: comparison of max distance parameter used in VMTS-o

Panel of Intermediate Geometries during VMTS Search

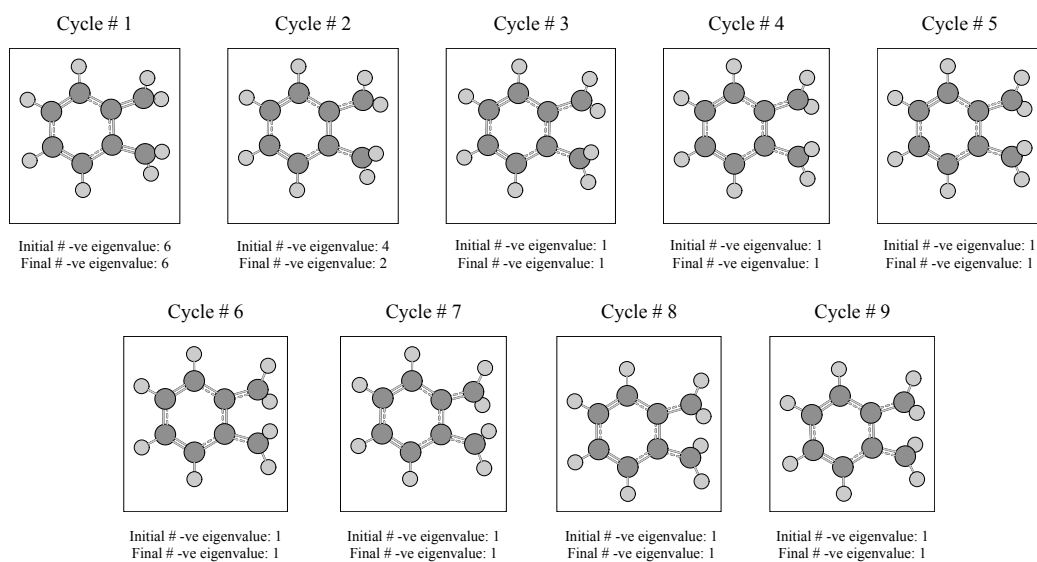


Figure 5.8: VMTS small scheme: intermediate geometries during TS search for Reaction 3

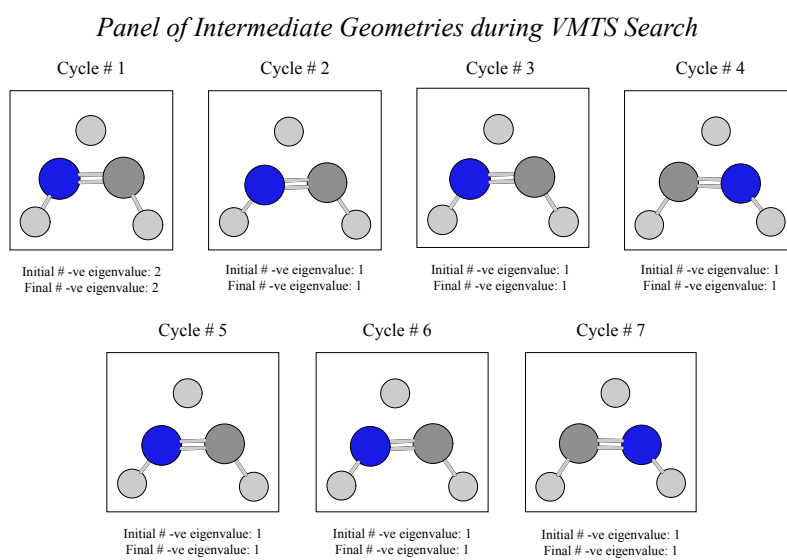


Figure 5.9: VMTS small scheme: intermediate geometries during TS search for Reaction 17

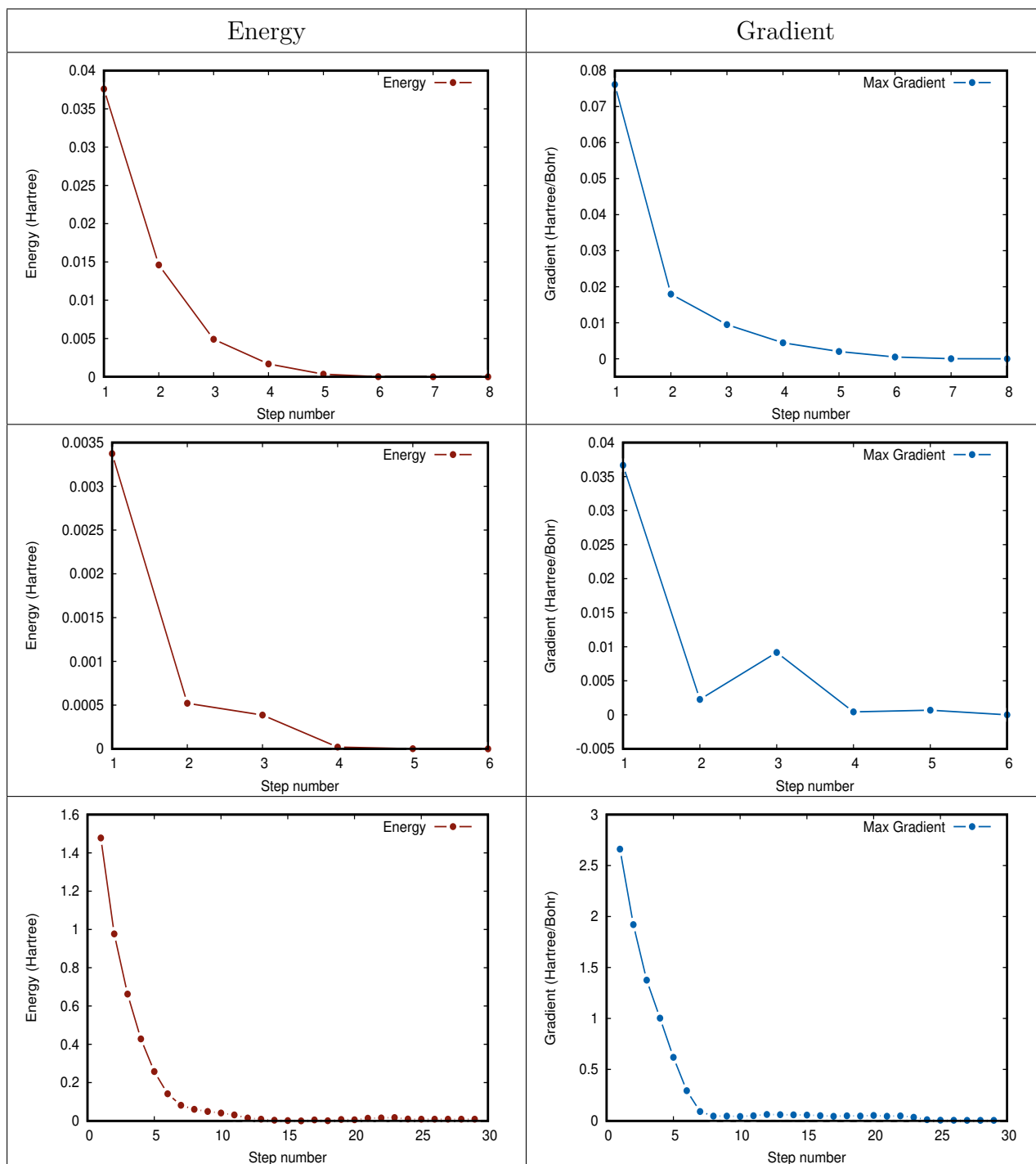


Table 5.6: Energy and gradient as a function of VMTS cycles for Reactions 3, 17 and 16 respectively

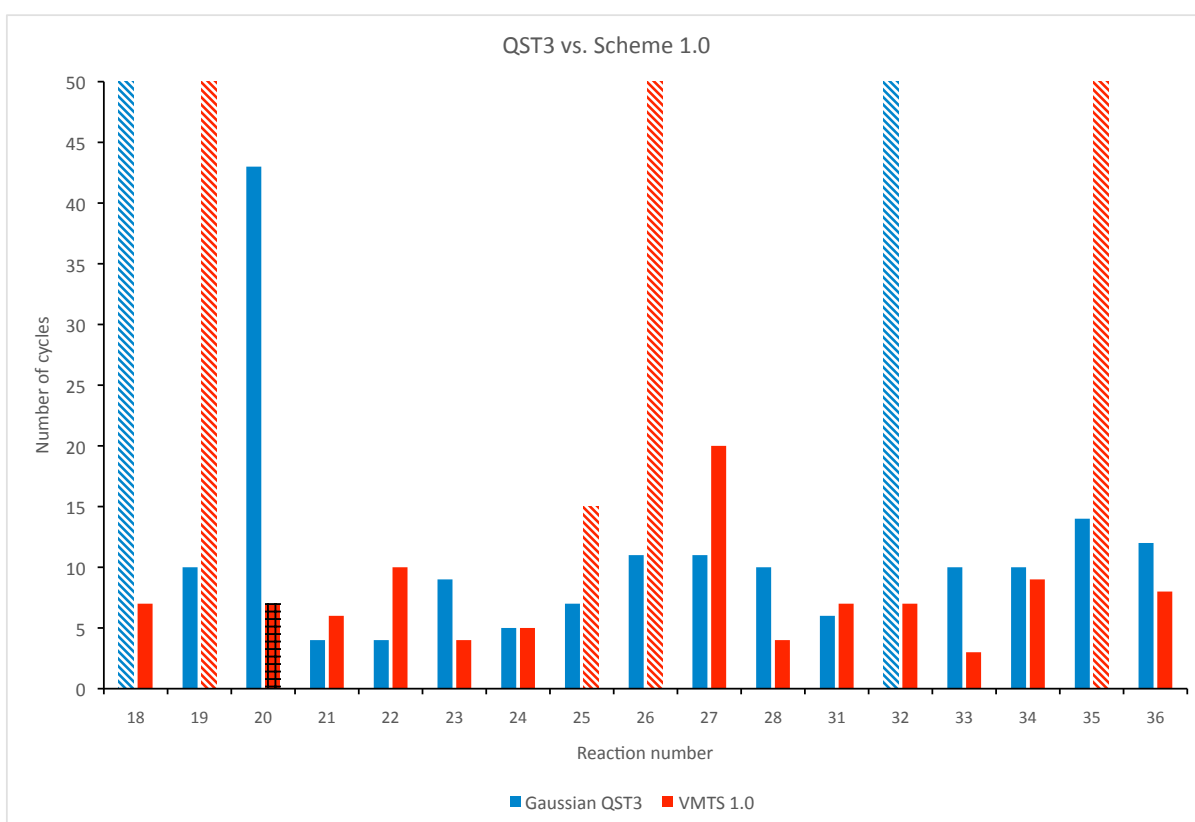
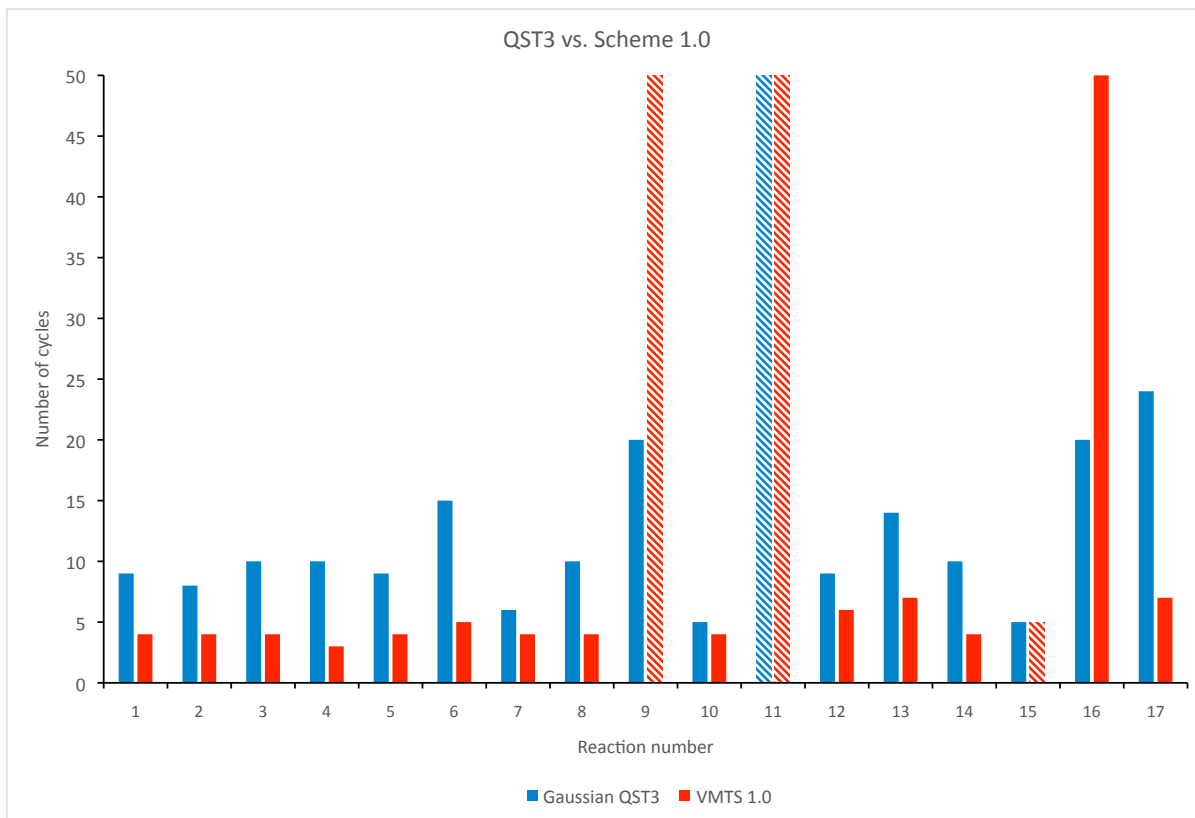


Figure 5.10: VMTS large scheme **2A** comparison with Gaussian's QST3 for HF/6-31G*

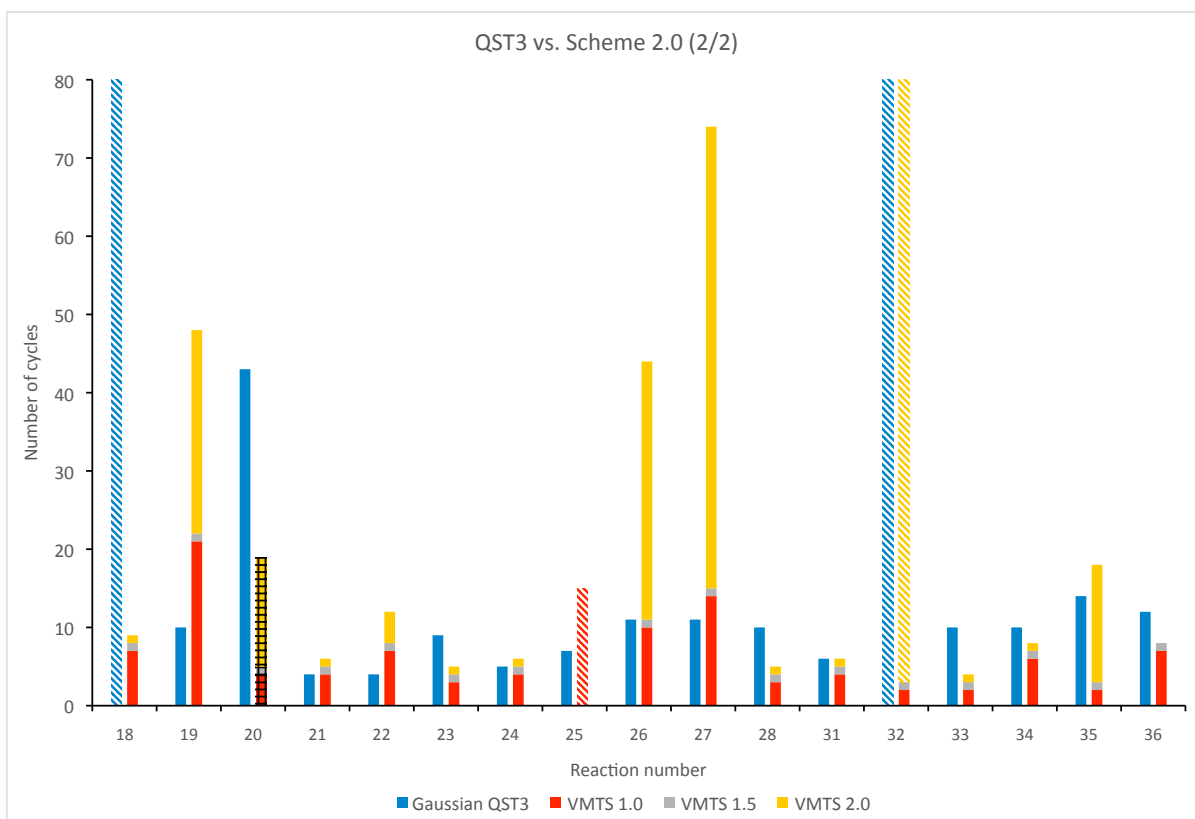
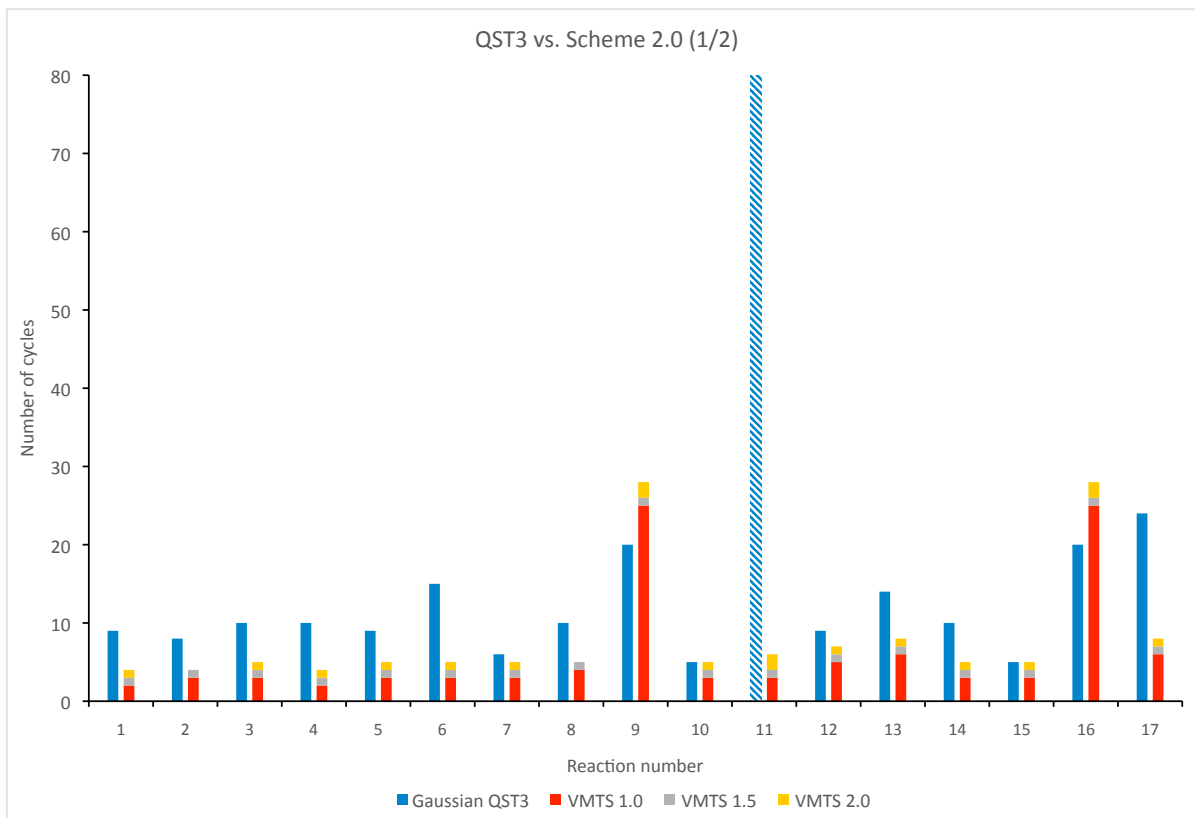


Figure 5.11: VMTS large scheme **2B** comparison with Gaussian's QST3 for HF/6-31G*

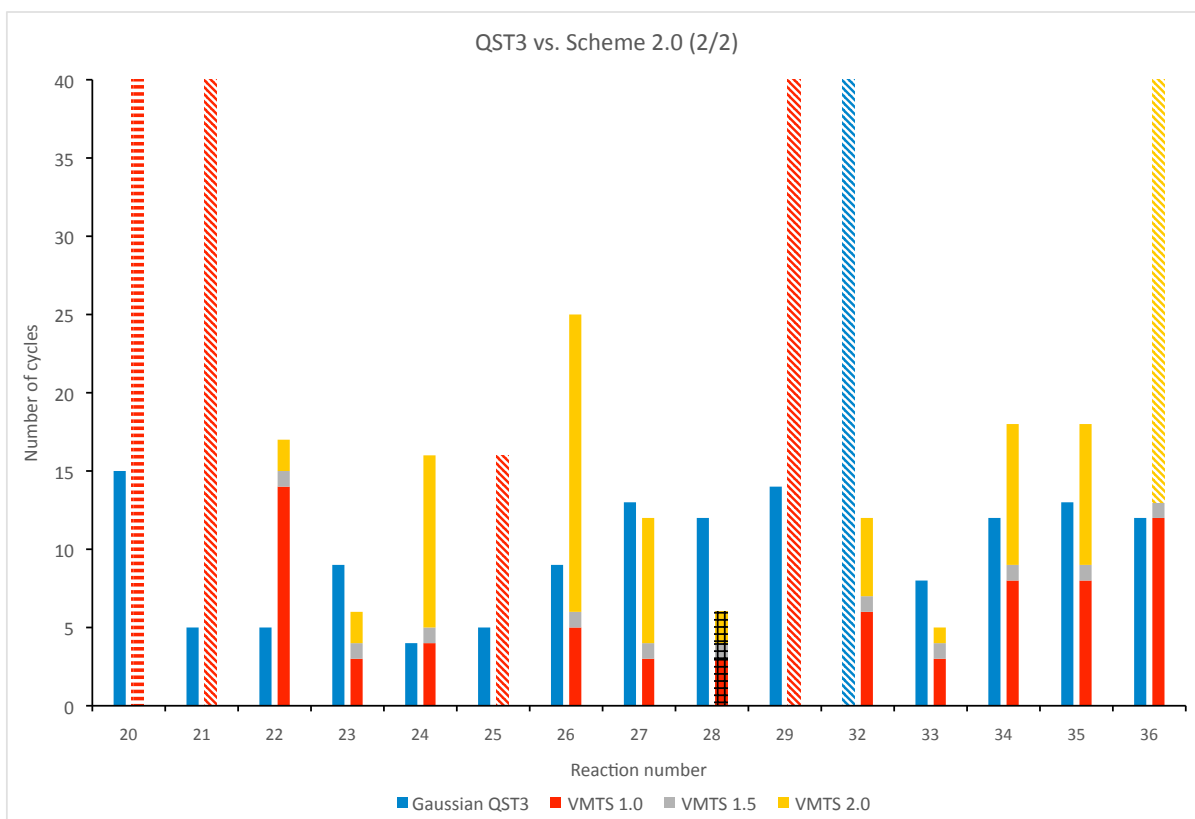
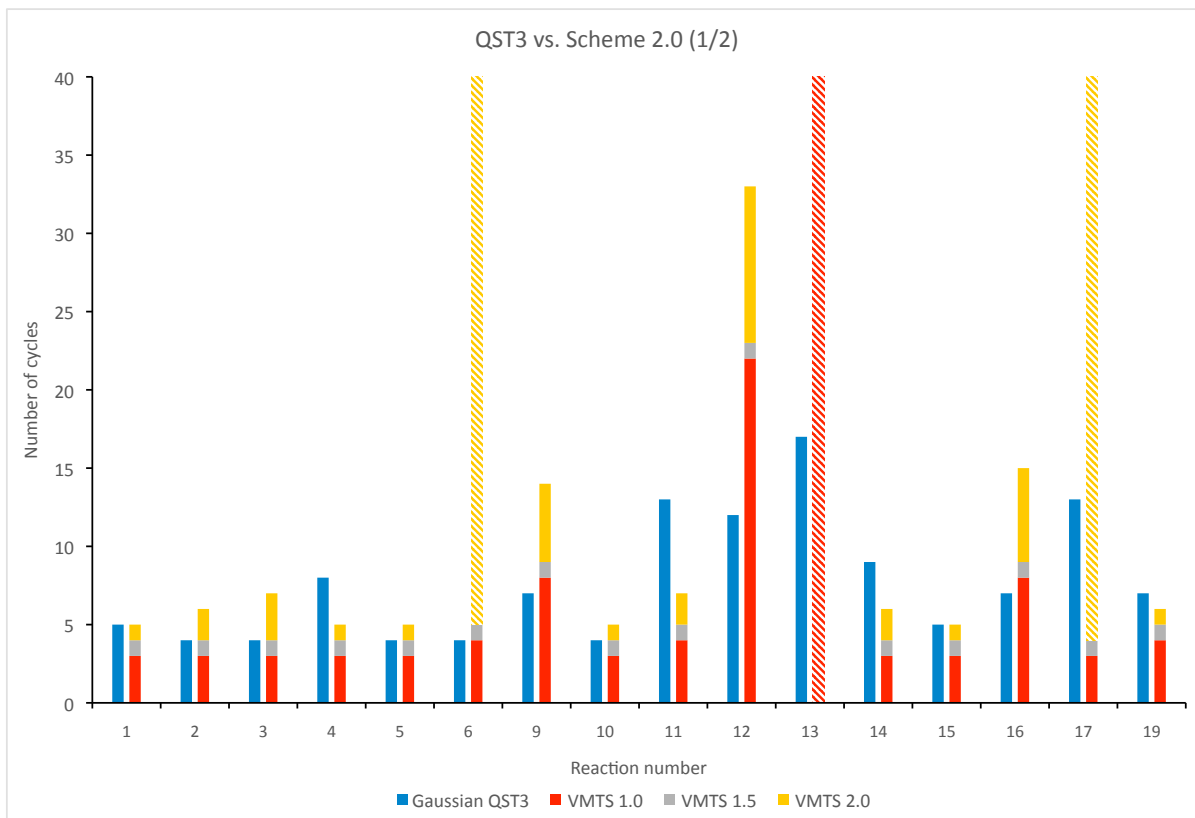


Figure 5.12: VMTS large scheme **2B** comparison with Gaussian's QST3 for B3LYP/cc-pVTZ

PART-B: Quantum Dynamics and Time-resolved Spectroscopy

Chapter 6

A proposed new scheme for vibronically resolved time-dependent photoelectron spectroscopy: pump-repump-continuous wave-photoelectron spectroscopy (prp-cw-pes)

6.1 Introduction

Femtosecond time-resolved spectroscopy has emerged as a major technique to study dynamical phenomena in the past three decades. A particular focus has been on studying nonadiabatic dynamics, where the coupling between electronic and vibrational (thus also named *vibronic* coupling) degrees of motion leads to interesting photochemical and photophysical processes such as internal conversion, radiationless transitions, isomerization, proton transfer amongst many others. [12, 59–61] A traditional femtosecond time-resolved experiment can be described in terms of a pump-probe configuration. Initially, an ultrafast (on the order of 10 fs) pump pulse prepares a nonstationary state, which is then mapped onto a set of chosen final states by the means of a suitable probe pulse. If the final states are chosen to be the ionized states of the molecule, such that the probe laser ionizes the nonstationary state by generating a free electron, the technique is known as Time-resolved photoelectron spectroscopy (TRPES). [62, 63] The merits associated with this specific probe technique have been widely discussed in the literature [64, 65] and there have been numerous applications of TRPES to study a wide variety of dynamical processes. [65, 66] [For an extensive discussion, refer to the review in reference [8], and references therein.]

Much of these studies performed by the means of TRPES have focused on long-time dynamics of

the molecule in question, where the time-delays were on the order of picoseconds. Such a time-scale is desired to investigate photochemical processes in order to probe the global features of the potential energy surfaces. The time-delayed spectra thus captured are often of low resolution in energy, but the global features vary significantly with the changing time-delay, where in principle one can monitor the *electronic* dynamics associated with the process. An example of such a process is the internal conversion between the $S_1 - S_2$ states of pyrazine, which was the first theoretical study performed using TRPES [67] and later followed by others. [68, 69] However, such an interpretation of the TRPES snapshots, in terms of a change of character in electronic states, is not always a straightforward task and relies heavily on the nature of electronic manifold of excited states. [65] A complementary technique which is often used to gain more insight in such complicated cases is to measure the angular distribution of the outgoing electrons, known as Time-resolved photoelectron angular distribution (TRPAD). [65, 70–72]

To raise the bar concerning the comparison between theory and experiment, it is of interest to investigate highly resolved time-dependent signals. Experimental techniques to obtain signal that provide high resolution feature both in time (in terms of time-delay) and frequency simultaneously are now well established. One of the earliest schemes to obtain such a signal was regarded as dynamic absorption spectroscopy, [73] where the measurement of the probe pulse spectrum is independent of the widths of pump and probe pulses. In the traditional detection techniques, which use a photo detector or laser-induced fluorescence, the measured spectra depend on the spectral resolution of the pump and probe pulses, which in turn are governed by their width in time (pulse duration). In the dynamic absorption experiment, the polarization response evoked by the probe pulse is measured as a continued evolution, in terms of the emitted radiation, over a desired period of time using a multichannel detector, which plays an important role in deciphering the detailed frequency resolved information. [74] It is important to note that the initial system prepared by the interaction of the probe pulse *is* dependent on the pump-probe time-delay and thus prepares a unique nonstationary state for each time-delay giving a series of time-resolved signals. The sharp features of the spectra are only dependent on the dephasing rate of the induced polarization (and thus on the lifetimes of the vibronic levels), and not on the pulse duration. [73–75] The key lies in detection. More recently, such signals have been obtained in a technique known as Femtosecond Stimulated Raman Spectroscopy (FSRS), [76–80] which uses a three pulse sequence, in which the use of a long Raman pulse ensures the high resolution in frequency domain.

Fundamentally, this limitation of time-energy resolution is different for TRPES as one can measure the kinetic energies of outgoing electrons with fine precision. In fact many experimental spectra obtained by TRPES are well resolved in both time and frequency. [66] The challenge lies in the interpretation of such high resolution spectra. Since these spectra depend on the phase re-

lations between the eigenstates (i.e. coherences), the vibronic features become very complicated and are hard to interpret theoretically. This argument also holds true for dynamic absorption spectroscopy. It is therefore not surprising that most simulations of such spectra have limited themselves to the low resolution regime in the frequency domain, focusing on the electronic dephasing, and not on the fine vibronic features. The spectroscopy is then most readily understood using a wave packet picture, moving in nuclear configuration space.

The goal of the scheme presented in this paper is to combine the high resolution features in energy and a time-dependent spectroscopy, such that one is able to analyze the results in a meaningful fashion, employing the interplay between theory and experiment. In the proposed scheme we make use of two short pulses (pump and repump) to create the initial nonstationary state and a long (cw) probe pulse to ionize this state. The populations in the vibronic levels of the excited state can be manipulated by changing the time-delay between the pump and repump pulses. The continuous laser acts for a long time and establishes resonance between excited states and continuum states of photoelectron spectroscopy, giving rise to sharp features in the final spectra. The kinetic energy of the outgoing electron is tuned to resonance, hence all transitions will be automatically resonant, independent of the frequency of the probe laser, if it is large enough. This is the primary reason to use ionized states in the detection mechanism. The fact that in the detection scheme resonance is established between the excited vibronic state and the photoionized state is a key concept. Only one vibronic state is exactly in resonance with a given photoionized state, and therefore the intensity of the transition depends on the population of this vibronic state, but there is no interference from other vibronic levels, akin to the process of Rabi oscillations. After the pump-repump sequence the nonstationary state moves as a wave packet, and this motion is essentially due to the interference between different eigenstates, also known as coherences. The populations of the eigenstates, however, do no longer change after the repump laser (neglecting excited state decay), and it is these populations (varying as a function of pump-repump time-delay) that determine the intensities for a particular time-delay. Each time-delayed snapshot spectrum is a weighted sum of so-called fingerprints, where a fingerprint is the vibrationally resolved photoelectron spectrum for a single vibronic eigenstate. The weight is essentially given by the population of the vibronic eigenstate after the pump-repump laser system has died out.

The proposed scheme is designed such that theory and experiment can work in unison. We believe the actual process that determines population is very complicated and hard to simulate from first principles. In addition, it would require very accurate absolute excitation energies, and a careful simulation of the time-dependent fields. Nonetheless, it is feasible to calculate fingerprints to fair accuracy using first principles calculations. [81-84] For this reason, to simulate experimental results the populations of vibronic excited state after the pump-repump action will be taken

as adjustable parameters. A number of individual experimental snapshots can be fitted using a (hopefully small) number of theoretical fingerprints. This then allows quantitative interpretation of experimental results, employing a direct interplay of theory and experiment.

The chapter is organized as follows: In section 6.2, we lay out the schematics of the proposed scheme in terms of time-dependent pulses and eigenstates of the molecular Hamiltonian. A key result is obtained in Equation 6.7, which expresses intensity of the final signal (snapshot) in terms of the populations of vibronic excited eigenstates as a function of pump-repump time-delay. It is shown how populations in excited state depend on the time-delay and phase relationship between the pump and repump pulses. This discussion leads to the various ways in which the proposed scheme can be realized experimentally. In section 6.3, we apply the proposed scheme to a vibronic model with two degrees of freedom, and discuss the scheme of fitting snapshots in terms of weighted fingerprints in significant detail. We conclude in section 6.4, with some thoughts on the possibilities that the proposed scheme presents and invite experimentalists to realize this setup in practice.

6.2 Schematics of the pump-repump-cw-photoelectron scheme

6.2.1 General discussions of the proposed scheme

On a fundamental level, the proposed scheme can be divided into two segments, mimicking the traditional setting of a pump-probe experiment. The first step consists of the preparation of a particular (non-stationary) initial state. The second step, which is also the detection step, projects this initial state onto a set of chosen final states, resulting in a final signal that can be analyzed to extract information about the system's structure and dynamics. We propose to make use of two short pulses ($\approx 10 - 30 fs$), which we shall refer to as pump and repump, for the preparation of the initial state. Let us find a form for this initial state wave function in terms of the time-delay between the two pulses. We first define the Hamiltonian of the system for nuclear motion, including molecular and interaction terms:

$$\begin{aligned}\hat{H}(t) &= \hat{H}_{mol}^{(0)} + \hat{W}(t) \\ \hat{W}(t) &= -\hat{\mu} \cdot \vec{E}_1^{pump}(t - t_1) - \hat{\mu} \cdot \vec{E}_2^{repump}(t - t_2)\end{aligned}\tag{6.1}$$

where $\hat{H}_{mol}^{(0)}$ is the molecular Hamiltonian for the neutral species and $\hat{W}(t)$ is the interaction between molecule and the external electric field, which has been defined in the second line within the dipole approximation. The quantities E_1 and E_2 denote the variation of the electric field for the pump and repump pulse, acting on the molecule at time t_1 and t_2 respectively. The time-delay between the two pulses is defined as $\tau = t_2 - t_1$ and will be referred to as the pump-repump time-delay. The quantity $\hat{\mu}$ refers to the dipole operator.

Initially, before any of the pulses are applied, the system is considered to be in its stationary ground state, $|\Psi_0(t = t_0)\rangle$. After the pump and repump pulses have acted on the system, the wavefunction at time t' , some time after the laser fields have died out, can be expressed as a coherent superposition of eigenstates:

$$|\Psi(t')\rangle = \sum_{\lambda} c_{\lambda}(\tau; t') |\lambda\rangle \quad (6.2)$$

where c_{λ} depend on the time-delay τ between the two pulses and the time t' . Once the pulses have died, each eigenstate evolves in a field-free environment with its own phase factor whereby the populations in each eigenstate remain constant:

$$|\Psi(t)\rangle = \sum_{\lambda} c_{\lambda}(t') e^{-\frac{i}{\hbar} E_{\lambda}(t-t')} |\lambda\rangle \quad (6.3)$$

It is to be noted that $|\lambda\rangle, E_{\lambda}$ refer to the stationary eigenstates of the molecular Hamiltonian:

$$\hat{H}_{mol}^{(0)} |\lambda\rangle = E_{\lambda} |\lambda\rangle \quad (6.4)$$

Having created a particular non-stationary state, we now want to project it onto a chosen set of final states, as our detection step to obtain the signal. These states are chosen to be the ionized states of the system. We propose to use a long monochromatic (cw) probe laser, which is supposed to ionize the system after time t' . In practice the cw laser might be always on and one would measure the difference in ionization signal upon the action of pump-repump laser system. The underlying idea is to be able to obtain sharp transitions (therefore requiring a *narrow band* laser), which are governed to a good approximation by an *exact resonance* condition:

$$\hbar\omega_{cw} + E_v = E_{kin}^{(\vec{k})} + E_{v^+} \quad (6.5)$$

Where ω_{cw} is the carrier frequency of the cw-probe pulse, $E_{kin}^{(\vec{k})}$ is the kinetic energy of the outgoing electron, and E_{v^+} and E_v denote the eigenenergies of the vibronic eigenstates corresponding to the ionized and excited electronic manifolds respectively. The measured kinetic energy of the outgoing electron can thus be expressed as:

$$E_{kin}^{(\vec{k})} = \hbar\omega_{cw} + E_v - E_{v^+} \quad (6.6)$$

It is important to emphasize that owing to the exact resonance condition, only a unique $v \rightarrow v^+$ transition energy is allowed as the outgoing electron comes out with a definite kinetic energy during each ionization process. Since the populations in vibronic excited states do not change after the pump and repump pulses have died, the detection time, or t' , does not play a role in the final signal. Therefore, the intensity of the transition can then be expressed as:

$$I_{v^{exc} \rightarrow v^+, \vec{k}} \propto |c_v(\tau)|^2 |\langle \psi_{v^+}^{N-1}, \Psi_{\vec{k}} | \hat{\mu} \cdot \vec{E}_{probe}(\omega_{cw}) | \psi_v^N \rangle|^2 \quad (6.7)$$

where ψ_v^N and $\psi_{v^+}^{N-1}$ denote the initial N -electron and final $(N - 1)$ -electron eigenstates respectively, while $\Psi_{\vec{k}}$ denotes the wave function of the outgoing electron.

It is to be noted that in the above derivation, the basic assumption we make is that the resonant ionization process is dominant. This process only considers the interaction between two eigenstates, and therefore the signal depends on the population of the eigenstate, and the transition dipole between the two states, according to equation 6.7 above. Let us examine Equation 6.7 closely. The first term in the equation $|c_v(\tau)|^2$ simply denotes the population in a particular vibronic level of electronic excited state and is a function of the pump-repump time-delay, τ . By virtue of varying this time-delay and the relative phase $\phi(\tau)$ between the two pulses (to be discussed later), one can generate unique nonstationary states providing the temporal resolution required for a time-resolved experiment. This corresponds to a wave packet interferometry or equivalently a coherent control type of experimental set-up. [85–90] If one uses a short pulse for the detection in order to project this nonstationary state onto some set of chosen final states, one would also measure the coherences between the excited state vibronic levels, in addition to the populations. It is precisely these coherences that are measured in a regular pump-probe experiment, such as TRPES, and make the signal extremely complicated. By using a long monochromatic laser, which results in a resonance condition as discussed above, we are able to kill the coherences, and only project the populations on the ionized manifold resulting in a simple expression for the final signal in Equation 6.7. This is a unique aspect of the proposed scheme.

The second overlap term, arising from the detection, is reminiscent of conventional photoelectron spectroscopic transitions, where the intensity is dependent on the outgoing continuum electron \vec{k} . To a good approximation the overlap part in Equation 6.7 is independent of \vec{k} (e.g. for low energy photoelectrons). However, this overlap is strongly dependent on the vibronic overlap between excited vibronic state and the vibronic states of the molecular ion. The set of transitions $v \rightarrow (v^+, \vec{k})$ for a particular excited vibronic level v is denoted as the corresponding fingerprint, which can be expressed as:

$$F_v(E_{kin}) \propto \sum_{v^+} |\langle \psi_{v^+}^{N-1} | \hat{\mu}^{eff} \cdot \vec{E}_{probe}(\omega_{cw}) | \psi_v^N \rangle|^2 \delta(E_{kin} - \Delta E) \quad (6.8)$$

where $\hat{\mu}^{eff}$ represents the electronic part of the ionizing transition, which can be modeled using the Condon approximation. The exact treatment of the ionization continuum is quite involved and mathematically demanding. [91, 92] Very recently, Gozem *et al.* have discussed different ways to treat this photoelectron wave function, in terms of plane wave and coulomb wave, and provide further insight into this problem. [93] Such a description would certainly be important to take into account if one is interested in obtaining information from photoelectron angular distributions (PADs). In contrast, if the interest lies in only the kinetic energy distribution of the outgoing electron, this dependence can be dropped making an assumption that the ion nuclei and

the electron decouple, [94] as will be done in this work. The condition for transition to take place emerges directly as a result of equation 6.6, such that $\Delta E = \hbar\omega_{cw} + E_v - E_{v+}$. The intensity pattern of a particular snapshot or time delay is most easily interpreted as a weighted sum of the fingerprints, where the weights are the populations of the vibronic levels. The final signal that will be observed experimentally can then be written as:

$$S(E_{kin}; \tau) = \sum_v P_v(\tau) \cdot F_v(E_{kin}) \quad (6.9)$$

where $P_v(\tau) = |c_v(\tau)|^2$ denotes the population in a particular vibronic level in excited state for a given time-delay. Let us emphasize the crucial role played by the populations, which do not change in the absence of a laser field (under the assumption of no excited state decay). This means the spectroscopy signal is independent of nuclear dynamics that happens between the time after the second laser has died out, and the (ill-defined) time of the probe laser. As a result an eigenstate picture is most appropriate to understand the proposed spectroscopy. This is very different from traditional time-resolved spectroscopy.

In the proposed experimental set-up, the resonant ionization process can start already after the first pulse has acted on the system. The second pulse will then change the population of the excited state, and the ionization rate will change accordingly. The overall ionization (photo-electron) count would reflect this changing population during the process. However, the transitions making up the fingerprint corresponding to a single excited vibronic state all go through the same process, and the signal can be modelled as a fingerprint times an effective population. In the light of this argument, our discussion of the proposed scheme above is elementary and assumes the ionization only takes place after the action of pump-repump pulse sequence. It serves the purpose of illustrating that the excited state population varies wildly with time-delay, but the calculations leave out much of the complexity of the process. In this respect, our description has a cartoon like flavour. However, it is important to realize that as long as the final signal can be expressed according to Equation 6.9, irrespective of the complexities of population evolution, the analysis scheme presented in this work remains perfectly valid and fruitful. Once again, we do not propose to calculate the populations, but rather obtain them as fitting parameters. If there are simultaneous processes that occur in such a way which leads to a final form of the signal that is not well described by Equation 6.9, the simplicity of description as well as analysis might perhaps break down and one will then need to describe the process using a density matrix formalism in its full complexity.

Below we will show how the populations can be expected to change as a function of time-delay using a very simple model. The phase relation between the two pulses will play a crucial role in monitoring this change. This analysis will lead us to anticipate some plausible experimental ways in which the proposed scheme can be realized in the lab. In addition, we will show that the

pump-repump time-delay can be used to create a large amount of experimental data, which in turn can be put to good use by comparing to theoretical simulations. In order to describe the wave packet interferometry and obtain the populations in excited state as a function of time-delay between the pump and repump pulses, we adopt the standard approach of treating the radiation-matter interaction using first order perturbation theory. The treatment presented here closely resembles to that of Leichtle *et al.* [89]. Assuming the dipole approximation, the interaction term of the Hamiltonian can be written as:

$$\hat{H}_{int} = -\hat{\mu}E(t) \quad (6.10)$$

where $\hat{\mu}$ is the electronic dipole operator in the direction of the field connecting the ground and excited state, and $E(t)$ is the electric field associated with the laser pulse, which can be represented as:

$$E(t) = f(t)e^{-i\omega_L t} + c.c. \quad (6.11)$$

We will first examine the action of a single pulse on the system. After the excitation, the resulting state vector can be expressed as a superposition of two components:

$$|\Psi(t)\rangle = c_g(t)|g\rangle e^{-\frac{i}{\hbar}E_g t} + \sum_v c_v(t)|v\rangle e^{-\frac{i}{\hbar}E_v t} \quad (6.12)$$

The first component of the state vector represents the ground state "wave packet", while the second component is the wave packet representing the coherent superposition of *vibronic* eigenstates in the excited electronic manifold. Employing the weak-field approximation and the rotating-wave approximation, the time-dependent coefficients in the excited state can be expressed as:

$$c_v(t) \approx \frac{i}{\hbar} \mu \langle v|g\rangle \int_{-\infty}^t dt' f(t') e^{[-i(\omega_L - \frac{E_v - E_g}{\hbar})t']} \quad (6.13)$$

where the Condon approximation has been employed as well. It is to be noted that the excited state coefficients depend on the *vibronic overlap* of the corresponding vibronic level in the excited state with the ground state, denoted as $\langle v|g\rangle$. For the simplicity of analysis, we choose the pulse envelope to be rectangular shaped, which in the short time limit acts as a delta function pulse. [75] A Gaussian shaped pulse would be equally suitable, as is used in the work of Leichtle *et al.* The underlying physics of the process does not depend on the shape of the pulse, and the choice of rectangular pulses has been made for mathematical simplicity and illustration of the scheme. Assuming impulsive excitation, the pulse profile can be expressed as:

$$f(t') = E_0 \Delta_t \delta(t' - t_1) \quad (6.14)$$

where E_0 is the height of the rectangle, which can be associated with the field amplitude, while Δ_t is the width of the rectangle denoting the duration of the pulse. The time $t = t_1$ is the time

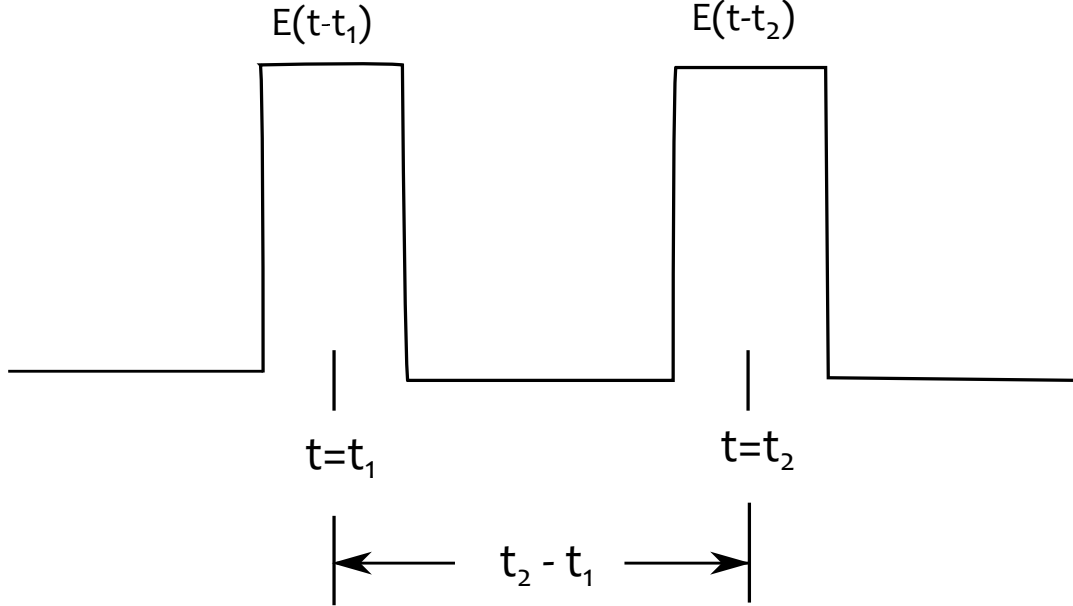


Figure 6.1: A diagrammatic representation of pump and repump pulse sequence with a time delay of $\tau = t_2 - t_1$

when the action of the pulse takes place under sudden approximation. The time-dependent coefficients in the excited state can now be expressed as:

$$c_v(t) \approx \frac{i}{\hbar} \mu E_0 \Delta_t \langle v|g\rangle e^{[-i(\omega_L - \frac{E_v - E_g}{\hbar})t_1]} e^{-\frac{i}{\hbar} E_v t} \quad (6.15)$$

After the pulse has died, the excited state wave packet evolves freely in coordinate space, while the populations $P_v = |c_v|^2$ do not change with time. This is a familiar picture of one-photon absorption process. Let us consider the action of a sequence of two identical pulses with a finite time-delay. The field envelop can now be written as:

$$f(t') = E_0 \Delta_t \delta(t') + E_0 \Delta_t \delta(t' - \tau) e^{-i\phi(\tau)} \quad (6.16)$$

where $\tau = t_2 - t_1$ is the time-delay between the two pulses, and $\phi(\tau)$ denotes the relative phase carried by the two pulses. A diagrammatic representation of the pulse sequence is shown in Figure ???. A first order perturbation theory analysis, essentially similar to the one pulse case discussed above, yields the time-dependent coefficients after both pulses have died, as:

$$c_v(t) \approx \frac{i}{\hbar} \mu E_0 \Delta_t \langle v|g\rangle e^{[-i(\omega_L - \frac{E_v - E_g}{\hbar})t_1]} e^{-\frac{i}{\hbar} E_v t} \left(1 + e^{-i\phi(\tau)} e^{[-i(\omega_L - \frac{E_v - E_g}{\hbar})\tau]} \right) \quad (6.17)$$

Therefore, the population in the v th vibronic level in excited state, $P_v = |c_v|^2$, can be expressed as:

$$P_v = \frac{\mu^2 (E_0 \Delta_t)^2 |\langle v|g\rangle|^2}{\hbar^2} \left(1 + \cos\left[\left(\omega_L - \frac{E_v - E_g}{\hbar}\right)\tau + \phi(\tau)\right] \right) \quad (6.18)$$

Using the definition of snapshots from Equation 6.9, and substituting the populations with the above expression, the snapshots can now be expressed as:

$$S(E_{kin}; \tau) = \sum_v \frac{\mu^2 (E_0 \Delta_t)^2 |\langle v|g\rangle|^2}{\hbar^2} \left(1 + \cos\left[\left(\omega_L - \frac{E_v - E_g}{\hbar}\right)\tau + \phi(\tau)\right] \right) \cdot F_v(E_{kin}) \quad (6.19)$$

We have obtained a closed form expression for the populations, as well as the snapshots, in terms of the time-delay and phase relationship between the two pulses, and their carrier frequency (which is the same for both pulses in this case). If one has a knowledge of vibronic eigenstates for the excited and ionized electronic manifold, in principle one has all the knowledge to obtain the snapshots.

It is evident that the time-dependence of the signal arises from the population term, as the fingerprints do not change with time. We would now like to explore how these populations, and in turn the snapshots, change with respect to the time-delay, as well as with respect to the phase relationship between the two pulses. This analysis is of vital importance, and will govern what kind of information can be retrieved from these signals, or how one can meaningfully analyze the signals as a spectroscopic signature of the molecule in question.

6.2.2 Various realizations of prp-cw-pes

In order to explore the pattern of the snapshots generated according to the Equation 6.19 with respect to the pump-repump time-delay, we will consider two cases for the phase relationship $\phi(\tau)$. As the first case, we consider the relative phase between the two pulses $\phi(\tau)$ to be the geometric path difference of the two pulses, such that,

$$\phi(\tau) = \omega_L \tau \quad (6.20)$$

Therefore, the snapshots can now be written as:

$$S(E_{kin}; \tau) = \sum_v \frac{\mu^2 (E_0 \Delta_t)^2 |\langle v|g\rangle|^2}{\hbar^2} \left(1 + \cos\left[\left(\omega_L - \frac{E_v - E_g}{\hbar}\right)\tau + \omega_L \tau\right] \right) \cdot F_v(E_{kin}) \quad (6.21)$$

Snapshots corresponding to Equation 6.21 for a simple one-dimensional harmonic oscillator model are shown in Figure 6.2. Individual snapshots are well resolved in energy, and the features change significantly with varying time-delays. With the definition of phase according to Equation 6.20, the populations, as well as the snapshots, can be expected to change very rapidly in time, with a characteristic frequency $\omega = 2\omega_L - \frac{E_v - E_g}{\hbar}$. If the electronic excitation energy is of the order of 4.0 eV, and the carrier frequency is also close to the excitation energy (resonant excitation), the snapshots then change completely within a time-delay of 0.1 fs. This behavior is shown for the populations of select vibronic levels in Figure 6.3 for the above mentioned model. The corresponding snapshots then also change rapidly at the same rate, which is illustrated in the supplemental Movie M1. The rapidly changing nature of the populations and snapshots makes it difficult to monitor the dynamics from an experimental point of view. In addition, as noted earlier, first principles simulation of populations and an attempt at direct interpretation of the experimental signals is a challenging task. Keeping this in mind, we propose that experimentally

recorded snapshots can be analyzed in terms of theoretically obtained fingerprints by the means of a fitting procedure. If one has a priori knowledge of fingerprints, populations in excited state can be obtained by fitting experimental snapshots to fingerprints for many time-delays. Under this scheme, the time-delays are not used to gain insight into the dynamics. Rather, it serves to generate a large amount of experimental data, which can be used to characterize individual molecules or as a tool to identify closely related molecular structures. The possibility of distinguishing between closely related conformers can be demonstrated by a simple gedanken experiment. One can prepare sample of a molecule for which the stereo-chemistry (cis vs. trans or the conformational isomer) is not known. Conventional spectroscopy methods such as absorption spectra might fail to distinguish between the two conformers. In such a situation, one can record the snapshots for this sample experimentally. If one calculates the fingerprints for possible conformers and attempts to fit the experimental snapshots for *all* time-delays, one should only be able to fit the snapshots with the *correct* fingerprints. The aforementioned fitting scheme will be discussed and illustrated in the next section with the help of a simple 2x2 vibronic model. Given such an application of the proposed scheme, it is safe to argue that the phase relation does not play an important role and therefore one does not need a perfectly stable interferometer for this experiment. Random-phased experiments, such as in the case of COIN experiments [90] will be good enough for our proposal, leading to a much simpler experimental arrangement.

As the second case for the phase relation, following the technique of Scherer *et al.*, [88] the relative phases between the two pulses can be locked and kept at a constant value $\phi(\tau) = \phi_0$. Therefore, for this case, the snapshots can be expressed as:

$$S(E_{kin}; \tau) = \sum_v \frac{\mu^2(E_0\Delta_t)^2 |\langle v|g\rangle|^2}{\hbar^2} \left(1 + \cos\left[\left(\omega_L - \frac{E_v - E_g}{\hbar}\right)\tau + \phi_0\right] \right) \cdot F_v(E_{kin}) \quad (6.22)$$

The choice of this phase constant, along with tuning the carrier frequency of the laser pulse, will greatly alter the dynamics of the process. If one considers the case when the laser carrier frequency is on resonance with excited state manifold $\omega_L = E_{exc}$ and if one chooses $\phi_0 = 0$, the populations (and therefore the snapshots) vary rather slowly with a characteristic frequency $\omega = \omega_L - \frac{E_v - E_g}{\hbar}$, compared to the previous case. This behavior is depicted for the one-dimensional harmonic oscillator model in supplemental movie M2. Such a set up eliminates the practical concern of monitoring the rapidly oscillating snapshots corresponding to the conventional interferometry setup. The more exciting prospect emerging from the phase-locked set up is perhaps the idea of monitoring the population dynamics of a particular vibronic level in the excited state, and obtaining the fingerprints directly from the experiments. Keeping the phase constant to be $\phi_0 = 0$, if one fine tunes the pulse carrier frequency such that $\omega_L = \frac{E_v - E_g}{\hbar}$, for a particular v th vibronic level in excited state, the populations in this level will become independent of the time-delay. Such behavior is shown in the supplemental movie M3. As a result, the weighted fingerprint fea-

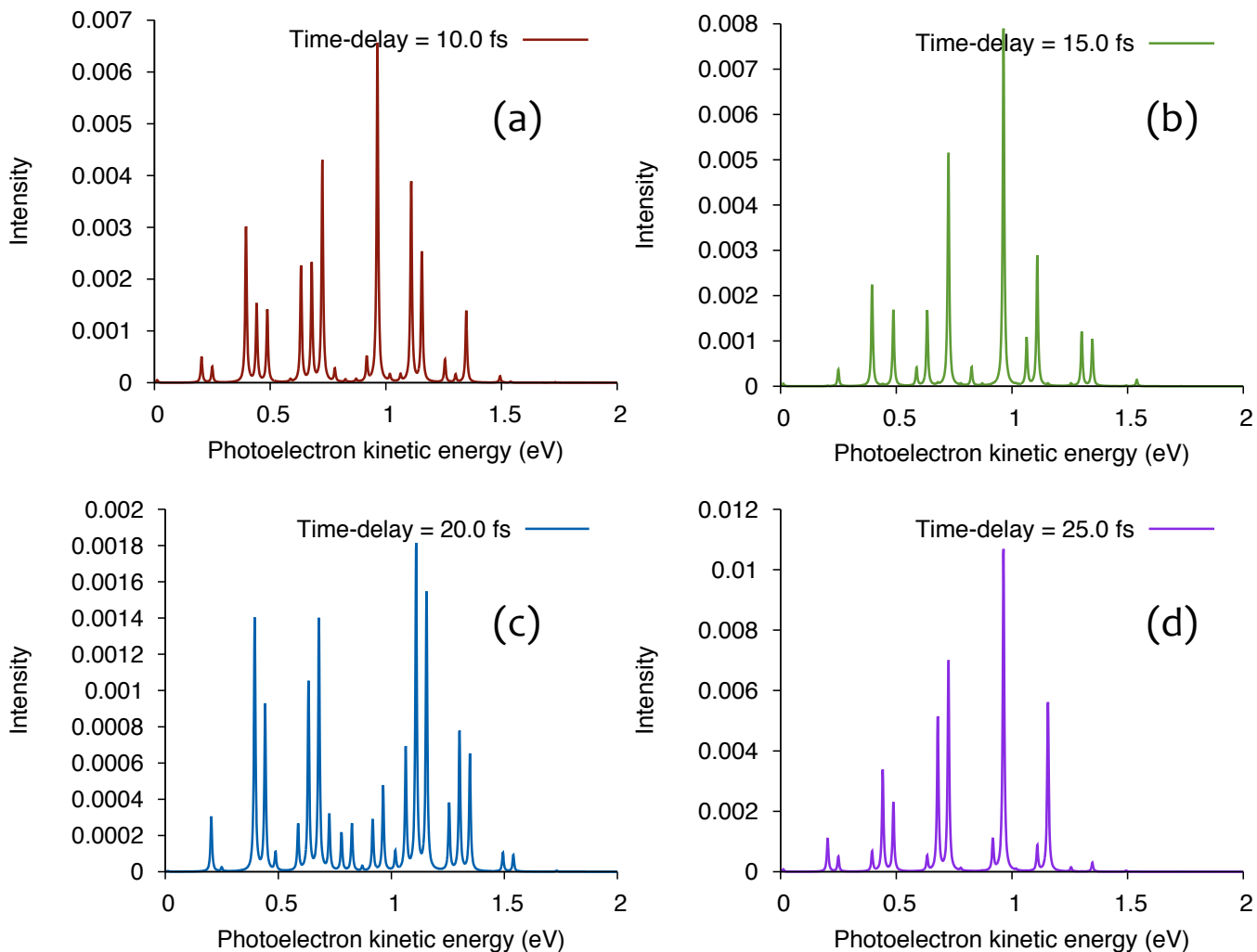


Figure 6.2: Snapshots of prp-cw-pes for a 1D model system at different values of pump-repump time-delays.

tures in the snapshots corresponding to this particular level will remain frozen for all time-delays. Separating out these peaks will give the corresponding fingerprint for this vibronic excited state. On the other hand, if these peaks are seen to be diminishing with increasing time-delay, it is indicative of population decay due to collisions. These observations can potentially lead to a deeper understanding of the excited state decay process.

Theoretical simulation of time-resolved spectroscopy experiments is usually performed by a numerical solution of the Time-dependent Schrödinger Equation (TDSE), which describes the time-evolution of the initial state vector, both in the presence and absence of the time-dependent electric field. A knowledge of molecular eigenstates is not necessary in this description as one solves an initial value problem in the time-domain. The dynamical observables can be obtained in terms of time-correlation functions and their Fourier Transforms. Interpretation and physical insights are gained in terms of the moving wave packet in nuclear configuration space. For the scheme proposed in this work, an eigenstate representation seems more suitable since the spectra depend on the populations in vibronic excited state, as discussed in previous sections. It should be noted

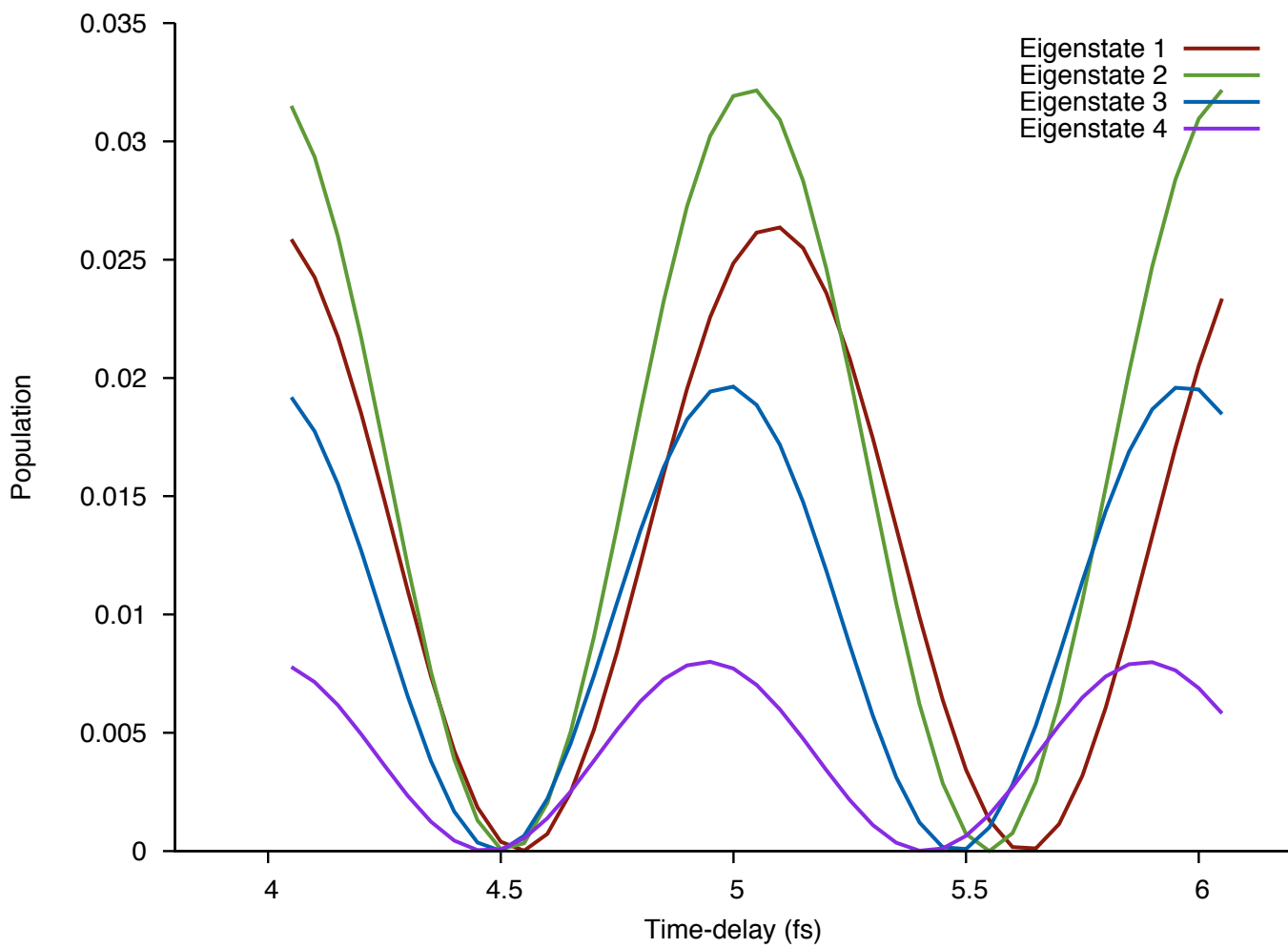


Figure 6.3: Rapid oscillations of populations in vibronic levels of excited state on a short time-scale.

that a wave packet description would be equally valid, and one may prefer to use time-dependent techniques in actual calculations for efficiency reasons.

First principles theoretical simulation of snapshots will provide one with the predictive power for complicated molecules, and will indicate the interest (or a lack thereof) to perform the experiment. In order to simulate the full time-dependent signal, a knowledge of accurate vibronic model for excited state manifold is necessary. This is a challenging task for Electronic Structure Theory. One can expect to encounter additional difficulties in terms of loss of populations (excited state decay), decoherence and dephasing, all of which seem to be nontrivial processes to incorporate in a first principles description. Given this scenario, alternative approaches to analyze the experimental data are necessary. Such a scheme is presented in the next section, where experimentally obtained snapshots are fitted against the theoretically obtained fingerprints, thereby giving the populations as fitting parameters as a function of time-delay. Under this analysis scheme, prp-cw-pes snapshots provide unique spectroscopic signature of molecular structure. In the next section, we will discuss the proposed fitting procedure with the help of a 2x2 vibronic model for excited state.

6.3 Application of prp-cw-pes to a 2x2 vibronic model

One of the goals of the proposed scheme is to employ the complexity of vibronic models by capturing vibrationally resolved features as a function of the pump-repump time-delay. In this section, we will obtain a working equation for the experimental signal in terms of vibronic eigenstates and pump-repump time-delay, using which the analysis scheme mentioned earlier will be discussed using a model system with two degrees of freedom.

Vibronic models have been used extensively to study the short time dynamics of nonadiabatic systems, often in conjunction with the MCTDH wave packet propagation scheme. [13] A detailed account of the description of vibronic models and its application to spectroscopic problems can be found in the literature, [12,61,95,96] and will not be discussed here. The vibronic coupling Hamiltonian (VCH) consists of the KE operator for the nuclei and a potential energy matrix $V_{ab}(\mathbf{q})$ in a diabatic representation of electronic states for a given coordinate system. In general, the coordinates are chosen to be the reduced normal modes of the ground state. Each potential energy matrix is then expanded in a Taylor series expansion using the ground state geometry (also known as the reference geometry) as the expansion point $\mathbf{q} = 0$:

$$V_{ab}(\mathbf{q}) = E_a \delta_{ab} + \sum_{i=1, N_q} E_{ab}^i q_i + \frac{1}{2} \sum_{i=1, N_q} E_{ab}^{ij} q_i q_j + \dots \quad \forall a, b = 1, \dots, N_e \quad (6.23)$$

Here E_a represents the vertical excitation (or ionization) energies, E_{ab}^i represent the linear coupling constants, while E_{ab}^{ij} represent quadratic coupling constants. In this representation, the dia-

batic states are essentially the electronic eigenstates at the reference geometry. One can in principle include the higher order coupling constants in order to capture the complexity of the potential and improve its accuracy. The coupling constants can be computed *ab initio* by making use of diabaticization schemes available in electronic structure packages, such as ACES2. [97]

The vibronic eigenstates can then be expressed as:

$$\begin{aligned} |\psi_v^{ex}\rangle &= \sum_{\mathbf{n},a} |\mathbf{n}, a\rangle c_{\mathbf{n},a}^v \\ |\psi_{v^+}^{ion}\rangle &= \sum_{\mathbf{m},i} |\mathbf{m}, i\rangle c_{\mathbf{m},i}^{v^+} \end{aligned} \quad (6.24)$$

for the excited and ionized manifolds respectively, which can be thought of arising as a result of diagonalizing the vibronic Hamiltonian in a given basis $|\mathbf{m}, i\rangle$, such as a DVR. In the above equation, the symbols v and v^+ denote the vibronic indices for a particular eigenstate corresponding to the excited and ionized electronic manifold respectively, \mathbf{n} and \mathbf{m} denote the multidimensional index for vibrational degrees of freedom, while a and i denote the labels of the diabatic electronic states.

Based on this definition of vibronic model and the corresponding eigenstates, we will obtain an expression for the final signal following the discussion in previous section. Using the vibronic nomenclature in this section, the fingerprints can be expressed as:

$$F_v(E_{kin}) = \sum_{v^+} \sum_{i,a} |\mu_{ia}|^2 \sum_{\mathbf{m},\mathbf{n}} \langle \mathbf{m} | \mathbf{n} \rangle c_{\mathbf{n},a}^v c_{\mathbf{m},i}^{v^+} \delta(E_{kin} - \Delta E) \quad (6.25)$$

Where $\langle \mathbf{m} | \mathbf{n} \rangle$ defines the vibrational overlap between the vibrational basis states, while μ_{ia} denotes the *electronic* transition dipole moment between the diabatic excited and ionized states that can be calculated *ab initio*. The principal quantity to calculate is the Dyson orbital between ionized and excited state, at the reference geometry. The norm of this orbital can be taken to be proportional to μ_{ia} , or a more sophisticated treatment can be invoked. [93] The populations in the excited state can be expressed as before employing the sudden approximation:

$$P_v(\tau) = \frac{\mu^2(E_0\Delta_t)^2 |\langle v|g\rangle|^2}{\hbar^2} \left(1 + \cos\left[\left(\omega_L - \frac{E_v - E_g}{\hbar}\right)\tau + \omega_L\tau\right] \right) \quad (6.26)$$

Therefore, the snapshots can also be expressed as before as a weighted sum of fingerprints:

$$S(E_{kin}; \tau) = \sum_v P_v(\tau) \cdot F_v(E_{kin}) \quad (6.27)$$

According to the above definitions, we will calculate these quantities for a vibronic model with two normal modes. The model considered here consists of four electronic states, of which one is

the ground state (S_0), two coupled states form the excited manifold (S_1 and S_2), while one represents the ionized manifold (I_0). The modes are referred as the tuning mode (v_t) and the coupling mode (v_c). The parameters for this model can be found in Table 6.1. Concerning the transitions with respect to an external electric field, we consider S_1 to be the dark state, while S_2 is the bright state with respect to transitions from the ground state. For the ionization process, both S_1 and S_2 couple to I_0 , though with different dipole strengths.

Parameter	ω	S_1	$\langle S_1 v_c S_2\rangle$	S_2	I_0
E		4.24		4.84	9.63
v_t/κ	0.074	-0.2		0.15	0
v_c/λ	0.118	0	0.175	0	0
$\mu_{S_0 \rightarrow S_1}$		0.0			
$\mu_{S_0 \rightarrow S_2}$				1.0	
$\mu_{S_1 \rightarrow I_0}$					0.5
$\mu_{S_2 \rightarrow I_0}$					0.1

Table 6.1: Parameters for the 2D vibronic model Hamiltonian. All quantities in electron Volts.

The first step is to obtain the vibronic eigenstates for individual electronic manifolds. The eigenstates are calculated in the Harmonic Oscillator basis using a DVR scheme. The molecular vibronic Hamiltonian can be represented as:

$$\mathbf{H}_{mol} = \begin{pmatrix} \mathbf{H}_{h.o.} & 0 & 0 & 0 \\ 0 & \mathbf{H}_{h.o.} + E_1 + \kappa_1 v_t & \lambda v_c & 0 \\ 0 & \lambda v_c & \mathbf{H}_{h.o.} + E_2 + \kappa_2 v_t & 0 \\ 0 & 0 & 0 & \mathbf{H}_{h.o.} + E_3 \end{pmatrix} \quad (6.28)$$

Where $\mathbf{H}_{h.o.} = -\frac{\omega_t}{2} \frac{\partial^2}{\partial q^2} - \frac{\omega_c}{2} \frac{\partial^2}{\partial q^2} + \frac{1}{2} \omega_t v_t^2 + \frac{1}{2} \omega_c v_c^2$ represents the harmonic oscillator Hamiltonian, and is taken to be the same for each electronic state. The parameters κ_1 and κ_2 correspond to the linear displacements in mode v_t for the two excited states, while λ represents the interstate coupling between the two excited states, S_1 and S_2 . The parameters in the model are chosen to illustrate features of prp-cw-pes. They are not modeled after a particular molecule. The matrix elements for the above Hamiltonian are built as $\langle \mathbf{m}, a | \mathbf{H} | \mathbf{n}, b \rangle$. Diagonalizing this vibronic Hamiltonian gives the eigenvalues and eigenvectors as $E_\lambda, c_{\mathbf{n},b}^\lambda$ and the vibronic wavefunctions can be expressed as:

$$|\Psi_\lambda\rangle = \sum_{\mathbf{n},b} c_{\mathbf{n},b}^\lambda |\mathbf{n}, b\rangle \quad (6.29)$$

The components of the wave function corresponding to different electronic manifolds can be obtained by projecting onto the desired electronic subspace. The pump and repump pulses act at

a uniformly defined grid of pump-repump time-delays. The snapshots corresponding to selected time-delays are shown in Figure 6.4. The features of the spectra change significantly with respect to the time-delay, as one would expect. Let us consider these spectra in terms of the two component structure of snapshots according to Equation 6.27. The time-delay features of snapshots arise due to the change in populations of excited eigenstates as discussed previously. Since we know the eigenstates of this system, the populations as a function of pump-repump time-delay can be computed according to Equation 6.26. These populations are plotted for the same time-delays as for the snapshots in Figure 6.5. The populations change significantly as one varies the time-delay between the two pulses, manifesting the interference effects between the two wave packets created by the pump and repump pulses.

Let us next consider the other component of the spectrum, namely the fingerprints. As mentioned previously in section 6.2, fingerprints can be thought of as photoelectron spectra originating from each individual vibronic eigenstate in the excited manifold acting as the absorbing state. Fingerprints can be characterized based on the knowledge of eigenstates corresponding to both electronic manifolds, i.e. excited and ionized. The complexity of fingerprints will depend on the character of electronic states. If there are low-lying states in any manifold, possibly with large anharmonicities and conical intersections, the resulting fingerprint will be diffuse and might display complicated features. In this model, the ionized state is taken to be simple Harmonic Oscillator. Quite often, the ground ionized state is well-separated, even though not harmonic, and is well-characterized by energy-resolved photoelectron spectroscopy. On the contrary, the manifold of excited electronic states can be quite complicated in nature by the presence of several low-lying states and the presence of conical intersections and thus characterizing eigenstates of such systems in terms of electronic characters is a challenging task. In the present model, the state S_2 crosses through conical intersection around its minimum on diabatic surfaces. Consequently, there are no eigenstates in the Franck-Condon region that have a dominant S_2 character. Most eigenstates in that region have *mixed* character, part S_1 and part S_2 . On the contrary, eigenstates originating in the vicinity of S_1 minima can be characterized as being *pure* S_1 eigenstates. These characteristics reflect in the fingerprints as shown in Figure 6.6 where the fingerprints corresponding to the mixed states have more complicated features.

Analysis of the snapshots: the fitting procedure

In this section, we present a scheme to analyze the prp-cw-pes snapshots in terms of fingerprints by the means of a simple least square fitting procedure. In section 6.2, we proposed that the *experimentally* obtained snapshots can be fitted with *theoretically* computed fingerprints to extract populations of vibronic eigenstates as a function of pump-repump time-delay. We aim to fit the spectra with *fewest* fingerprints possible, and use the same set of fingerprints to fit the snapshots

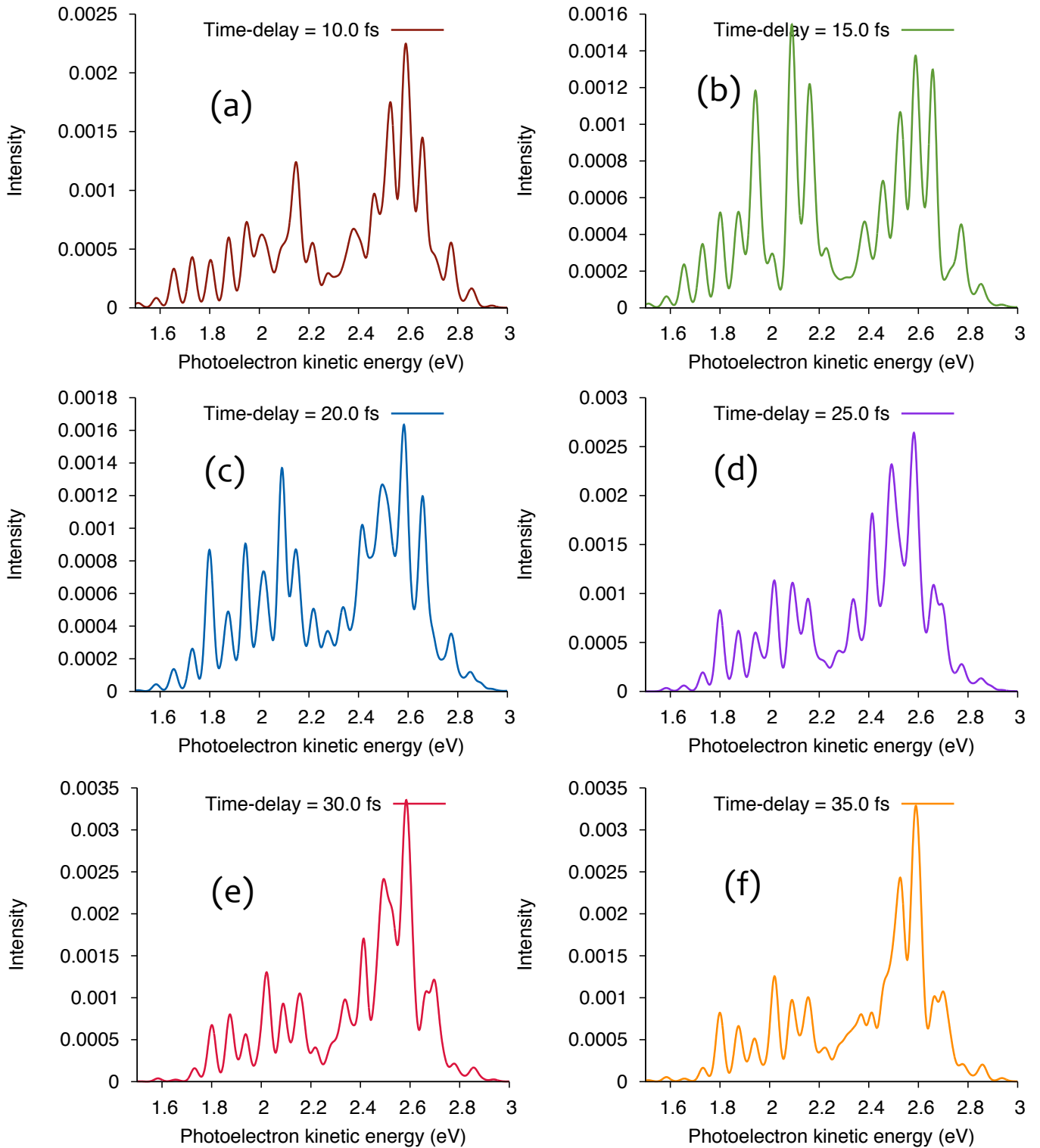


Figure 6.4: Snapshots of prp-cw-pes for the 2D vibronic model at select values of pump-repump time-delays.

corresponding to all time-delays, in order to keep the fitting procedure robust and non-redundant.

A natural question that arises at this stage is, "Which fingerprints should one choose to fit the snapshots?" If the fitting is performed with selecting the fingerprints corresponding to lowest vibronic levels in the excited manifold first, and then gradually adding the higher ones, a large

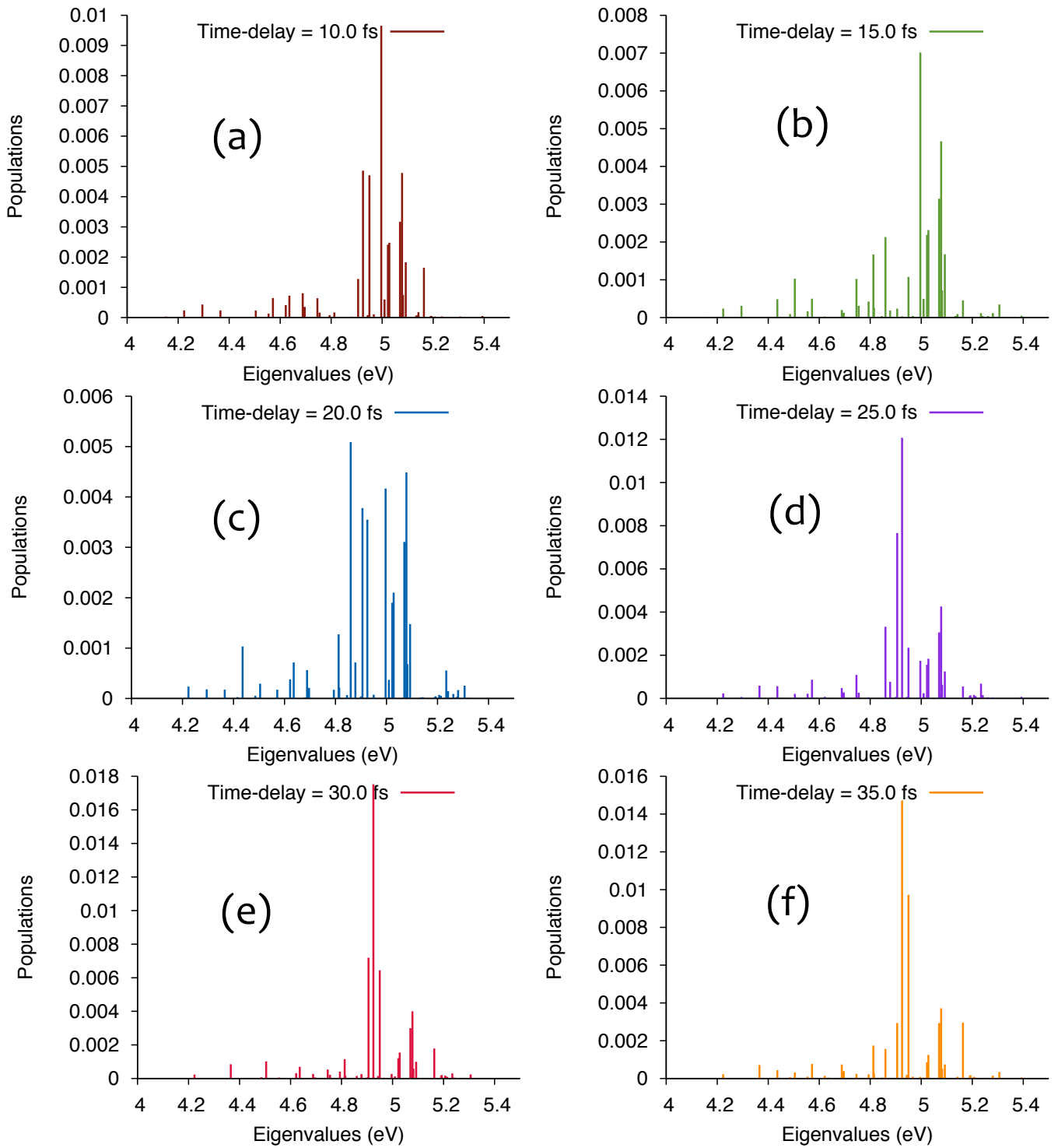


Figure 6.5: Populations in vibronic levels of excited states for the 2D vibronic model at select values of pump-repump time-delays. Eigenvalues characterize the vibronic levels.

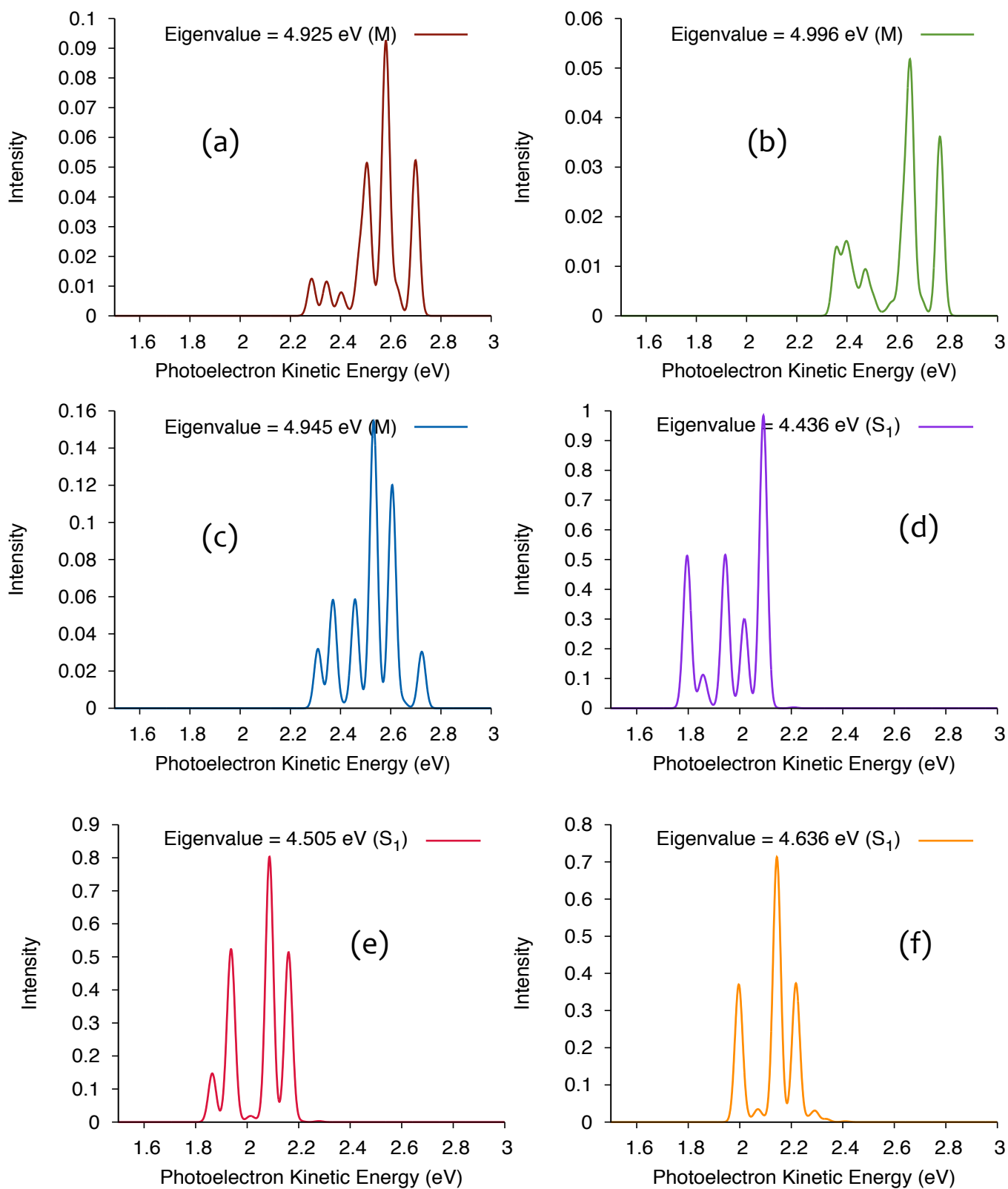


Figure 6.6: Select fingerprints of vibronic excited states for the 2D vibronic model displaying the *primary* character of excited electronic state of its origin

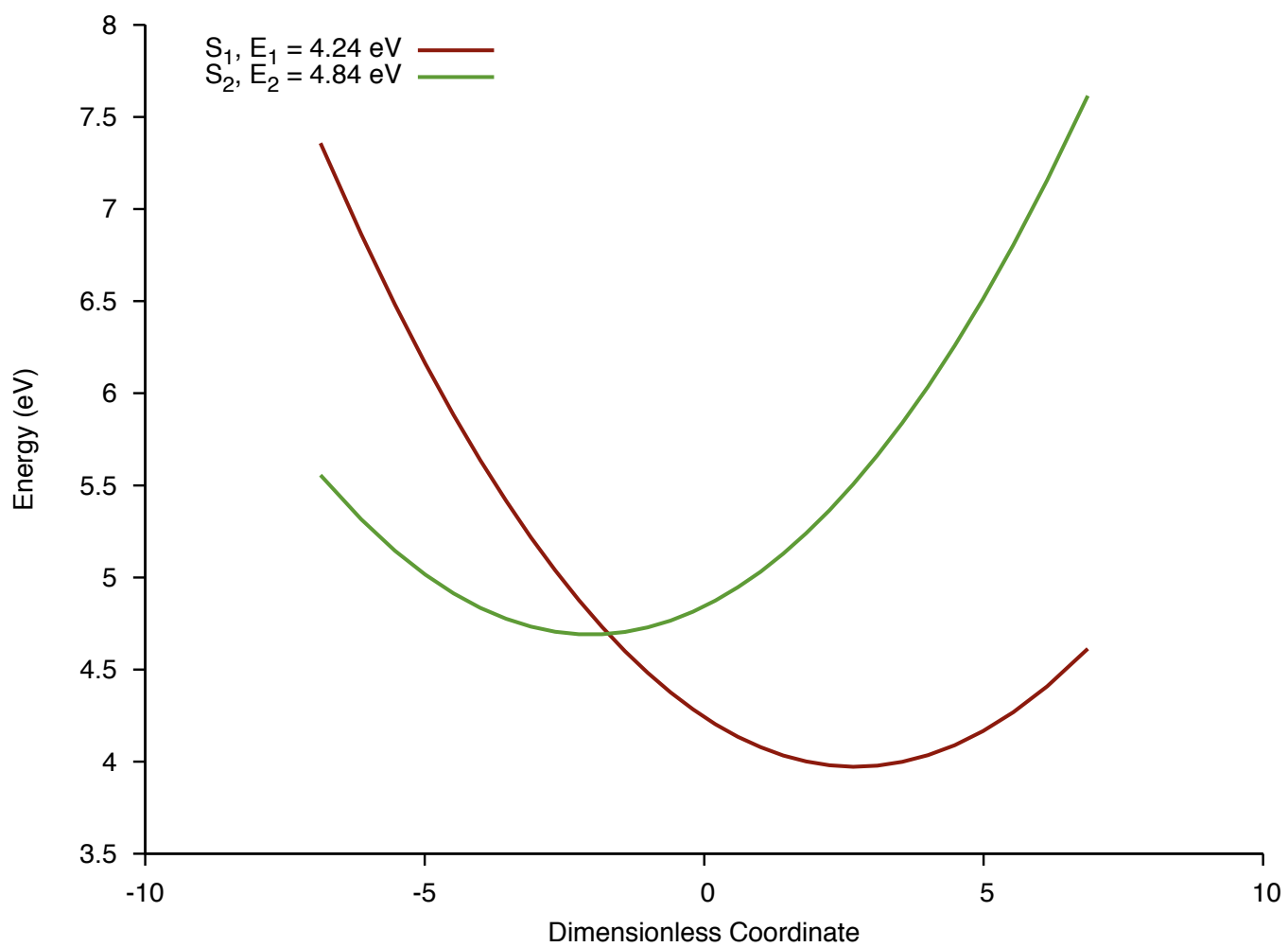


Figure 6.7: 1d cut of PES along the normal mode v_t for excited states S_1 and S_2 corresponding to the parameters shown in Table 6.1

number of fingerprints might be needed in order to obtain a decent fit. Simply because fingerprints corresponding to the low-lying levels in excited manifold might not have any significant contribution to the snapshots, which could be due to the low to zero transition dipole moment or just the lack of any significant overlap of the corresponding excited eigenstate with the initial ground state. The latter argument provides us with some hint in order to choose the suitable fingerprints needed for fitting the snapshots. If a particular vibronic eigenstate in the excited manifold has negligible overlap with the ground state to begin with, from which the pump and repump had originated, it is never going to get a significant population later on as well. As a result, the fingerprints corresponding to these eigenstates will contribute little to the final snapshot. If one observes, however, that for a particular time-delay an eigenstate which had originally minuscule population is now significantly populated, it will indicate a strong interference pattern occurred due to the repump pulse. By the same argument, an eigenstate which is highly populated initially may lose all its population at some particular time-delays. These are states which can be readily identified by observing the pattern of population one gets from the fitting procedure. Therefore, in order to fit the snapshots, we will select fingerprints in order of increasing overlap of vibronic levels in excited state with the initial ground state.

Having discussed the route for the analysis, we now apply these ideas to our 2D vibronic model. The total number of vibronic levels for excited states is 1800 in the basis set, using 30 primitive basis functions along each mode ($30 \times 30 \times 2$). Out of these large number of vibronic states, only a few with largest overlap with the ground state are selected for the fitting procedure because of the reasons discussed above. The fitting results are shown in Figure 6.8 for the time-delay of $\tau = 10.0 fs$. Starting from 10 fingerprints, one only gets part of the full spectrum reproduced, while adding more fingerprints recovers the rest of the features. With about 35 fingerprints or so, one starts to see almost a complete convergence where the fitted spectrum and original spectrum match quite well. This is confirmed quantitatively as well by the root mean square error (RMSE) values. As one increases the number of fingerprints to fit the spectrum, the RMSE values reduce and converge to a smaller value. It is important to note that adding more fingerprints (let's say up to a 1000) has no effect on the fitting of the spectrum as these states have essentially no contribution to the spectrum. Furthermore, although we show the fitting spectra only for the time-delay of $\tau = 10.0 fs$, this behavior is observed for almost all time-delays, as is confirmed by the pattern of RMSE values in Figure 6.9.

The pattern of convergence provides information about the features of the vibronic model for excited states. With the first 10 fingerprints, we are able to fit the *right* side of the spectrum, but not the *left* side at all. This is because the eigenstates with largest overlap belong to a higher energy range as a result of S_2 being the bright state. These fingerprints contribute almost exclusively to the right side of the spectrum. As one moves towards a higher number of fingerprints,

the lower overlap eigenstates, mostly originating in the vicinity of S_1 minima, also get included and one starts to see the left side of the spectrum recovered until one reaches convergence to get all the features. This is also confirmed by the nature of fingerprints themselves as seen in Figure 6.6. Moreover, going a step further, we can also assign these eigenstates an electronic character, based on the *pieces* coming from S_1 or S_2 . This is shown in Table 6.2. States with high overlap actually have *mixed* $S_1 - S_2$ character (M) because the S_2 minima crosses the conical intersection, something which we noticed earlier in the description of the vibronic model. Due to vibronic coupling, low lying eigenstates corresponding to the *pure* S_1 state get significant overlap, contributing significantly to the snapshots.

The prp-cw-pes scheme thus is able to capture the complexity of vibronic models without sacrificing the vibrational resolution. A simpler case is observed if one makes S_1 the bright state, while S_2 becomes the dark state. Snapshots corresponding to this situation are shown in Figure 6.10. The changing pattern of snapshots with respect to the pump-repump time-delay is relatively simple. All the peak positions correspond to a particular $v^{exc} \rightarrow v^+$ transition, only the intensity varies reflecting the change in population in the v state with varying time-delay. This simplicity is reflecting the "Franck-Condon" behavior of the vibronic model. Even though there is significant vibronic coupling, the fingerprints which have major contribution to the snapshots correspond to the *pure* S_1 states, eigenstates lying in the vicinity of S_1 minima. One can in principle monitor the ratio of intensities of snapshots with respect to the time-delay and disentangle the pieces which correspond to the same v level, i.e. contribution from a particular eigenstate in the excited state. These pieces will grow in unison, moving up and down together, as the corresponding population changes at the same rate. This behavior is illustrated in Movie M4. Such an analysis would be complicated for a complex vibronic model, such as the case of S_2 being the bright state. Nonetheless, one can identify parts of the snapshots for which only a few fingerprints are needed for fitting (states with the high vibronic overlap), while some other parts might be more complicated to reproduce and will require more fingerprints. This behavior is shown for the present model when S_2 is the bright state in Movie M5. It is important to emphasize that the transition dipole moments are chosen in such a way that the photo-ionization cross section corresponding to both S_1 and S_2 states get significant intensities in the final spectra.

Finally, we comment on the pattern of populations obtained from the fitting procedure. If we look at the Table 6.2, the vibronic levels in excited state that have large overlap with the ground state, also have large populations irrespective of the time-delay. As anticipated earlier, there are exceptions to this behavior. These particular time-delays can be readily identified. Using this data, one can also monitor the growth and decay of populations for a particular eigenstate. Certain eigenstates display strong changes in population, as seen in Figure 6.11. One could identify a particular intense transition corresponding to such a state, and then monitor closely the intensity

of the peak as a function of time-delay.

No	Eigenstate	$E_v(eV)$	Overlap	Populations					Character
				$\tau = 10.0$	$\tau = 15.0$	$\tau = 20.0$	$\tau = 25.0$	$\tau = 30.0$	
1	70	4.925	0.1968	0.0071	0.0001	0.0054	0.0144	0.019	M
2	82	4.996	0.1360	0.0144	0.0129	0.0064	0.0025	0.0003	M
3	75	4.945	0.1144	0.0068	0.0019	-2.21E-06	0.0031	0.0069	M
4	66	4.906	0.0899	0.0019	0.0005	0.0057	0.0091	0.0079	M
5	60	4.860	0.0573	0.0001	0.0044	0.008	0.0044	0.0005	M
6	99	5.078	0.0544	0.0066	0.008	0.0067	0.0050	0.0044	M
7	116	5.163	0.0376	0.00245	0.001	8.76E-05	0.0007	0.002	M
8	95	5.07	0.0355	0.0058	0.0065	0.0046	0.0049	0.0036	M
9	88	5.028	0.0291	0.0034	0.004	0.0032	0.0022	0.0017	M
10	87	5.023	0.029	0.0036	0.004	0.003	0.0015	0.0015	M
11	101	5.093	0.0218	0.0026	0.0024	0.002	0.0011	0.0009	M
12	53	4.812	0.0206	-0.0001	0.0029	0.002	1.48E-05	0.0013	M
13	44	4.746	0.0135	0.0014	0.0019	-7.14E-05	0.0013	0.0005	M
14	15	4.436	0.0114	-8.07E-06	0.0007	0.001	0.0007	-8.06E-05	S1
15	20	4.505	0.0113	0.0003	0.002	0.0006	0.0003	0.0012	S1
16	26	4.572	0.0099	0.0011	0.0010	0.0003	0.001	4.51E-05	S1
17	37	4.688	0.0098	0.0012	0.0005	0.001	0.0006	0.0004	S1
18	11	4.366	0.0095	0.0003	3.39E-05	0.0003	0.0007	0.0009	S1
19	64	4.878	0.0093	0.0005	0.0012	0.0014	0.0008	0.0006	S1
20	100	5.081	0.0086	0.0008	0.0009	0.0008	0.0007	0.0004	M

Table 6.2: Change in populations as a function of pump-repump time-delay for select vibronic levels in excited states depending on the vibronic overlap with the ground state. All time-delays are in fs .

6.4 Concluding Remarks

We have proposed a new scheme for time-resolved photoelectron spectroscopy denoted as prp-cw-pes, which has potential to become a tool to identifying molecular structures, in addition to monitor population dynamics in excited states. Different ways of performing the experiment have been discussed. In the actual experiment the process that determines the final populations after the action of pump and repump may be very complicated and they are also hard to predict theoretically. Experimentally one would measure the *change* in spectra depending on the time delay between pump and repump pulses. This change in the spectra is expected to be the weighted sum of fingerprints, regardless of the complications. The burden is on the theory to calculate fingerprints to sufficient accuracy. If this can be achieved by theory, and the resolved spectra can be obtained by experiment, comparisons can be made employing the fitting tools discussed in this work. If these comparisons are satisfactory, it presumably means that the vibronic model used in the simulations is accurate. That means one has obtained a detailed molecular model of ground, excited and ionized states of the molecular system under consideration. In this manner, a direct interplay between theory and experiment emerges by the means of the proposed scheme.

Moreover, population in excited state might decay through collisions. There is also possible interest of monitoring the decay of population of a particular vibronic excited state. If one would monitor a particular known feature in the spectrum which is independent of the time-delay, achieved by tuning the carrier frequency of the pump and repump laser in the phase-locked version of the experiment, one might observe these features disappearing over a period of time because of population decay. One might be able to see the phenomena for several vibronic states. This is an exciting prospect, and it may yield an increased understanding of excited state decay.

The discussion of cw laser field as the probe deserves further examination. A picosecond pulse, which is relatively quite long compared to the femtosecond duration of pump and repump, will be able to achieve resonant transitions and therefore provide the desired energy resolution. A high energy picosecond laser will also be able to provide the sufficient incident flux and power density in order to ionize the system. Such lasers are either currently available in the market or can be obtained with a custom order. Furthermore, experimentally there is the underlying question of which experimental set up one should use for the proposed scheme in regards to the phase relation between pump and repump. We emphasize that the analysis scheme based on the fitting of snapshots to fingerprints is independent of a precise phase relation, inasmuch as it depends on the final population in excited state after the action of pump and repump, which are in turn obtained as fitting parameters. A phase-locked experiment has its own virtues, although amounting to a difficult experimental set-up. The answer then is slightly subjective, guided by the motivation of problem at hand, and the experimental resources available to oneself. Perhaps more possibilities of performing the experiment exist, which could possibly lead to new kind of information

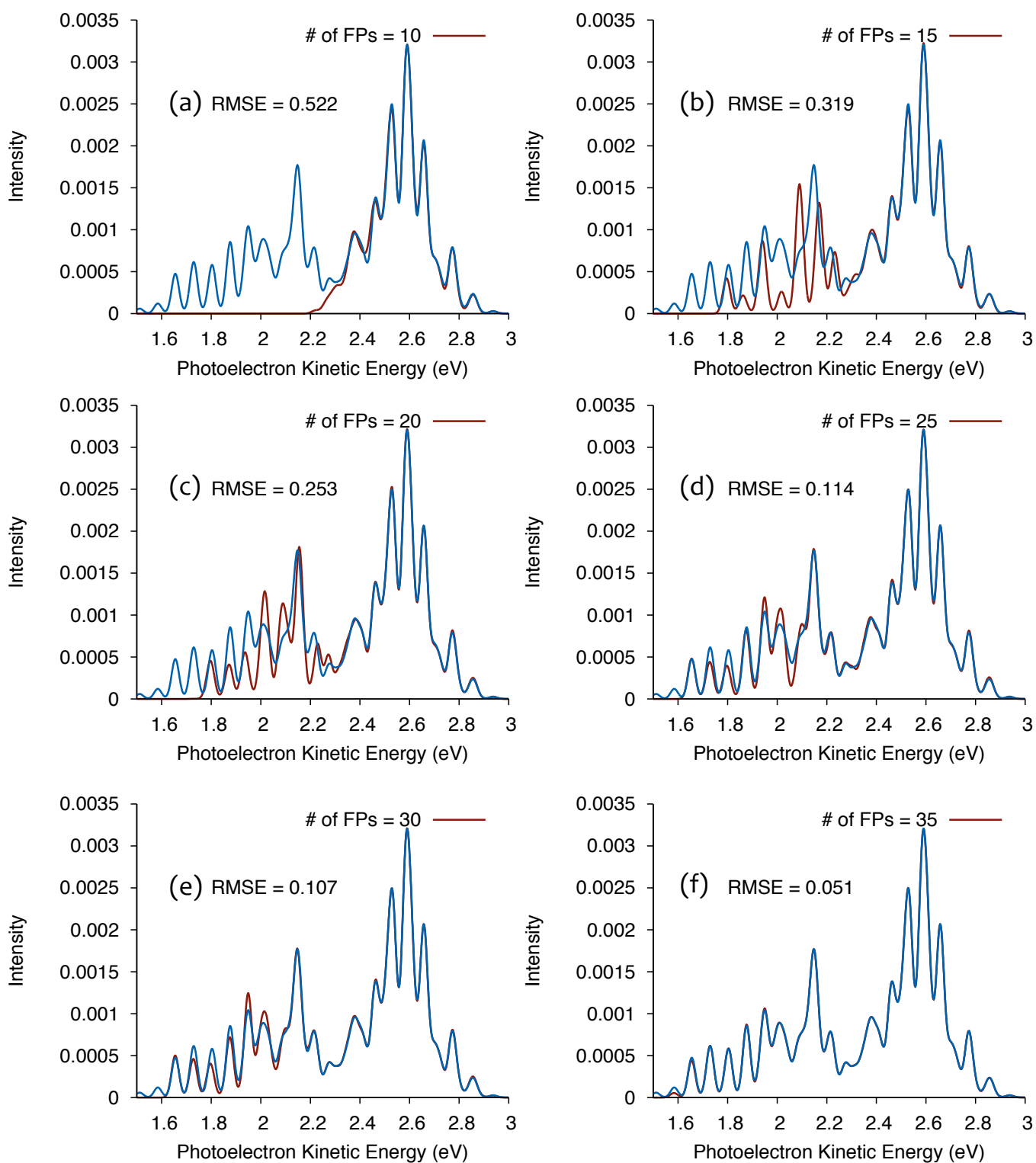


Figure 6.8: Results of fitting for the snapshot corresponding to time-delay 10.0 fs for the 2D vibronic model with varying number of fingerprints. Convergence is reached at 35 fingerprints.

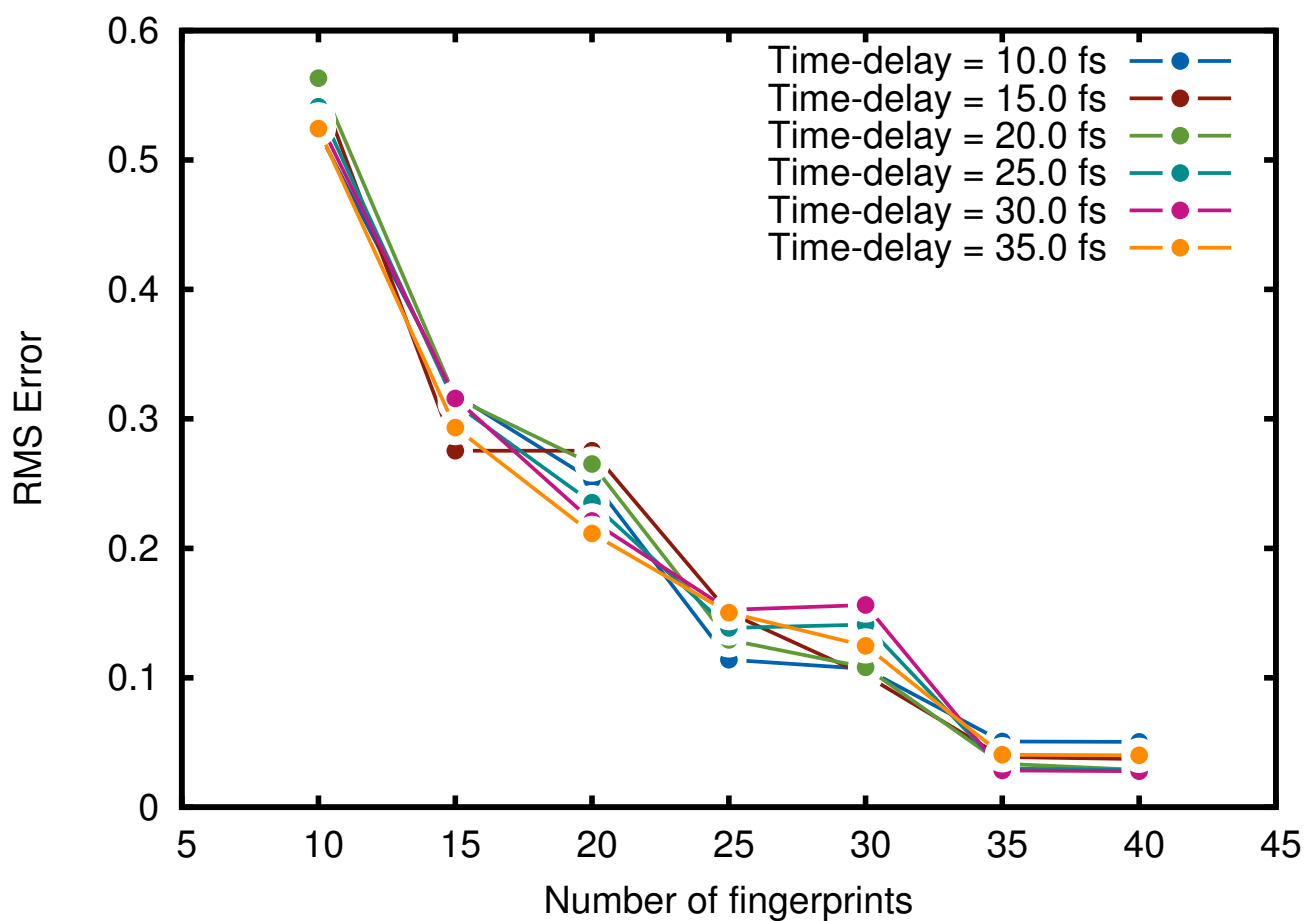


Figure 6.9: RMSE values associated with the fitting of snapshots with varying number of fingerprints for select time-delays. The pattern is similar for all time-delays and convergence is reached after 35 fingerprints.

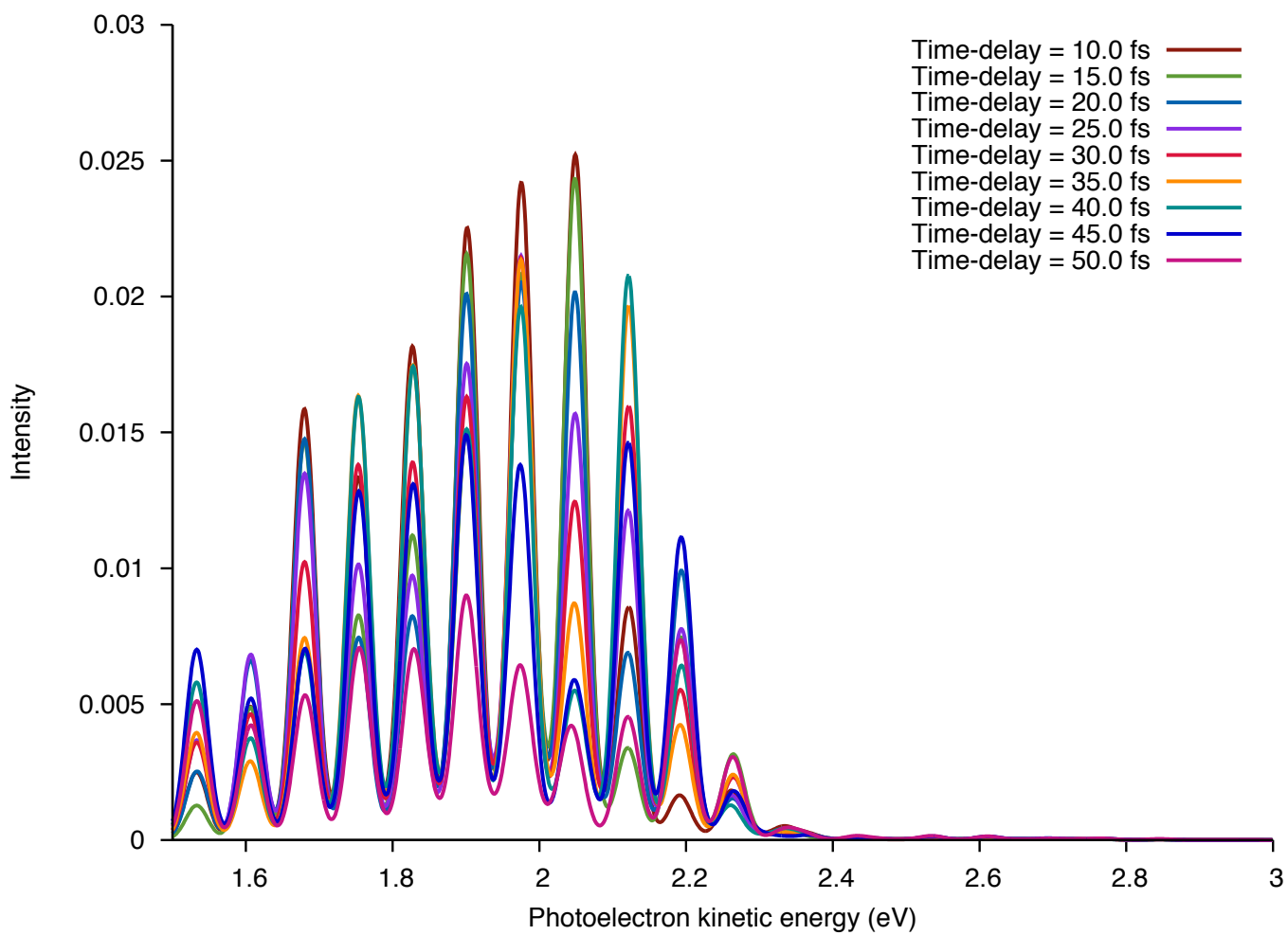


Figure 6.10: Snapshots of prp-cw-pes for the 2D vibronic model at select values of pump-repump time-delays for the case when the state S_1 is bright.

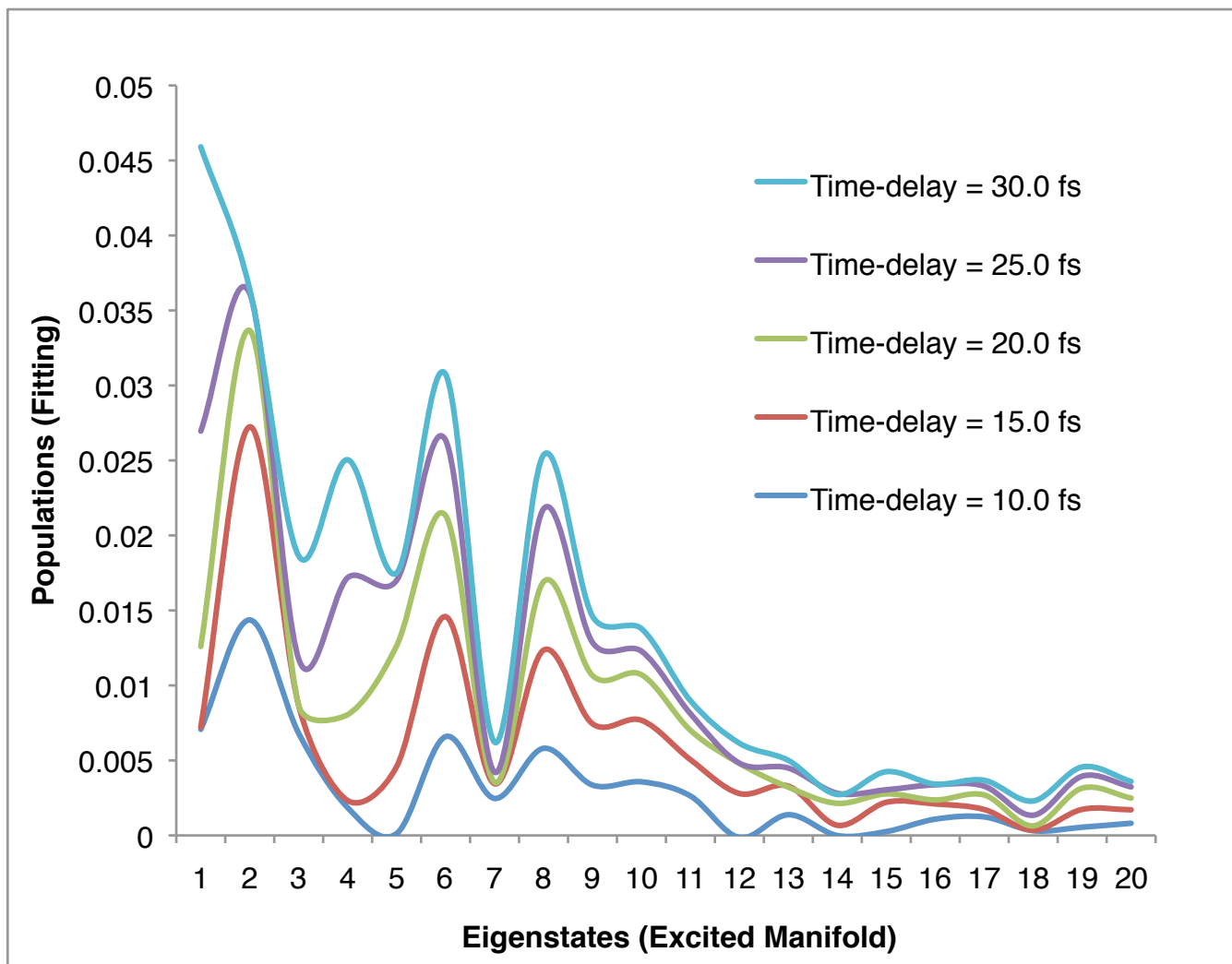


Figure 6.11: Population dynamics associated with vibronic levels in excited state at select values of time-delays. Some eigenstates display large changes while others only have small effect of time-delay on the net population.

and understanding of molecular structure and associated dynamics. We look to the experimental spectroscopy community for further inspiration.

Supplementary Information

The Supplementary Information (movies) can be accessed from PCCP: P. Goel and M. Nooijen, *Phys. Chem. Chem. Phys.*, 18, 11263-11277, 2016

References

- [1] C. J. Cramer, *Essentials of computational chemistry: theories and models* (John Wiley & Sons, 2013).
- [2] F. Jensen, *Introduction to computational chemistry* (John Wiley & Sons, 2017).
- [3] D. G. Truhlar, B. C. Garrett, and S. J. Klippenstein, *The Journal of physical chemistry* **100**, 12771 (1996).
- [4] A. Fernández-Ramos, J. A. Miller, S. J. Klippenstein, and D. G. Truhlar, *Chemical reviews* **106**, 4518 (2006).
- [5] J. H. Baraban et al., *Science* **350**, 1338 (2015).
- [6] H. B. Schlegel, *Wiley Interdisciplinary Reviews: Computational Molecular Science* **1**, 790 (2011).
- [7] R. Collepardo-Guevara, Y. V. Suleimanov, and D. E. Manolopoulos, *The Journal of chemical physics* **130**, 174713 (2009).
- [8] W. H. Miller, N. C. Handy, and J. E. Adams, *The Journal of chemical physics* **72**, 99 (1980).
- [9] W. Mizukami, S. Habershon, and D. P. Tew, *The Journal of chemical physics* **141**, 144310 (2014).
- [10] S. Pratihar, X. Ma, Z. Homayoon, G. L. Barnes, and W. L. Hase, *Journal of the American Chemical Society* **139**, 3570 (2017).
- [11] A. Warshel and R. M. Weiss, *Journal of the American Chemical Society* **102**, 6218 (1980).
- [12] H. Koppel, W. Domcke, and L. Cederbaum, *Advances in Chemical Physics* **57**, 59 (1984).
- [13] M. H. Beck, A. Jäckle, G. Worth, and H.-D. Meyer, *Physics reports* **324**, 1 (2000).
- [14] Y. Kim, J. C. Corchado, J. Villa, J. Xing, and D. G. Truhlar, *The Journal of Chemical Physics* **112**, 2718 (2000).
- [15] J. L. Sonnenberg and H. B. Schlegel, *Molecular Physics* **105**, 2719 (2007).
- [16] R. Fletcher, *Practical methods of optimization* (John Wiley & Sons, 2013).

- [17] C. J. Cerjan and W. H. Miller, *The Journal of chemical physics* **75**, 2800 (1981).
- [18] J. Simons, P. Joergensen, H. Taylor, and J. Ozment, *The Journal of Physical Chemistry* **87**, 2745 (1983).
- [19] J. Nichols, H. Taylor, P. Schmidt, and J. Simons, *The Journal of chemical physics* **92**, 340 (1990).
- [20] J. Simons and J. Nichols, *International Journal of Quantum Chemistry* **38**, 263 (1990).
- [21] A. Banerjee, N. Adams, J. Simons, and R. Shepard, *The Journal of Physical Chemistry* **89**, 52 (1985).
- [22] J. Baker, *Journal of Computational Chemistry* **7**, 385 (1986).
- [23] P. Culot, G. Dive, V. H. Nguyen, and J.-M. Ghuysen, *Theoretica Chimica Acta* **82**, 189 (1992).
- [24] E. Besalú and J. M. Bofill, *Theoretical Chemistry Accounts: Theory, Computation, and Modeling (Theoretica Chimica Acta)* **100**, 265 (1998).
- [25] J. M. Anglada and J. M. Bofill, *International journal of quantum chemistry* **62**, 153 (1997).
- [26] B. A. Murtagh and R. W. Sargent, *The Computer Journal* **13**, 185 (1970).
- [27] C. Bryoden, *J. Inst. Math. App1* **7**, 76 (1971).
- [28] R. Fletcher, *The computer journal* **13**, 317 (1970).
- [29] D. Goldfarb, *Mathematics of computation* **24**, 23 (1970).
- [30] D. F. Shanno, *Mathematics of computation* **24**, 647 (1970).
- [31] J. E. Dennis Jr and R. B. Schnabel, *Numerical methods for unconstrained optimization and nonlinear equations* (SIAM, 1996).
- [32] J. M. Bofill, *Journal of Computational Chemistry* **15**, 1 (1994).
- [33] P. Császár and P. Pulay, *Journal of Molecular Structure* **114**, 31 (1984).
- [34] Ö. Farkas and H. B. Schlegel, *Physical Chemistry Chemical Physics* **4**, 11 (2002).
- [35] X. Li and M. J. Frisch, *Journal of chemical theory and computation* **2**, 835 (2006).
- [36] C. Lanczos, *An iteration method for the solution of the eigenvalue problem of linear differential and integral operators* (United States Governm. Press Office Los Angeles, CA, 1950).
- [37] T. A. Halgren and W. N. Lipscomb, *Chemical Physics Letters* **49**, 225 (1977).
- [38] C. Peng and H. Bernhard Schlegel, *Israel Journal of Chemistry* **33**, 449 (1993).
- [39] D. A. Liotard, *International journal of quantum chemistry* **44**, 723 (1992).

- [40] S. Fischer and M. Karplus, *Chemical physics letters* **194**, 252 (1992).
- [41] R. Czerminski and R. Elber, *International Journal of Quantum Chemistry* **38**, 167 (1990).
- [42] G. Henkelman, B. P. Uberuaga, and H. Jónsson, *The Journal of chemical physics* **113**, 9901 (2000).
- [43] B. Jiang and H. Guo, *The Journal of chemical physics* **139**, 054112 (2013).
- [44] A. Warshel, *Computer modeling of chemical reactions in enzymes and solutions* (Wiley New York, 1991).
- [45] Y. T. Chang and W. H. Miller, *Journal of Physical Chemistry* **94**, 5884 (1990).
- [46] H. B. Schlegel and J. L. Sonnenberg, *Journal of chemical theory and computation* **2**, 905 (2006).
- [47] B. Hartke and S. Grimme, *Physical Chemistry Chemical Physics* **17**, 16715 (2015).
- [48] S. Grimme, *Journal of chemical theory and computation* **10**, 4497 (2014).
- [49] F. Jensen, *Journal of computational chemistry* **15**, 1199 (1994).
- [50] F. Jensen and P.-O. Norrby, *Theoretical Chemistry Accounts* **109**, 1 (2003).
- [51] M. Sierka and J. Sauer, *The Journal of Chemical Physics* **112**, 6983 (2000).
- [52] P. R. Bunker and P. Jensen, *Molecular symmetry and spectroscopy* (NRC Research Press, 2006).
- [53] S. V. Krasnoshchekov, E. V. Isayeva, and N. F. Stepanov, *The Journal of Chemical Physics* **140**, 154104 (2014).
- [54] M. Page and J. W. McIver Jr, *The Journal of chemical physics* **88**, 922 (1988).
- [55] R. H. Byrd, R. B. Schnabel, and G. A. Shultz, *SIAM Journal on Numerical Analysis* **24**, 1152 (1987).
- [56] B. K. Dey, M. R. Janicki, and P. W. Ayers, *The Journal of chemical physics* **121**, 6667 (2004).
- [57] P. Pulay, *Chemical Physics Letters* **73**, 393 (1980).
- [58] W. Quapp, M. Hirsch, and D. Heidrich, *Theoretical Chemistry Accounts* **100**, 285 (1998).
- [59] M. Bixon and J. Jortner, *The Journal of Chemical Physics* **48**, 715 (1968).
- [60] W. Domcke and G. Stock, *Advances in Chemical Physics*, Volume 100 , 1 (1997).
- [61] G. A. Worth and L. S. Cederbaum, *Annu. Rev. Phys. Chem.* **55**, 127 (2004).
- [62] D. M. Neumark, *Annual review of physical chemistry* **52**, 255 (2001).

- [63] G. Wu, P. Hockett, and A. Stolow, *Physical Chemistry Chemical Physics* **13**, 18447 (2011).
- [64] A. Stolow, A. E. Bragg, and D. M. Neumark, *Chemical reviews* **104**, 1719 (2004).
- [65] A. Stolow and J. G. Underwood, *Advances in chemical physics* **139**, 497 (2008).
- [66] T. Suzuki, *International Reviews in Physical Chemistry* **31**, 265 (2012).
- [67] M. Seel and W. Domcke, *The Journal of chemical physics* **95**, 7806 (1991).
- [68] S. Hahn and G. Stock, *Physical Chemistry Chemical Physics* **3**, 2331 (2001).
- [69] Y.-I. Suzuki, T. Fuji, T. Horio, and T. Suzuki, *The Journal of chemical physics* **132**, 174302 (2010).
- [70] T. Seideman, *Annual review of physical chemistry* **53**, 41 (2002).
- [71] K. L. Reid, *Annual review of physical chemistry* **54**, 397 (2003).
- [72] Y.-i. Suzuki, M. Stener, and T. Seideman, *The Journal of chemical physics* **118**, 4432 (2003).
- [73] W. T. Pollard, S.-Y. Lee, and R. A. Mathies, *The Journal of chemical physics* **92**, 4012 (1990).
- [74] W. T. Pollard and R. A. Mathies, *Annual review of physical chemistry* **43**, 497 (1992).
- [75] D. Tannor et al., *Introduction to quantum mechanics* (University Science Books, 2007).
- [76] P. Kukura, D. W. McCamant, and R. A. Mathies, *Annu. Rev. Phys. Chem.* **58**, 461 (2007).
- [77] P. Kukura, D. W. McCamant, S. Yoon, D. B. Wandschneider, and R. A. Mathies, *Science* **310**, 1006 (2005).
- [78] D. W. McCamant, P. Kukura, S. Yoon, and R. A. Mathies, *Review of scientific instruments* **75**, 4971 (2004).
- [79] P. Kukura, D. W. McCamant, and R. A. Mathies, *The Journal of Physical Chemistry A* **108**, 5921 (2004).
- [80] S.-Y. Lee, D. Zhang, D. W. McCamant, P. Kukura, and R. A. Mathies, *The Journal of chemical physics* **121**, 3632 (2004).
- [81] A. Hazra and M. Nooijen, *Physical Chemistry Chemical Physics* **7**, 1759 (2005).
- [82] A. Hazra, H. H. Chang, and M. Nooijen, *The Journal of chemical physics* **121**, 2125 (2004).
- [83] J. Bloino, M. Biczysko, F. Santoro, and V. Barone, *Journal of Chemical Theory and Computation* **6**, 1256 (2010).
- [84] R. Borrelli, A. Capobianco, and A. Peluso, *Canadian Journal of Chemistry* **91**, 495 (2013).
- [85] K. Ohmori, Y. Sato, E. E. Nikitin, and S. A. Rice, *Physical review letters* **91**, 243003 (2003).

- [86] K. Ohmori et al., Physical review letters **96**, 093002 (2006).
- [87] K. Ohmori, Annual review of physical chemistry **60**, 487 (2009).
- [88] N. F. Scherer et al., The Journal of chemical physics **95**, 1487 (1991).
- [89] C. Leichtle, W. Schleich, I. S. Averbukh, and M. Shapiro, The Journal of chemical physics **108**, 6057 (1998).
- [90] C. Warmuth et al., The Journal of Chemical Physics **114**, 9901 (2001).
- [91] T. N. Rescigno and V. McKoy, Phys. Rev. A **12**, 522 (1975).
- [92] A. W. Fliflet and V. McKoy, Phys. Rev. A **18**, 2107 (1978).
- [93] S. Gozem et al., The journal of physical chemistry letters **6**, 4532 (2015).
- [94] M. Wollenhaupt, V. Engel, and T. Baumert, Annu. Rev. Phys. Chem. **56**, 25 (2005).
- [95] H.-D. Meyer, F. Gatti, and G. A. Worth, *Multidimensional quantum dynamics* (John Wiley & Sons, 2009).
- [96] F. Gatti, *Molecular Quantum Dynamics* (Springer, 2014).
- [97] M. Nooijen, International journal of quantum chemistry **95**, 768 (2003).
- [98] W. Domcke et al., *Conical intersections: electronic structure, dynamics and spectroscopy*, volume 15 (World Scientific, 2004).
- [99] L. Noordam, D. Duncan, and T. Gallagher, Physical Review A **45**, 4734 (1992).